

Christy Rouault

# Extreme Multiple Landslide Events in Norway

An Investigation of Rainfall and Snowmelt Induced Soil Landslide Detection and Forecasting

Master's thesis in Cold Climate Engineering

Supervisor: Steinar Nordal (NTNU), Erin Lindsay (NTNU), Morten Andreas Dahl Larsen (DTU), & Luca Piciullo (NGI)

June 2020





Christy Rouault

# **Extreme Multiple Landslide Events in Norway**

An Investigation of Rainfall and Snowmelt Induced Soil Landslide Detection and Forecasting

Master's thesis in Cold Climate Engineering

Supervisor: Steinar Nordal (NTNU), Erin Lindsay (NTNU), Morten Andreas Dahl Larsen (DTU), & Luca Piciullo (NGI)

June 2020

Norwegian University of Science and Technology

Faculty of Engineering

Department of Civil and Environmental Engineering



Norwegian University of  
Science and Technology



## Abstract

Extreme events with multiple landslides can cause major economic costs, damage, and loss of life. While a single landslide can be destructive, multiple landslides are often the culprit of major losses. They can isolate communities and overwhelm emergency response by blocking transportation arteries and disrupting power and communication lines in several locations. In Norway, no red level warnings have been issued from 2015-2019, despite at least three events with severe damage and  $\geq 20$  landslides. Early warnings greatly benefit in mitigating the consequences of landslides. Due to the uncertainty in forecasting rare, high consequence events, improved understanding of past events is needed. This study aimed to (1) improve the landslide inventory and (2) analyse forecasting tools and warnings given for past events with multiple landslides, to assist in issuing more reliable warnings in the future.

21 Norwegian and four international multiple landslide case studies between 2015-2019 were investigated. Selected Norwegian case studies included days with  $\geq 10$  registered, geographically clustered, soil landslides. Two satellite landslide mapping techniques were tested using Sentinel-1 (SAR) and Sentinel-2 ( $\delta$ NDVI) images. Detection of registered landslides was attempted, and additional unreported landslides were mapped. Only 10% of landslides were detectable using SAR. Limiting factors of detection of selected landslides using SAR intensity, phase, and coherence, included snow, slope aspect, and spatial resolution. 45% of selected landslides were detectable using  $\delta$ NDVI. However, if only considering ideal conditions, the detection rate increased to 94%. In  $\frac{1}{3}$  of cases,  $\delta$ NDVI mapping nearly tripled the landslide inventory.  $\delta$ NDVI-mapping is hindered by snow and cloud cover, low sun angle, short daylight hours, and landslide size ( $>1000 \text{ m}^2$ ). International test sites in arctic, urban, tropical, and monsoon conditions showed great potential for  $\delta$ NDVI-mapping, but limited success using SAR.

Forecasting tools, including the HYDMET threshold model, susceptibility maps, geology maps, rainfall and snowmelt, were analysed for the selected Norwegian case studies to identify correlations. Published warnings and warning evaluations of case studies were compared, in order to determine the main challenges in forecasting. Finally, the temporal and spatial trends of multiple landslide events were identified. Forecasting tools for the selected cases revealed varied usefulness. The HYDMET model underestimated hazard levels in 67% of cases. 84% of landslides occurred in high or very high susceptibility zones and have quaternary geology mapped as till, colluvium, or bare bedrock. Rainfall and snowmelt were the ultimate instigator of all selected cases, with normalized 24-hour water supply between 2.4% and 8.5% of mean annual precipitation. Return periods of 1, 3, and 24-hr water supply are  $\leq 5$  years in 11 cases and  $\geq 100$  years in six cases. Peak water-supply may not be captured by models or observed by rain gauges. The most challenging forecasting days are 1) uncertain high return period rainstorms and 2) spring melt with wet antecedent conditions.  $\frac{1}{3}$  of case studies were under-warned according to NVE evaluations. Days with  $\geq 10$  landslides are most common in Western Norway, due to a tempered climate and high precipitation, and rare north of Trondelag due to lower rainfall and cold, stable winters. These days occur nearly five times/year, with  $\frac{3}{4}$  occurring in September to January.

Using  $\delta$ NDVI, landslide inventories in Norway could be drastically improved, albeit limited by cloud, snow, daylight, and landslide size. Improved inventories would help develop more reliable thresholds. However, this analysis indicates that despite a strong correlation in the majority of selected cases, rainfall and snowmelt alone cannot predict landslides. Better understanding of the role of the other influencing factors could reduce the number of under-warned multiple landslide events.

## Preface

This report fulfills the requirements for the Joint Nordic Master of Science Degree in Cold Climate Engineering, Land Track, with an Arctic specialization at the Norwegian University of Science and Technology (NTNU) and the Technical University of Denmark (DTU). It was written at the Department of Civil and Environmental Engineering at NTNU in conjunction with the Department of Civil Engineering at DTU. It was written entirely by myself, with much support from my advisors, cooperating organizations, the scientific community, friends, and family.

Two weeks into writing my master's thesis, the World Health Organization declared a Public Health Emergency. A highly contagious virus sent us all into months of isolation. Despite the obvious tragedy that struck, many important lessons have shined through in this time:

1. Despite us all bearing the same storm, everyone is on a different lifeboat. While writing my thesis was one of the most isolating experiences of my life, greatly exaggerated by the pandemic restrictions, I was on a deluxe lifeboat. This period of life has been humbling, in noticing those things I've taken for granted, not least, these past two years living in Denmark, Greenland, Svalbard, Norway, and Canada.
2. I am eternally grateful for the countless hours I've spent on the phone with loved ones while in isolation. I count myself lucky to have a mom who loves to chat.
3. The COVID-19 pandemic, not unlike landslides, was predictable. The onslaught of scientists whose warnings went relatively unheard serve as a reminder that a warning must be measured in both accuracy and communication of predictions. While my thesis delves only into the former, my understanding and interest in how those warnings are communicated has been ignited by this pandemic.

Thanks to the organizations who made this work possible. At NGI, for not only formal supervision, but also inspiration and knowledge provided, as is evident in my reference list. To NTNU and DTU, having given me this extraordinary opportunity to be educated in Scandinavia. At NVE, I was provided with invaluable comments and data. To all those at BGC, who motivated me to complete my masters in the first place, and this incredible organization for supporting me throughout.

My four advisors each brought something exceptionally valuable to me and this research. To Steinar, it was a privilege to be supervised by an engineer whose name precedes you. Your energy and wise words always fuelled my motivation. To Luca, you have been my compass through this research. Your ideas, knowledge, and criticism have been essential. To Morten, you have a true gift in making students feel important; thank you for giving me your time and inspiration to write a great thesis. To Erin, you have become such a dear friend. I am in debt to you for this opportunity to work with you and I can't thank you enough for teaching me much about navigating academia, landslides, and babies.

# Contents

Abstract.....	i
Preface .....	ii
List of Figures .....	v
List of Tables .....	vi
List of Equations.....	vii
Abbreviations.....	viii
1 Introduction .....	1
1.1 Landslide Early Warning Systems.....	1
1.1.1 Thresholds.....	2
1.1.2 Landslide Inventories .....	2
1.1.3 Extreme Landslide Events .....	2
1.2 Research Problem .....	4
1.3 Limitations.....	4
1.4 Contributions .....	5
1.5 Structure .....	6
2 Background .....	7
2.1 Norwegian Landslide Early Warning System .....	7
2.1.1 Warning Levels.....	7
2.1.2 Weather Conditions .....	9
2.1.3 Current Norwegian Thresholds.....	12
2.1.4 Susceptibility Maps .....	12
2.1.5 Quaternary Geology Maps.....	13
2.1.6 Warning Communication .....	13
2.1.7 Performance.....	14
2.2 National Landslide Database.....	14
2.2.1 Landslide Classification .....	14
2.3 Remote Sensing .....	15
2.3.1 SAR Theory .....	15
2.3.2 $\delta$ NVDI Theory .....	16
3 Methods.....	18
3.1 Case Study Selection .....	18
3.1.1 Norway.....	18

3.1.2	International .....	18
3.2	Landslide Inventory.....	19
3.2.1	Sentinel-1 .....	19
3.2.2	SAR Pre-Processing .....	19
3.2.3	Sentinel-2 .....	20
3.2.4	$\delta$ NVDI Pre-processing .....	20
3.2.5	Landslide Detection .....	21
3.2.6	NVE Landslide Database Limitations.....	21
3.3	Landslide Forecasting.....	22
3.3.1	Landslide Database Trends .....	22
3.3.2	Susceptibility Mapping.....	22
3.3.3	Quaternary Geology Mapping .....	23
3.3.4	Weather .....	24
3.3.5	HYDMET Model.....	26
3.3.6	Landslide Warnings.....	26
4	Results & Discussion .....	28
4.1	Case Studies .....	28
4.1.1	Norway.....	28
4.1.2	International .....	29
4.2	Landslide Inventory.....	30
4.2.1	SAR .....	30
4.2.2	$\delta$ NDVI .....	34
4.2.3	International Test Sites .....	41
4.2.4	Method Comparison & Opportunities.....	46
4.2.5	NVE Landslide Database Limitations.....	47
4.3	Landslide Prediction.....	50
4.3.1	Landslide Database Trends .....	50
4.3.2	Susceptibility Mapping.....	51
4.3.3	Quaternary Geology Mapping .....	52
4.3.4	Weather .....	54
4.3.5	HYDMET Model.....	63
4.3.6	Landslide Warnings.....	65
5	Conclusions .....	71



5.1	Landslide Inventory.....	72
5.2	Landslide Forecasting.....	73
5.3	Future Studies .....	74
6	References .....	75
	Appendix A: Python Code .....	82
	Appendix B: Landslide Database Selection .....	88
	Appendix C: SAR Analysis.....	95
	Appendix D: $\delta$ NDVI Analysis .....	99
	Appendix E: Weather Data.....	105
	Appendix F: HYDMET Model Results .....	114

## List of Figures

Figure 1.	Landslides at Jølster on July 30, 2019, Slåtten (left), Årnes (right) (photo credit: NGU).....	3
Figure 2.	Report Structure .....	6
Figure 3.	Warning regions of the Norwegian Landslide Early Warning System, figure made using NVE data (NVE, 2020c) .....	9
Figure 4.	Mean annual precipitation in Norway (reference period 1971-2000), figure reprinted from (Meteorologisk institutt, 2020a).....	10
Figure 5.	Normalized water supply intensity thresholds plotted on log-log axes, figure reprinted from (Meyer, Dyrddal, Frauenfelder, Etzelmuller, & Nadim, 2012).....	11
Figure 6.	Landslide warning based on relative degree of soil water saturation thresholds, figure reprinted from (Krøgli, et al., 2018) .....	12
Figure 7.	Communication sequence of the NLEWS , figure reprinted from (Krøgli, et al., 2018).....	14
Figure 8.	Spectral response from different vegetation surfaces, figure reprinted from (Clark, 1999) .....	17
Figure 9.	Catchment level susceptibility map of Norway, figure made using NVE data (NVE, 2020a).....	23
Figure 10.	Quaternary geology map of Norway, figure made using NVE data (NVE, 2020c) .....	24
Figure 11.	Map of selected case studies in Norway.....	29
Figure 12.	Map of international test sites.....	30
Figure 13.	Comparison of A: Sentinel-2 natural colour image and Sentinel-1 SAR with registered landslides identified with white points and detectable landslides identified with white arrows on B: intensity, C: phase, and D: coherence interferograms (case 19, July 30, 2019, Sogn og Fjordane) .....	32
Figure 14.	A: Optical image and B: SAR intensity of a debris flow with an approximate area of 0.06 km <sup>2</sup> (case 19, July 30, 2019, Sogn og Fjordane) .....	33
Figure 15.	Sentinel-2 $\delta$ NDVI landslide detection success for various conditions as a percentage of landslides per category with the absolute number in brackets as (landslides detected/total landslides in category) .....	36
Figure 16.	Comparison of satellite image with A: natural colours, B: false colour infra-red, C: $\delta$ NDVI, and D: $\delta$ NDVI with landslides mapped in case 19 (July 30, 2019, Sogn og Fjordane) .....	37
Figure 17.	Processes and objects causing a significant change in NDVI obstructing landslide detection: A: agricultural crops (case 10, July 24, 2017, Oppland). B: snow melt (case 15, April 18, 2018, Oppland). C	

elongated lakes and rivers (case 16, September 26, 2018, Hordaland). D: clouds (case 19, July 30, 2019, Sogn og Fjordane) .....	38
Figure 18. Norwegian cloud cover presented as mean annual frequency, ranging from 60-90% (left) and seasonality, slightly weighted to May through August (right), figure adapted from (Wilsom & Jetz, 2016). .....	40
Figure 19. Detectable landslide, knowing its location, marked by the white arrow, using SAR intensity, at site D (October 15, 2016, Longyearbyen, Svalbard) .....	42
Figure 20. $\delta$ NDVI images with mapped landslides at Site A (December 4, 2019, Nyempundu, Burundi)..	43
Figure 21. $\delta$ NDVI images with mapped landslides at Site B (August 17, 2019, Wenchuan, China) .....	43
Figure 22. $\delta$ NDVI images with mapped landslides at Site C (March 3, 2020, Baixada Santista, Brazil).....	44
Figure 23. $\delta$ NDVI images with mapped landslides at Site D (October 15, 2016, Longyearbyen, Svalbard)	44
Figure 24. Comparison of false colour infra-red before and after, and $\delta$ NDVI change detection, with arrows pointing to a large landslide scar from a previous event (Site A, December 4, 2019, Nyempundu, Burundi) .....	45
Figure 25. Comparison of $\delta$ NDVI SAR mapped landslide(in white) on natural colour optical image(left), $\delta$ NDVI (centre), and SAR intensity (right) in case 19 .....	46
Figure 26. Road map with landslides registered in NVE landslide database in case 2 (November 26, 2015, Sogn og Fjordane) (road data downloaded from kartkatalog.geonorge.no (Kartverket, 2016)) .....	48
Figure 27. Distance of registered and $\delta$ NDVI mapped landslides from road centreline .....	48
Figure 28. Seasonal distribution of landslides registered in the NVE landslide database from 2000-2019 .....	50
Figure 29. Spatial distribution of selected case studies, identified by season .....	51
Figure 30. Histogram of landslides recorded and mapped in the catchment level landslide susceptibility classes .....	52
Figure 31. Debris flow initiation zone with quaternary geology mapped as bare bedrock at a scale of 1:250,000 (case 19, July 30, 2019, Sogn og Fjordane) (Photo credit: Lena Rubensdotter, NGU) .....	53
Figure 32. Large- and small-scales quaternary geology map intersections with registered and $\delta$ NDVI mapped landslides .....	53
Figure 33. Mean annual precipitation at weather station for all years on record (left) and 24-hour water supply at weather station from rain gauge and snowmelt model (right) .....	55
Figure 34. Normalized 24-hr initiation water supply from A: weather station rain gauge and modelled snowmelt B: mean seNorge v2.0 and C: maximum seNorge v2.0 .....	59
Figure 35. HYDMET Model results for case 2 (November 26, 2015, Sogn og Fjordane) where maximum hazard level is orange and the modal hazard level is yellow.....	65
Figure 36. Landslide warnings from model results, published results, and corrections based on NVE and number of landslides .....	67
Figure 37. Corrected hazard levels based on NVE evaluation, reported landslides, and average water supply as a percent of annual average precipitation.....	68

## List of Tables

Table 1. Awareness level for flood and landslide forecasting and warning colour legend (NVE, 2019a) ....	8
Table 2. Summary of landslide initiation water supply thresholds in Norway by various authors .....	11
Table 3. Norwegian landslide database classification system (NVE, 2018) .....	15

Table 4. Quantitative thresholds for landslide warning hazard levels .....	27
Table 5. Norwegian multiple landslide event case studies .....	28
Table 6. International $\delta$ NDVI landslide mapping test sites.....	30
Table 7. Sentinel-1 SAR landslide mapping results for Norwegian case studies .....	31
Table 8. Sentinel-1 SAR change detection landslide mapping results by landslide type(Y = mappable, M = mappable if location is known, N = not detected, Y/M = detectable).....	34
Table 9. Sentinel-2 $\delta$ NDVI landslide mapping results for Norwegian case studies .....	35
Table 10. Landslides mapped with $\delta$ NDVI method, by area.....	37
Table 11. Sentinel-2 $\delta$ NDVI change detection landslide mapping results by landslide type (Y = mappable, M = mappable if location is known, N = not detected, Y/M = detectable).....	39
Table 12. Sentinel-2 $\delta$ NDVI change detection landslide mapping results by landslide type (Y = mappable, M = mappable if location is known, N = not detected, Y/M = detectable).....	41
Table 13. Climate, geography, and vegetation of international test sites.....	41
Table 14. Number of landslides mapped and Sentinel-2 $\delta$ NDVI challenges for international test sites....	42
Table 15. Landslide types in Norwegian case studies.....	49
Table 16. Precipitation during event (1-, 3-, 24-hr) and mean annual precipitation from rain gauges (Meteorologisk institutt, 2020b).....	54
Table 17. seNorge v2.0 24-hr precipitation and equivalent snowmelt maximum and mean of grid over case study area data from (NVE, 2020a) .....	56
Table 18. Weather and hydrological factors recorded for Norwegian case studies from a selected case study landslide on xgeo.no relative to reference years 1981-2010 .....	57
Table 19. Normalized 24-hr Water Supply from weather stations points and mean and maximum seNorge v2.0 areas.....	58
Table 20. Return period of rainfall and snowmelt of case studies .....	61
Table 21. Weather categorization and storm name for Norwegian case studies .....	62
Table 22. HYDMET Model Results (data from xgeo.no).....	64
Table 23. Percentage of days with landslide hazard levels warned in 2013-2019, data from (NVE, 2020a) .....	65
Table 24. Published landslide warnings by NVE for Norwegian case studies (data from www.varsom.no) .....	66
Table 25. Details of selected case studies that were under-warned according to NVE post-event evaluations.....	68
Table 26. Proposed area water supply thresholds using seNorge v2.0.....	69
Table 27. Hazard level based on proposed area thresholds.....	70

## List of Equations

Equation 2-1. Normalized difference vegetation index (NDVI) (CCMEO, 2013).....	17
Equation 3-1. Equation for $\delta$ NDVI using band maths operator in SNAP 7.0 software .....	20
Equation 3-2. Normalized water supply for landslide initiation .....	25
Equation 3-3. Return period of a given water supply .....	25

## Abbreviations

Bane NOR	Norwegian Rail Administration
CIM	Crisis Information Management
DEM	Digital elevation model
EWS	Early Warning System
GAM	Generalized Additive Model
hrs	Hours
IDF	Intensity-Duration-Frequency
DInSAR	Interferometric Synthetic Aperture Radar
km	Kilometres
LEWS	Landslide Early Warning System
m	metres
MAP	Mean Annual Precipitation
masl	Metres above sea level
MET	Norwegian Meteorological Institute
MSI	Multi-spectral instrument
NDVI	Normalized Difference Vegetation Index
NGI	Norwegian Geotechnical Institute
NGU	Norwegian Geological Survey
NIR	Near infrared range
NLEWS	Norwegian Landslide Early Warning System
NPRA	Norwegian Public Road Administration
NTNU	Norwegian University of Science and Technology
NVE	Norwegian Water Resources and Energy Directorate
PDN	Precipitation Day Normal
RCP	Representative Concentration Pathway
SAR	Synthetic Aperture Radar
SVG	SynopVis Grosswetterlagen (SVG)
SWIR	Short wave infrared spectral range
UNISDR	United Nations International Strategy for Disaster Risk Reduction
VIR	Visual Red wavelengths
yrs	Years
$\delta$ NDVI	Difference in Normalized Difference Vegetation Index

# 1 Introduction

Landslides are a natural hazard, present on earth for all of history, and ubiquitous in steep terrain. While they are common hazards, found throughout the solar system on Mars (Lucchitta, 1979), Mercury, and the Moon (Brunetti et al., 2015), they only cause disasters on earth where vulnerable people and man-made infrastructure are in their path (Kelman, 2020). Landslides worldwide annually incur losses of hundreds of millions in damages (Clague & Stead, 2012) and thousands of fatalities (Foude & Petley, 2018). From 2004 through 2016, at least 55,997 people were killed by landslides worldwide (Foude & Petley, 2018). An analysis of recorded fatal landslides around the world hypothesizes that there has been an increase in landslides associated to extreme rainfall and population distribution in the past two decades (Haque, et al., 2019).

In Norway, landslide incidents are frequent and widespread due to steep mountainous terrain and high precipitation. Over the past 150 years, it is estimated that there have been 125 landslide related fatalities in Norway (Colleuille, et al., 2017). 25 of these deaths occurred from 1995-2014, 12 of which were snowmelt and rainfall induced landslides (5 debris flows and 7 slushflows) (Haque, et al., 2017). Due to climatic changes increasing the frequency and severity of precipitation and increasing the proportion of precipitation falling as rain rather than snow, consequences from landslides are expected to increase unless properly managed (Jaedicke, et al., 2008), (Hannsen-Bauer, et al., 2017).

Early warning systems (EWS), alongside a well-informed population, can drastically reduce vulnerability to landslides, letting natural processes take place but avoiding disasters (Kelman, 2020). The Norwegian landslide early warning system (NLEWS) has been operational since 2013 with its main goal being the reduction of economic and human losses caused by landslides (Krøgli, et al., 2018).

This research is a part of KLIMA 2050, an initiative funded by the Research Council of Norway and consortium partners intending to reduce societal risks associated with climate change within the built environment. As part of the KLIMA 2050 program, research is being carried out on Early Warning Systems for landslides induced by heavy rainfall.

## 1.1 Landslide Early Warning Systems

The United Nations International Strategy for Disaster Risk Reduction (UNISDR) defines early warnings systems as, “the set of capacities needed to generate and disseminate timely and meaningful warning information to enable individuals, communities and organizations threatened by a hazard to prepare and to act appropriately and in sufficient time to reduce the possibility of harm or loss” (UNISDR, 2009). The UNISDR emphasizes the four key elements of the system are: knowledge of the risks, forecasting, communication, and response.

When other mitigation solutions are not feasible, Landslide Early Warning Systems (LEWS) are becoming an increasingly common tool used as a cost-effective solution to reducing exposure to extreme events (Calvello, 2017). Warning systems can, if executed well, decrease vulnerability and educate citizens about the natural hazards they live near (Kelman, 2020). They are used on both local scales (a single slope) and regional scales (ranging from a basin to an entire nation) (Calvello & Piciullo, 2016). Regional LEWS are sometimes referred to in literature as a territorial LEWS (Piciullo, et al., 2018). LEWS have three main categories, alarm, warning, and forecasting (Calvello, 2017). In a recent study of 26 territorial LEWS, Guzzetti et al., describes landslide forecasting as “a difficult and uncertain task that lays at the fuzzy boundary between science, technology, and decision making”, pointing out that the success of

forecasting landslides is not only dependant on quality and quantity of data, but also largely dependant on experience and judgement (Guzzetti, et al., 2019).

### 1.1.1 Thresholds

A threshold is defined as a quantitative condition, expressed in terms of a mathematical law, that when exceeded results in a change of state of a system (White, et al., 1996). LEWS are designed under the assumption that landslides are predictable, given correct data of past landslides is collected (Meyer, et al., 2012). Thresholds indicating the likelihood of a landslide, can thus be statistically derived using known past events. To create a threshold a dataset must include: a period of analysis, source of landslide data, landslide number and type, source of rainfall, rainfall timescale, and spatial density of rainfall measurements (Segoni, et al., 2018). The most common threshold parameters include (Segoni, et al., 2018):

- intensity-duration (ID): peak, mean, and combinations of intensity
- antecedent rainfall: 30-day, 15-day, 3-day, 1-day, and degree of saturation
- total rainfall during an event: defined, often, with limits of 48-hour and 96-hour dry periods

Among many variables (e.g. snowmelt, Jökulhlaup, seismicity, volcanic activity, wind), rainfall is the main trigger of landslides worldwide (Guzzetti, et al., 2007). Rainfall thresholds were first introduced in literature by (Endo, 1969), further developed by (Caine, 1980), and have since been thoroughly researched and documented, including a review of international literature by (Guzzetti, et al., 2007), (Guzzetti, et al., 2008), and more recently by (Segoni, et al., 2018). Such studies conclude that the most crucial inputs of rainfall thresholds are the landslide database and the rainfall data. Often, the validation process is not completed due to the low number of inventoried landslides (Segoni, et al., 2018). Improvements to landslide databases are therefore of utmost importance to the improvement of initiation thresholds.

### 1.1.2 Landslide Inventories

Landslide risk assessments and LEWS thresholds inherit the quality of the database they are created from (Foude & Petley, 2018), (Segoni, et al., 2018). A high-quality landslide database is essential in producing susceptibility maps, rainfall thresholds, hazard maps, and to validate new landslide mapping methods. Landslide inventories are also essential in quantifying the performance of a LEWS (Piciullo, et al., 2017). Landslide mapping is still commonly performed using first-hand accounts, media reports, and aerial photographs, but developments over recent decades have increased the use of remote sensing in creating landslide inventories (Fiorucci, et al., 2019).

### 1.1.3 Extreme Landslide Events

Landslides can be labelled “extreme” for many reasons, including size, consequences, and number of landslides. Herein, extreme refers to the number landslides that occur due to a common trigger. Extreme landslide events are defined, in this study, as those days with more than ten soil landslides recorded in the NVE database, with at least five within 40 km radially of one another. The landslides selected are classified in the database as shallow soil landslides, including debris flows, debris floods, debris avalanches, soil slides, unspecified landslides in soils, and slushflows. Slushflows are included, despite being a type of snow avalanche, to test if they can be detected using the studied satellite mapping methods.

An individual landslide can have enormous consequences, and there is no shortage of examples to prove this point (e.g. Huascarán Debris Fall, Peru, 1962, destroyed a town and killed 4,500 people). The large majority of deadliest landslide events in history are, however, a series of multiple landslides with the same trigger (Oishimaya, 2017). Landslides are frequently induced by regional phenomena, such as earthquakes and rainstorms, resulting in regional consequences; loss of power and communication infrastructure, isolation from blocked or destroyed transportation routes, and insufficient emergency response resources turn even small isolated landslides into catastrophes.

On July 30<sup>th</sup>, 2019, dozens of landslides were triggered in Jølster, Norway, by intense heavy rainfall exceeding the magnitude 200-year 24-hour precipitation event (NVE, 2019b). The landslides resulted in damage to infrastructure, private property and one fatality of a man whose car was swept into the lake. Five large debris flows (10-25,000 m<sup>3</sup>) and at least 40 smaller debris flows/floods occurred, and although each were devastating, the scale of the consequences of this event are due to the sequence of events and the sheer number of landslides that occurred. Figure 1 includes photographs of two of these large debris flows.



*Figure 1. Landslides at Jølster on July 30, 2019, Slåtten (left), Årnes (right) (photo credit: NGU)*

Three large landslides ravaged the slopes of Slåtten at 15:00 (left in Figure 1) sending emergency response to the region. Three hours later, the main town had a large debris flow and many slides on the north side of the lake washed out two bridges and cut off road access, trapping vehicles, including an ambulance, overnight and eventually requiring boat evacuation (NTB, 2019). With communication lines down, and only satellite phones, road authorities, opened the re-opened road on the south side of the lake to evacuate the area (Torheim, 2019). At 21:00 a debris flow washed a car into the lake on the south side of the lake, taking the life of one man (Rubensdotter, 2019). This fatal decision was the product of a complex series of events, each exacerbating the crisis.

Jølster is one of several case studies of extreme landslide events in Norway that are investigated in this report. Only a level yellow warning was given, in what should have been an orange or red hazard level, revealing that such events are challenging to forecast (NVE, 2020a). Previous studies demonstrated that

the number of landslides was drastically under-reported, highlighting the need for systematic landslide mapping to build a complete inventory used to improve tools for landslide forecasting (Rouault, et al., 2020). The landslide event in Jølster is the canary in the coal mine (i.e. the early warning) of the potential of devastating and the challenges in forecasting landslides in changing climate.

## 1.2 Research Problem

Extreme multiple landslide events in populated areas cause widespread effects and damage. These events have the ability to isolate communities and overwhelm emergency response efforts by blocking transportation arteries in landslide prone areas of Norway. Due to the scale of potential destruction and capacity to devastate an area, events with numerous landslides require more research.

While rare, such events are challenging to forecast, and often go under-warned in Norway (Devoli, 2019). Landslide early warning systems rely on historical landslide inventories to reliably forecast future events. Unfortunately, the Norwegian landslide database is spatially biased toward transport routes, limiting the success of the warning system. More knowledge of extreme multiple landslide events in Norway is needed, to help landslide forecasters give more reliable warnings for these low frequency, high consequence events. Using case studies of recent multiple landslide events in Norway, the following research questions will be answered:

1. In what conditions can landslide inventories be improved with the use of two remote sensing change detection techniques? An optical method ( $\delta$ NDVI) and a synthetic aperture radar method (SAR), using Sentinel-2 and Sentinel-1 satellite imagery, respectively, are tested to determine their limitations and opportunities. What are the limitations of the current landslide database and can the proposed methods address these limitations?
2. When and where are extreme multiple landslide events recorded in Norway in the past five years? How do forecasting tools, including HYDMET threshold model, susceptibility maps, geology maps, and weather, rain gauge and snow melt, correlate with selected cases? Are these landslide events warned at the appropriate level? Which events are most challenging to forecast?

## 1.3 Limitations

There are many high consequence landslides in Norway. While it only takes a single landslide to destroy an entire community, multiple landslides in a small area are of interest due to the frequency they occur in Norway, their complex consequences, and that they are generally understated. This report is limited to landslides under a strict limitation of soil slides and flows, registered in the NVE landslide database, categorized as 140, 142, 144, and 133: unspecified landslides in soils, debris flows/floods/avalanches, soil slides, and slushflows, respectively. Selected cases occur on a day with at least ten landslides in Norway, five of which occurred within a 40 km radius of each other. The landslides that occurred on the same date are collectively named an extreme landslide event, herein.

The communication of warnings is not addressed, despite being essential, if not the most critical piece of any warning system. Additional research is needed in this field to improve the effectiveness of landslide warning systems.

Landslide triggers are complex, and ultimately require in-depth geotechnical field investigations to fully explain. In the absence of such investigations, the most important weather indicators reported in literature of shallow soil landslides triggers in Norway were investigated to assess their correlation. This



is not to undermine the importance of geotechnical soil properties, frost, groundwater, de-forestry, construction, or any other factor that may lead to landslides in Norway.

Finally, the remote sensing methods considered are two of many techniques available. They are intended to test and compare possibilities of optical and radar satellite mapping techniques that could be implemented nearly anywhere in the world on a small budget. They are simple to conduct and utilize free ESA Copernicus software and satellite imagery. Other than those registered in the NVE database and many of those investigated at Jølster (case 19), the landslides mapped using remote sensing methods are not confirmed in the field in this work.

#### 1.4 Contributions

These research questions were developed with the four advisors and built off the investigative work completed by the author with Erin Lindsay in autumn 2019 for a specialization project on the debris flows in Jølster, Norway (Rouault, et al., 2020).

A literature review was completed independently by the author, the results of which are written in Section 2 – Background. Techniques for literature review and literature sources were provided by the four advisors.

All data was collected and downloaded by the author, with permission as cited, including all satellite images (ESA, 2020c), GIS files (geology (NGU, 2019), roads, bodies of water (NGU, 2019), NVE landslide database (NVE, 2020c), digital elevation model (NGU, 2019), cloud cover (Wilson & Jetz, 2016)), landslide warnings (NVE, 2020b), HYDMET model results (NVE, 2020c), rain gauge data (Meteorologisk institutt, 2020b), intensity-duration-frequency (IDF) curves (Meteorologisk institutt, 2020a). Data provided by NVE includes the catchment level susceptibility maps (.shp), seNorge v2.0 rainfall and snowmelt (.csv), and daily evaluation of landslide warning assessments (.pdf) (NVE, 2020a).

The analyses the author personally completed are the following:

- Landslide database statistical analysis: downloaded NVE landslide database, with the programming language Python, and performed a statistical analysis to determine the temporal and spatial trends of shallow soil landslides. These results were used to choose the Norwegian case studies. Additionally, the four international test sites were chosen by researching interesting landslide cases with varied conditions on the Landslide Blog (Petley D., 2020a).
- Remote sensing landslide mapping: The selection of the satellite mapping techniques drew upon the master's thesis written by Mads Fjeld in 2018 (Fjeld, 2018). The author was taught the  $\delta$ NDVI method by Erin Lindsay and the SAR method in a RUS Copernicus seminar. Both methods were completed on all cases (Norwegian and International) entirely by the author, using SNAP 7.0 (ESA, 2020e) and ArcGIS (ESRI, 2019).
- Forecasting tools: completed a statistical analysis of the catchment level susceptibility map from NVE (NVE, 2020a) and quaternary geology maps from NGU (NGU, 2019) using ArcGIS and Python code.
- Weather analyses: calculated mean annual precipitation, absolute 1, 3, 12, 24-hour, 1 and 3-day antecedent precipitation values and normalized water supply for each event and plotted each in ArcGIS. The absolute water supply was plotted on IDF curves to determine return periods and, finally, categorized the events based on my own description of the weather.

- Landslide warning evaluations: completed a visual interpretation of the HYDMET model results from xgeo.no and calculated the number of warnings of each warning level from 2015-2019. The NVE evaluations were compared for each Norwegian case study with two quantitative evaluations defined in work by others.

All climate change projections and conclusions regarding landslides are the work of others, which are have included to highlight their importance in LEWS.

All maps, figures and tables, and appendices are self-made, in ArcGIS and Microsoft Excel, unless explicitly stated otherwise. All code is included in Appendix A. This report was written entirely the author, with comments and guidance from advisors.

### 1.5 Structure

This report takes the reader through an introduction of LEWS, the motivation for research, and the research problem. It then delves into background and literature review of the NLEWS, the NVE landslide database, and the remote sensing techniques that are tested for mapping landslides in Norway. An investigation of extreme multiple landslide events in Norway is conducted, with the methods used, followed by results and discussion. International test sites are included only to test the limitations of the mapping techniques. Figure 2 illustrates the structure of this study.

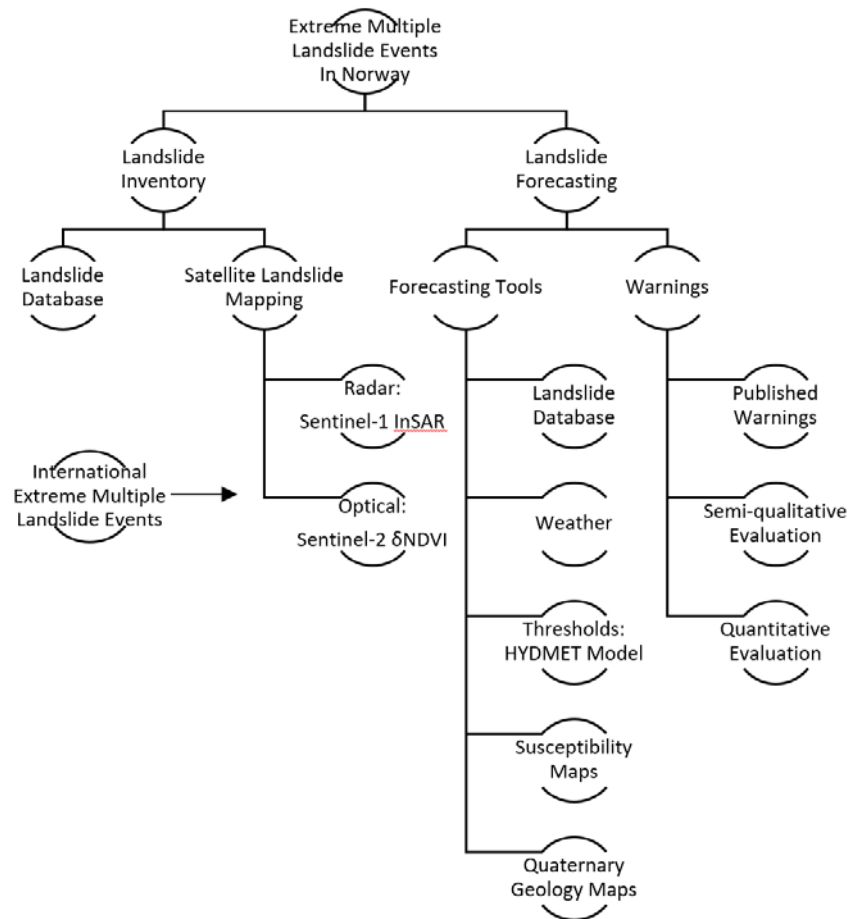


Figure 2. Report Structure

## 2 Background

### 2.1 Norwegian Landslide Early Warning System

The Norwegian Landslide Early Warning System (NLEWS) is a territorial LEWS. It was developed starting in 2010 and became operational in 2013 as a joint initiative of Norwegian Water Resources and Energy Directorate (NVE), Norwegian Meteorological Institute (MET), the Norwegian Public Road Administration (NPRA), and the Norwegian Rail Administration (Bane NOR). (Krøgli, et al., 2018). It is run in conjunction with the flood and avalanche warning systems and is operated by NVE and MET (NVE, 2020d) who collaborate in daily meetings to ensure clear and consistent communication across their platforms (Devoli, 2019).

The NLEWS was originally developed to alert the road and rail authorities so that they could allocate appropriate emergency responses. Although it is publicly available, it continues to be designed for decision making authorities. Surveys to users were conducted in 2009, 2016, and 2019 (Colleuille & Engen, 2020). Respondents include emergency responders, municipalities, and infrastructure owners. In the 2019 survey one third of the respondents were members of the general public. The survey results show that most users find the service to be “useful or very useful” and have “quite or very much confidence with the warning notifications” (Colleuille & Engen, 2020). Members of the general public had the lowest opinion of the NLEWS and emergency responders in the transport sector had the highest.





Four areas of improvement were suggested by Krøgli et al. (2018) to increase accuracy, precision, and usefulness of the Norwegian LEWS: hazard assessment, weather forecasts and hydrological models, better verification of landslide events, and increased communication and build the user’s capacity.

It is proposed that the third suggestion, verification of landslide events, can be drastically improved with a relatively low cost and effort with the use of remote sensing techniques. While eyewitness accounts and field investigations cannot be replaced, the landslide inventory can be augmented using remote sensing mapping, especially in those more remote locations where landslides might otherwise go unnoticed.

#### 2.1.1 Warning Levels

The NLEWS has four hazard levels that relate roughly to the number of landslides anticipated in one day within an area of 10,000 – 15,000 km<sup>2</sup> (Piciullo, et al., 2017). The warning levels used in the NLEWS and their respective description and consequences are included in Table 1. The colour coded warning is delivered alongside a description and suggested precautions in order to give the public and administration as much information as possible. There is no estimate of uncertainty associated with the warning. Adding an uncertainty estimate could both make the warning more difficult to understand due to complexity and be more explicit and clearer due to the transparency of the warning.

Table 1. Awareness level for flood and landslide forecasting and warning colour legend (NVE, 2019a)

Warning Colour	Description	Flood Return Period	Consequences
<b>Green</b> 	Generally safe conditions.	<2 Yr	<ul style="list-style-type: none"> <li>• No consequences</li> <li>• Very few, small landslides caused by local rain showers</li> </ul>
<b>Yellow</b> 	Situation that requires vigilance and may cause local damages. Moderate landslide hazard.	2-5 Yr	<ul style="list-style-type: none"> <li>• Expected some landslide events, certain large events may occur. <ul style="list-style-type: none"> <li>• Local flooding and/or erosional damage due to rapid increase of discharge in streams/ small rivers, ice drift, ice in streams/rivers and frozen soil.</li> </ul> </li> <li>• High flow/water level in comparison to normal seasonal variations.</li> </ul>
<b>Orange</b> 	Severe situation that occurs rarely, requires contingency preparedness and may cause severe damages. High landslide hazard.	>5 Yr	<ul style="list-style-type: none"> <li>• Expected many landslide events, some with considerable consequences.</li> <li>• Extensive flooding, erosional damage and flood damage to certain prone areas.</li> </ul>
<b>Red</b> 	Extreme situation that occurs very rarely, requires immediate attention and may cause severe damages. Very high landslide hazard.	>50 Yr	<ul style="list-style-type: none"> <li>• Expected many landslide events, several with considerable consequences.</li> <li>• Extensive flooding, erosional damage and flood damage to buildings and infrastructure.</li> </ul>

Landslide warnings are given for regions of varying area. In many cases, uncertainty in the weather forecast merits a warning for a very large area, causing large disruptions and use of resources. Additionally, weather systems do not align with municipal boundaries as the warnings do (Piciullo, et al., 2017). The subdivisions that make up the smallest areas for a landslide warning were downloaded from NVE ([www.atlas.nve.no](http://www.atlas.nve.no)) and are illustrated in Figure 3.

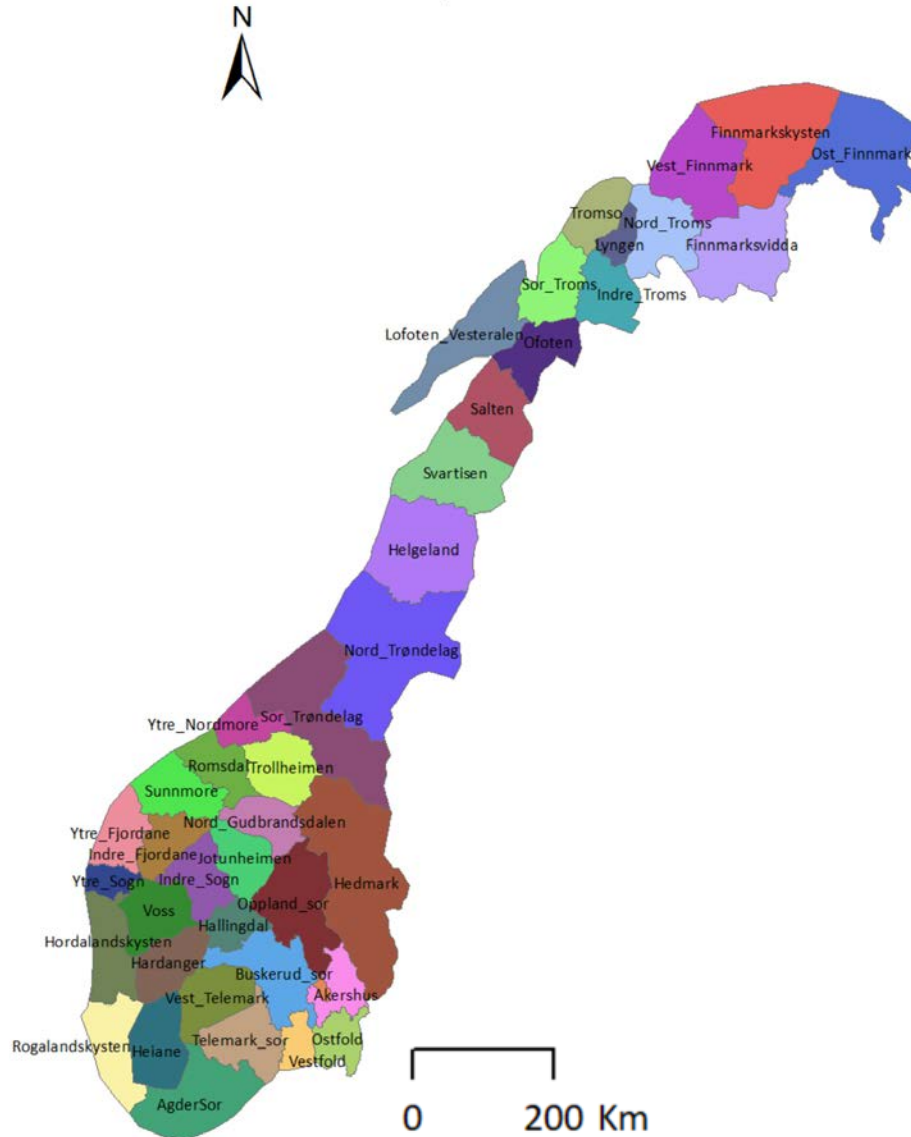


Figure 3. Warning regions of the Norwegian Landslide Early Warning System, figure made using NVE data (NVE, 2020c)

### 2.1.2 Weather Conditions

Debris flows in Norway are most commonly triggered by rapid snowmelt and intense rainfall (Nadim, et al., 2009). One study considered 41 meteorological elements found that soil landslides in Norway have the strongest correlation to precipitation, both short and intensive (<1 day) and rain accumulation up to 15 days, and snowmelt (Jaedicke, et al., 2008). These triggers lead to high soil saturation, high pore water pressures, low effective shear strength, and surface erosion. Another study found the strongest correlation to shallow soil landslides is 24-hour precipitation (Devoli, et al., 2017).

The largest rainfall events occur in late autumn and early winter, while the heaviest rainfall events occur in late summer and early autumn (Devoli, et al., 2017). There are three main types of rainfall, which can all induce landslides. A description of each follows (S-Cool, 2020):

- Frontal – when two air masses of different temperatures meet, the warmer less dense air rises over the colder one, it cools as it rises and condensates, producing moderate to heavy rainfall and various clouds
- Convective – the earth is heated by the sun, as the air rises it cools and condensates, producing heavy rainfall, cumulonimbus clouds, and often thunderstorms. Common in late summer and autumn
- Relief – prevailing winds pick up moisture from the sea, the moist air rises, cools and condenses due to orographic lifting when it hits the mountainous coast. In Norway will cause higher precipitation on the west facing slopes and is common along the coast.

Precipitation ranges widely across Norway, from less than 300 mm to greater than 4000 mm per year in Norway (see Figure 4). Snow cover ranges from zero days, in some locations along the west coast, up to 200 days, inland and above 800 masl.

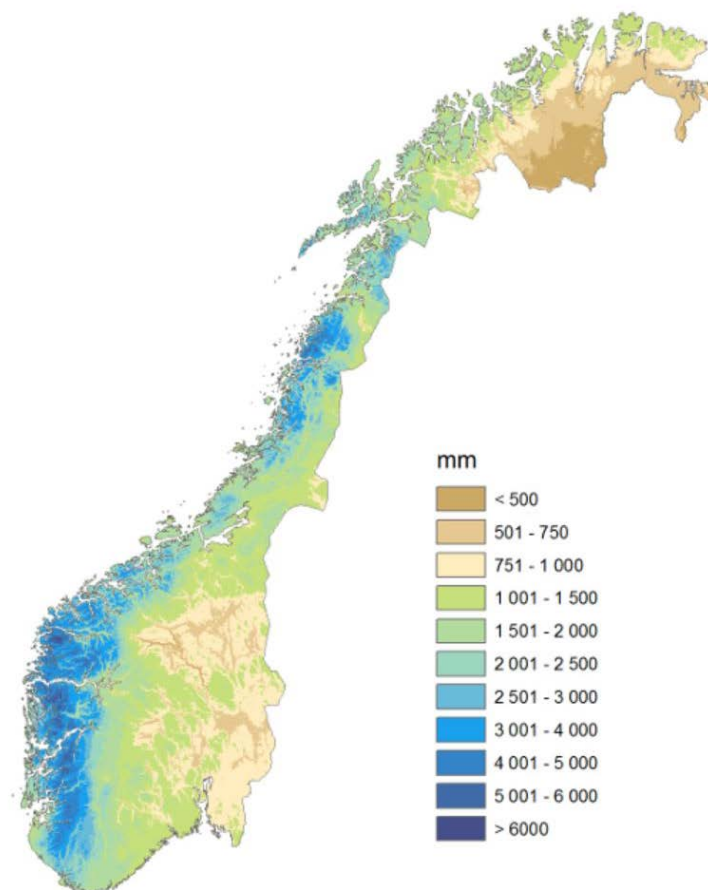


Figure 4. Mean annual precipitation in Norway (reference period 1971-2000), figure reprinted from (Meteorologisk institutt, 2020a)

A study was conducted to correlate large-scale synoptic weather types and landslides in southern Norway. Using the SynopVis Grosswetterlagen (SVG) classification, anticyclonic westerly (SVG 1) and anticyclonic southwesterly (SVG 5) are the weather classes that induce landslides most often (Devoli, et al., 2017). Zonal ridge across central Europe (SVG 10) has the highest predictive probability of weather-induced landslides, with 90% of such weather systems inducing landslides. Landslides in Western Norway have the highest correlation with weather, and in Eastern Norway, the lowest correlation (Devoli, et al., 2017).

Ultimately, the relative water supply (rainfall and equivalent snowmelt) over a period up to 15 days can be used as an indicator of the likelihood of shallow soil landslides. Normalized values can use mean annual precipitation (MAP), precipitation day normal (PDN), calculated as MAP/average days of precipitation per year, or a relative saturation of the soil. Thresholds calculated in previous studies are summarized in Table 2. This list is not exhaustive, and rather, is intended to illustrate the variety and general range of water supply needed to initiate landslides in Norway according to a selection of previous studies.

Table 2. Summary of landslide initiation water supply thresholds in Norway by various authors

Threshold	Notes	Author
>8% [mm/day]/PDN	Relative value of debris flow initiation in Norway	(Sandersen, Bakkehøi, Hestnes, & Lied, 1996)
2.18 – 8.66% [mm/day]/PDN	Relative value of debris flow initiation in Norway	(Meyer, Dyrddal, Frauenfelder, Etzelmuller, & Nadim, 2012)
15-107 mm/day	Absolute value of debris flow initiation in Norway	(Meyer, Dyrddal, Frauenfelder, Etzelmuller, & Nadim, 2012)
20-30 mm/hr or 50-100 mm/day	Absolute value of infrastructure damage from geohazards in Europe	(Groenemeijer, et al., 2016)
17 mm/day	Absolute value of debris flows initiation in the Norangselva catchment	(Cepeda, Høeg, & Nadim, 2010)

The relative thresholds calculated by Meyer, et al., 2012 are illustrated in Figure 5.

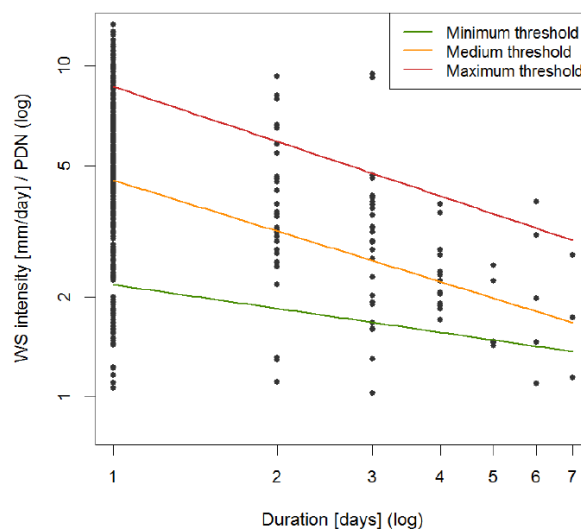


Figure 5. Normalized water supply intensity thresholds plotted on log-log axes, figure reprinted from (Meyer, Dyrddal, Frauenfelder, Etzelmuller, & Nadim, 2012)

### 2.1.3 Current Norwegian Thresholds

The Norwegian system uses minimum, medium, and maximum thresholds of relative water supply and relative groundwater conditions that are calculated based on real-time hydro-meteorological observations that inform a 1 km square grid precipitation-runoff model (Pecoraro, et al., 2019). The hydro-meteorological (HYDMET) model is used by NVE to inform landslide forecasters of a landslide index calculated from water supply (rainfall and equivalent snowmelt) and soil saturation, weighted at 0.61 and 0.39, respectively (NVE, 2020c). This value is then weighted according to susceptibility mapping. The resulting indices range from one to four, corresponding to the hazard levels of the NLEWS on a 1 km square grid.

Notably, thresholds are not only relative to normal local conditions, but vary between both different regions and different types of landslides (Krøgli, et al., 2018). Regional refinement is ongoing, including studies combining local and regional LEWS (Pecoraro, et al., 2019). Although the thresholds have been calculated from historic events, a lack of registries and errors in the landslide inventory add to the uncertainty of thresholds (Krøgli, et al., 2018). The national thresholds, used where local refinements have not been made, are illustrated in Figure 6.

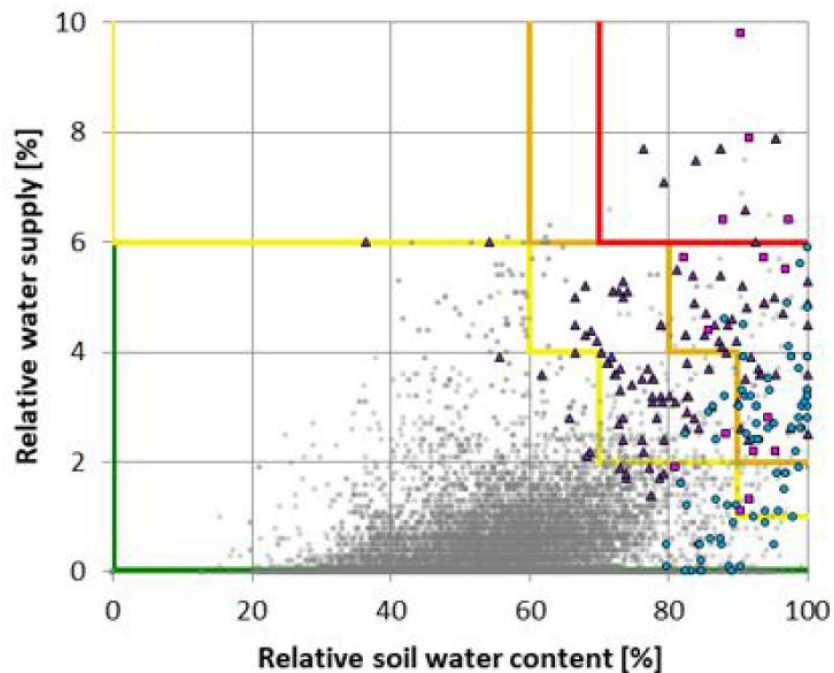


Figure 6. Landslide warning based on relative degree of soil water saturation thresholds, figure reprinted from (Krøgli, et al., 2018)

### 2.1.4 Susceptibility Maps

Landslide susceptibility maps give an indication of the likelihood of a landslide occurring in an area (Corominas, et al., 2013). These subdivisions aid in the initial phase of landslide hazard and risk assessments, landslide awareness and education, land planning, and spatial resolution of rainfall thresholds (Devoli, et al., 2019). NVE's catchment level susceptibility map of landslides in soils was created using catchment areas, historic landslide events, quaternary geology maps, land cover, rainfall, runoff properties, and slope properties derived from a 15 x 15 m DEM, in a Generalized Additive Model



(GAM). Not only was the map used directly in the development of updated landslide thresholds (HYDMET), it is used by local authorities to know where to expect landslides (Devoli, et al., 2019).

### 2.1.5 Quaternary Geology Maps

Norway has a rugged terrain, with deep fjords, and mountainous U-shaped valleys. It has been shaped by several glaciations over the past 2-3 million years, eroding and depositing glacial sediment, shifting tectonics due to loading and unloading of ice pressure (NGU, 2013). As an example, Jølster is made up of deep valleys with steep slopes that were once fjords connected to the sea. These bedrock-controlled valleys have steep slopes, climbing to elevations from 100 to 1200 masl, and a shallow soil cover on their slopes with deep lakes at their base. Soil depth increases downslope, from thin pockets in bedrock crevices, to several metres thick at the base of the slopes (NGU, 2019).

The soil cover of a slope is indicative of the likelihood, triggers, and types of landslides occurring. High risk soils include fine grained soils and colluvium. Soils with high fines content (ablation till, marine clays, moraine till), can build up higher pore water pressures resulting in lower effective shear strength when saturated. Colluvium is a product of past slope movement, revealing likely locations of future slope movement. Low risk soils include coarse grained soils and bedrock. Coarse grained soils (fluvial, glaciofluvial, marine beach) are well drained and have a higher shear strength. The presence of bare bedrock negates the possibility of a soil landslide, in the absence of soil.

### 2.1.6 Warning Communication

Warnings are published on varsom.no, yr.no, halo.met.no, twitter (@meteorologene) and to anyone who subscribes to the free email service via Crisis Information Management (CIM), a Norwegian emergency communication software system (NVE, 2020d). Users can choose to receive an SMS, email, or both, with a link to the warning bulletin (Krøgli, et al., 2018). The communication of the LEWS is designed to have redundant communication avenues, each varying in effectiveness by demographic, and in technology in the event that the internet is down and/or mobile network is down. Since 2017, warnings are published in CAP format, an international data format for emergency messages created to improve effectiveness of emergency communication around the world. As of January 2018, warnings are published in Norwegian and English (Krøgli, et al., 2018).

In the event of orange or red warning, CIM is used to inform the county's emergency personnel, MET, NPRAs traffic service, and NVE regional offices via email (NVE, 2020d). The county governor and road authorities must respond to confirm receipt of the warning and are responsible to convey the message to the municipality and road traffic centres (NVE, 2020d). Municipal emergency plans are then followed. Yellow warnings are sent to subscribers and warnings of all levels are always published on [www.varsom.no](http://www.varsom.no), with no required response. A schematic of the sequence of communication is included in Figure 7.

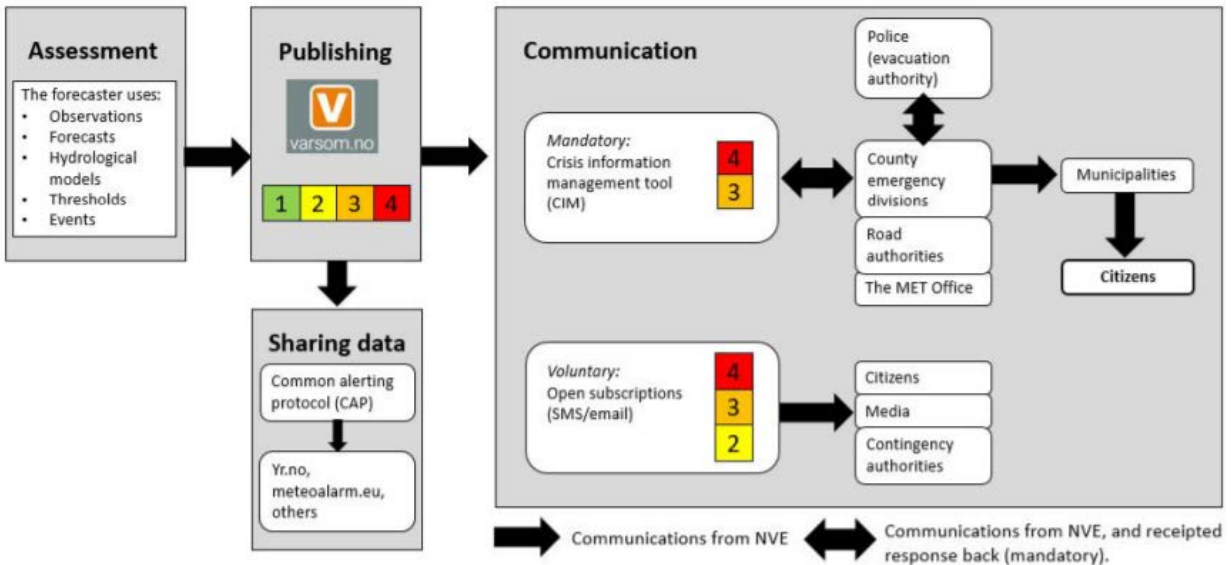


Figure 7. Communication sequence of the NLEWS , figure reprinted from (Krøgli, et al., 2018)

### 2.1.7 Performance

(Krøgli, et al., 2018) report a 96% accuracy of the Norwegian Flood and Landslide Early Warning System. When the values are disseminated to determine the accuracy by warning colour, however, it becomes evident that the system is underestimating severe storms. Considering only the challenging days, during snow melt and high rainfall (25-30% of the year), there is an 88% accuracy of warnings. This may be due to the risk tolerance of the individuals or a systematic bias of the model or decision-making process. When a red warning is delivered, there must be certainty that the storm will have severe consequences for the public. It is costly and problematic if a false red warning is released; as a result, decision makers are reluctant to deliver such a warning when there is such great uncertainty in their models. Throughout the entire duration of the Norwegian LEWS, only one red warning has been issued, in 2013.

The threshold models used by NVE have changed several times over the duration of the LEWS lifetime, making it more difficult for the forecaster to be confident in modelling results (Devoli, 2019). Furthermore, the Norwegian LEWS thresholding lacks objectivity, is highly dependent on staff training and consistency, and, hence, difficult to reproduce results (Krøgli, et al., 2018).

## 2.2 National Landslide Database

Norway has a crowdsourced and public landslide and avalanche database created in 2001 ([www.skredregistrering.no](http://www.skredregistrering.no)) and can be downloaded from NVE ([www.atlas.nve.no](http://www.atlas.nve.no)) (Jaedicke, et al., 2009). The database serves as an essential tool for future landslide prediction and is used as the basis for determination of warning thresholds for the NLEWS (Krøgli, et al., 2018).

### 2.2.1 Landslide Classification

Registered landslides are categorized into seven classifications. Table 3 translates the category code to the Norwegian terminology and the closest English translation as defined by the updated Varnes classification (Hungri, et al., 2014). The database classifications are not only broad, each including many subclassifications, classifications may also be erroneous (Krøgli, et al., 2018).

Table 3. Norwegian landslide database classification system (NVE, 2018)

Code	Norwegian Term	English Term
133	Sørpeskred	Slushflow
140	Løsmasseskred	Landslide in soils, unspecified
142	Flomskred	Debris flow/flood
144	Jordskred	Debris/soil slide/avalanche
143	Leirskred	Clay slide
111	Steinskred	Landslide in rocks
160	Utglijning	Debris/earth slump

## 2.3 Remote Sensing

Remote sensing is a common tool used to map landslides. It is powerful due to the large areas that can be surveyed, valuable in both population dense regions and in remote locations of the world that have low accessibility. Methods to identify and map landslides using synthetic aperture radar (SAR) and optical methods are becoming increasingly common with the availability of free satellite data from the European Space Agency (ESA) Copernicus Sentinel-1 and -2 missions, respectively. Two satellite mapping methods, SAR and  $\delta$ NDVI, are investigated herein.

### 2.3.1 SAR Theory

SAR mapping techniques make use of the change in SAR C-bands to detect differences in intensity, phase, and amplitude between two images, measured using two-way travel time of radar signals from a satellite. C-bands are part of the electromagnetic spectrum in the microwave range, with frequencies between 4 to 8 GHz (Peebles, 1998). C-bands are also used in Wi-Fi, microwave ovens, satellite T.V., and weather radar (USGS, 2020).

SAR techniques are well established and has proved successful in many geohazard applications including volcanoes, earthquakes, land subsidence (USGS, 2020), avalanches (Wiesmann, et al., 2002), deep-seated landslide monitoring (Riedel & Walther, 2008), and rapid shallow soil landslides around the world (Mondidi, et al., 2011). DInSAR (Interferometric Synthetic Aperture Radar) is a method of mapping ground deformations, the height and displacement of the Earth surface, to create a DEM (USGS, 2020). InSAR has been cited over the past two years, as the “most exciting advancement in landslide sciences” (Petley D. , 2020b).

Optical images are often not available directly after a landslide takes place due to the weather that induces them; for example, monsoon season causes the majority of landslides in the Himalayas, but during this season it rains nearly every day from June to September (Surendranath, et al., 2008). This makes radar techniques, such as SAR, much more attractive than optical methods, such as  $\delta$ NDVI, for applications, such as emergency response and continuous monitoring programs (e.g. landslides, earthquakes, or volcanos), that need reliable monitoring in all weather. SAR can, however, be affected by weather, but to a lesser extent than optical images (ESA, 2007).

SAR images contain pixels with intensity and phase, with which amplitude is estimated (Lopez-Martinez, et al., 2005). Intensity is the proportion of microwaves backscattered and is a function of ground roughness, soil moisture content, and the incidence angle. The higher the roughness and the higher the moisture content, the higher the intensity. However, water, or flooding, reduces intensity. In landslide mapping, intensity may increase or decrease depending on the conditions, making landslide signatures complex. Phase is a function of the optical path travelled by the radar wave and is expressed as an angle

(Closson & Milisavljevic, 2017). Coherence is an index of how well the amplitude of the master and slave images match, ranging between 0 and 1. A high coherence, is caused by a large change, such as a body of water or a landslide. An interferogram is the image produced representing the deformation between two SAR images, herein as intensity, phase, and coherence (Closson & Milisavljevic, 2017). A complete background of SAR technology and methods is included in the textbook, Bistatic Sar System and Signal Processing Technology (Wang & Yunkai, 2017) and a practical application guide is written by the ESA (ESA, 2007).

### 2.3.2 $\delta$ NDVI Theory

The Normalized Difference Vegetation Index (NDVI) is a vegetation index obtained from optical images. It was first cited in literature by (Kriegler, et al., 1969), shortly followed by (Rouse, et al., 1973) who developed the index in the Great Plains study, following the launch of Landsat-1 in 1972, to examine the vegetation spring green-up and autumn dry-down across the North American Plains. They made use of the visible/near infrared and short wave infrared spectral range (SWIR) bands of satellite images to assess regional changes. Its success as a standard index is in large due to the simplicity and swiftness of calculation. For this same reasoning, it has since been utilized for many applications including landslide inventory mapping (Nichol & Wong, 2005), landslide susceptibility mapping (Weirich & Blesius, 2007), and more recently the development of semi-automatic landslide mapping (Mondidi, et al., 2011). Despite these developments in landslide mapping, NDVI and the change of NDVI between two optical images,  $\delta$ NDVI, have often been overlooked due the limitations of cloud cover, shadows and daylight. In dark, cloudy regions, like Norway, the opportunities of optical satellite methods are, thus, unexploited.

The  $\delta$ NDVI change detection method utilizes four 10 m spatial resolution bands in the visible and visible near infra-red spectrums: B2 (490 nm), B3 (560 nm), B4 (665 nm) and B8 (842 nm) of Sentinel-2 pre- and post-event images, to visually identify areas where there has been a loss of vegetation. Each pixel of the Sentinel-2 satellite image contains the magnitude of reflectance of the earth's surface, i.e. the spectral response, making it possible to classify and differentiate between surfaces (CCMEO, 2013). Green lush vegetation has high reflectance in near-infrared wavelengths (NIR) (centered at 0.842 m) and low reflectance in visible red wavelengths (VIR) (centered at 0.665  $\mu$ m). The reflectance of different surfaces is illustrated in Figure 8.

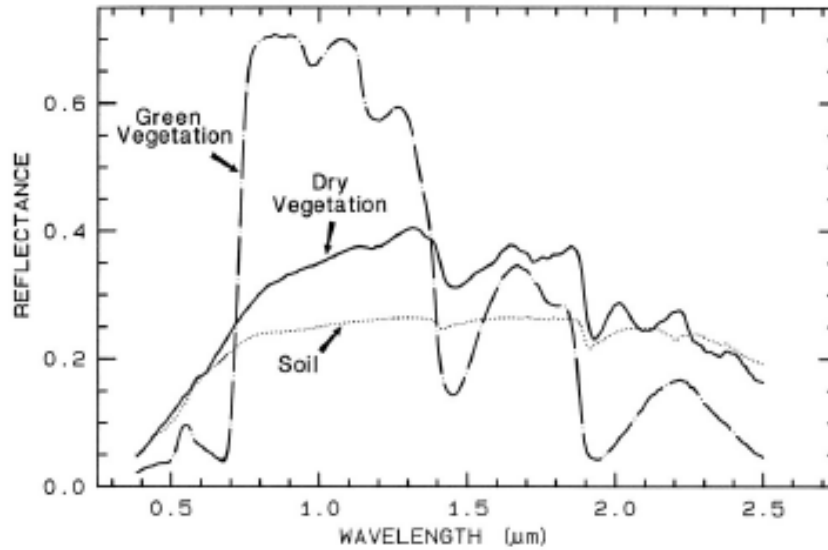


Figure 8. Spectral response from different vegetation surfaces, figure reprinted from (Clark, 1999)

The equation for NDVI, as defined by CCMEQ, 2013, is included in Equation 2-1:

Equation 2-1. Normalized difference vegetation index (NDVI) (CCMEQ, 2013)

$$NDVI = \frac{NIR - VIR}{NIR + VIR}$$

This results in a normalized value between -1.0 to +1.0 where perfectly lush green vegetation is close to +1.0. Soil or bare bedrock, which have similar NDVI values, are around 0 or slightly negative. Water and can be as low as -1.0 (CCMEQ, 2013).

For landslides that occur when no snow is present, the pre-event surface has a higher NDVI (green vegetation surface) than the post event surface (dark brown soil) (Clark, 1999). When snow is present, the change is, in theory, reversed, but often unclear due to snowmelt. In ideal conditions, the difference between the NDVI value of the pre-event imagery and the post-event imagery produces a clear signal where there has been a loss of vegetation compared to surrounding unchanged areas.

## 3 Methods

### 3.1 Case Study Selection

#### 3.1.1 Norway

The landslides studied herein were registered as unspecified landslides in soil, debris flows/floods, and soil slides (codes 140, 142, 144) in an attempt to encompass all shallow soil landslides, simply referred to in this report as landslides. Additionally, slushflows, code 133, are included in the analysis as they show similar geomorphological signatures as debris flows and there was interest in the potential of detection using the remote sensing techniques used in this study. Slushflows have similar meteorological trigger types as debris flows, however, they are a type of snow avalanche and differ from debris flows in their preconditions, initiation thresholds, and flow properties (Jaedicke, et al., 2013). High velocities, densities, and long runouts make slushflows, debris flows/floods/avalanches particularly destructive and of concern for landslide forecasters (Hestnes E. , 1998), (Dowling & Santi, 2014). Careful attention is thus paid to them in this research.

To select case studies of multiple landslide events in Norway, the NVE landslide database was filtered for days with more a combined ten or more soil landslides, codes 140, 142, 143, 144, and slushflows, 133, as classified in Section 2.2.1. Events were further filtered for those with Sentinel-1 and Sentinel-2 satellite imagery available, between July 1, 2015 and December 31, 2019. If subsequent days fit the aforementioned criteria, they were merged into one single event. Spatial limitations were used, only including an event if it has at least five registered landslides overlapping with a 20 km radius buffer around each (i.e. a group of five with no more than 40 km between each). This spatial limitation is based on the proximity of landslides in Jølster on July 30, 2019. In cases with several clusters, those achieving the most geographic variety and highest landslide concentration were chosen in order to be representative of the whole of Norway. The NVE database was downloaded from [www.nedlasting.nve.no/gis/](http://www.nedlasting.nve.no/gis/). Analysis of the NVE landslide database was completed using ArcGIS using the Python ArcPy module package (ESRI, 2020). The Python code written is included in Appendix A.

#### 3.1.2 International

In order to test the two satellite mapping methods, SAR and  $\delta$ NDVI, it is useful to consider sites outside of Norway. Landslide events, with greater than ten landslides, were selected from 'The Landslide Blog' ([www.blogs.agu.org/landslideblog/](http://www.blogs.agu.org/landslideblog/)) (Petley D. , 2020a), news articles, and scientific papers. Test sites with the following conditions, that differ from Norway, were sought:

- Slow growth and low density vegetation
- High growth and high density vegetation
- Permafrost soils
- Residual soils
- Urban environment
- Tropical climate and vegetation
- Monsoon influenced
- Slopes with frequent landslides and many scars from previous events

## 3.2 Landslide Inventory

The two specific methods were chosen to compare radar and optical change detection methods. SAR intensity and coherence change detection was chosen as it is the leading radar technique used in literature for landslide detection.  $\delta$ NDVI was chosen as it had the best results in the optical methods study in a previous NTNU master's thesis (Fjeld, 2018). His results found that change detection was superior to simply using the spectral signature of post-event images. Sentinel-1 and -2 imagery is freely available from Copernicus Open Access Hub ([www.scihub.copernicus.eu](http://www.scihub.copernicus.eu)) (ESA, 2020c) and all pre-processing of images was completed with ESA's free software, SNAP 7.0 (ESA, 2020e).

### 3.2.1 Sentinel-1

Sentinel-1 is satellite constellation made up of two SAR satellites that share the same orbital plane (ESA, 2020b). It is a part of the ESA Copernicus Programme, launched on April 3, 2014, with the intention of monitoring natural hazards. Sentinel-1 obtains C-band synthetic aperture radar images, operating day and night, and unaffected by weather. It has a repeat frequency (i.e. two images in the same orbit of the same location) of approximately 6 days, a revisit frequency (two images of the same location, regardless of orbit) of three days at the equator, decreasing to the poles. Spatial coverage is worldwide, varying temporally and in acquisition mode, but focused on Europe (ESA, 2020b).

Sentinel-1 satellite images are retrieved for pre- and post-event, as near to the date of landslide occurrence as possible. The favourable orbit is descending for eastward exposed slopes, ascending for westward facing slopes, and impartial for north and south facing slopes in order to reduce foreshortening (a shortening of features due to perspective) (ESA, 2007), but temporal proximity of satellite data to the landslide events is prioritized over acquisition mode to determine if SAR can be used for emergency purposes. SAR is limited in detecting landslides on north and south facing slopes using Sentinel-1 due to the orbit orientation; the orbit is pole to pole with the instrument antenna facing right, and thus has a poor perspective of north and south facing features.

All pre-processing was executed following the ESA tutorial (ESA, 2020a). Images are acquired in Interferometric Wide swath (IW) sensor mode with a 5x20 m spatial resolution in single look. Each contains three swaths and nine bursts, with the Terrain Observation with Progressive Scanning SAR (TOPSAR). Each burst can be processed as an independent image decreasing the size. This is the primary Sentinel-1 data acquisition mode and ensures alignment of interferometric pairs from pass to pass, essential for change detection (ESA, 2020b). The images are in Level-1 Single Look Complex (SLC) mode. They have VV-polarization, are geo-referenced with orbit and altitude and include amplitude and phase, the two main change detection parameters used for landslide detection (Mondidi, et al., 2011).

### 3.2.2 SAR Pre-Processing

With SNAP 7.0, the images are coregistered using S1 TOPS ESD Coregistration to the GETASSE30 digital elevation model (DEM) using the subswath and burst(s) of interest. Coregistration ensures that both master and slave images refer to the same pixel (ESA, 2007). GETASSE30 is a composite DEM with worldwide coverage and a 30 arc second resolution in longitude and latitude (Bouvet, 2020). Nearest neighbour interpolation with the pre-event image as the master and post-event image as the slave.

Subsequently, the coregistered image is processed to create an interferogram using the Graph Processing Tool with the following executions: TOPSAR-Deburst, topo phase removal, radar multilook (to obtain a mean square pixel near 28 by changing range looks), and Goldstein phase filtering (using 128,

higher for steeper topography). A complete guide to the processing steps is described in the ESA InSAR guidelines (ESA, 2007).

Viewing the coregistered image in RGB, with red = intensity before, green = intensity after, blue = null, the landslide should appear slightly green, meaning the pixels from the post-event image are more intense. Yellow indicates image intensity is the same before and after, and red indicates the pixels from the pre-event image are more intense.

Viewing the interferogram, the landslides should have low coherence values (dark, near zero), meaning the phase cannot be correlated between pixels of the pre- and post-event images. Phase of the landslide should appear random (like a rainbow) as phase was not able to be created, and the surrounding area should appear uniform.

Finally, a range doppler terrain correction is applied to export the intensity, phase and coherence source bands, on the original GETASSE30 DEM, as a georeferenced raster file (geotiff), for mapping in ArcGIS.

### 3.2.3 Sentinel-2

Sentinel-2 is a Copernicus Programme satellite constellation, consisting of two polar-orbiting satellites, launched on June 23, 2015 by the ESA supporting Copernicus core services: land monitoring, emergency management, security and climate change (ESA, 2020d). It is a single multi-spectral instrument (MSI) with 13 spectral channels in the visible/near infrared and short wave infrared spectral range (SWIR). Sentinel-2 has coverage around the world on all continental land surfaces from 56° south to 84° north, with a minimum a five-day combined constellation revisit frequency (ESA, 2020d).

Sentinel-2 images with a maximum of 30% cloud cover were chosen, with a minimum time before and after the landslide event date. For events that cloud-free images are not available within the same season, images with optimal vegetation conditions can alternatively be chosen, from the summer before and after, as close to the same date as possible. A maximum of one before and one after image are used in each case study, so in many cases, not all registered landslides are analyzed.

### 3.2.4 $\delta$ NVDI Pre-processing

Images are pre-processed in SNAP 7.0 with the following procedure:

1. Spatial subset: Keep only GRB and NIR bands B2, B3, B4, B8 so that all pixels are square 10 m resolution of the same area in both pre- and post-event images.
2. Collocate: collocate pixels of the images such that the post-event image is the master and the pre-event image is the slave.
3. Band maths: perform  $\delta$ NDVI calculation on the collocated image using Equation 3-1:

*Equation 3-1. Equation for  $\delta$ NDVI using band maths operator in SNAP 7.0 software*

$$\delta NDVI = \frac{B8\_M - B4\_M}{B8\_M + B4\_M} - \frac{B8\_S - B4\_S}{B8\_S + B4\_S}$$

The resulting  $\delta$ NVDI value ranges from -2 to 2 where negative values indicate a loss of vegetation.  $\delta$ NVDI is exported as a georeferenced raster file (geotiff), for mapping in ArcGIS.



### 3.2.5 Landslide Detection

#### 3.2.5.1.1 Norway

Using the  $\delta$ NVDI and SAR processed images, a search is completed for the registered landslides in the NVE database. Each registered landslide is scored to indicate the following:

- Y (yes) – detectable and mappable with high confidence, without knowing its location
- M (maybe) - detectable and mappable with low confidence, knowing its location
- N (no) - not detectable, even knowing its location
- D (duplicate) – landslide registered more than once

Landslides scored Y and M are together deemed “detectable.” For those cases that have registered landslides that are scored Y or M, an attempt is made to map landslides that occurred but were not registered in the area. The factors inhibiting landslide detection and ideal conditions are recorded. Wherever possible, a polygon is drawn to map the extent of the landslide to create an inventory of landslides not registered.

#### 3.2.5.1.2 International

Location maps, descriptions, and photos of the international extreme landslide events are used to search for landslides that are known and extending the search to those that are not known but are visible. When possible, landslides are mapped with polygons and a total number of mappable landslides is recorded for both methods, SAR and  $\delta$ NDVI.

### 3.2.6 NVE Landslide Database Limitations

Each landslide in the NVE database is assigned an assortment of metadata to record important information about the landslide. The Norwegian landslide database often has duplicate reports of the same event from several sources and can have erroneous landslide classification, trigger, and time of event (Krøgli, et al., 2018). These inconsistencies and errors make it challenging to correlate mass movement types with pre-conditions and triggers for forecasting purposes (Devoli, et al., 2017). The landslide types, uncertainty of time of occurrence, uncertainty in landslide location, the date and location of registries are all investigated for errors and limitations.

#### 3.2.6.1 Spatial Bias

Landslide registries that are known to be predominantly located along transportation routes as a consequence of the large majority of landslides being reported by the road and rail authorities. To quantify this spatial bias in the selected landslide events, the landslides registered in the NVE database from the Norwegian case studies are mapped on the network of roads downloaded from [kartkatalog.geonorge.no](http://kartkatalog.geonorge.no) (Kartverket, 2016). The proximity of landslides from the centreline of a road is recorded for all landslide registered in the NVE database.

It is possible that most landslides in Norway intersect transportation routes and that this phenomenon is not a systematic recording bias. To determine if the proximity to roads is a reporting bias or a true representation of landslides that occur in Norway, the distance of roads to the landslides in the NVE database is compared with to the distance of roads to the landslide polygons mapped using remote sensing methods. This assumes that in the best cases, the landslides mapped using remote sensing are near complete inventories of the landslides that occurred.

### 3.3 Landslide Forecasting

#### 3.3.1 Landslide Database Trends

A statistical analysis of the landslide database was completed for a better understanding of soil landslides across the country and trends by season. This analysis excludes slushflows to ensure it is not biased to events during winter. Seasons are defined by months, inclusively, as follows:

- Spring: March – May
- Summer: June – August
- Autumn: September – November
- Winter: December - February

Seasonal trends of all registered landslides and of multiple landslide events are then compared, where multiple landslide events are defined as days with ten or more landslides (codes 140, 142, 143, 144).

The spatial distribution of landslides by season is determined by mapping the Norwegian case studies to determine where they are most commonly located and if certain areas show a susceptibility to landslides in specific seasons.

#### 3.3.2 Susceptibility Mapping

The catchment level landslide susceptibility level map of Norway was provided by NVE (NVE, 2020a). These maps are used directly in the HYDMET threshold model (Devoli, et al., 2019) and by local authorities to allocate emergency response (Krøgli, et al., 2018). It is expected that the majority of landslides occur in high and very high susceptibility levels, with few events in medium and low levels. The usefulness of the susceptibility level can therefore be quantified by determining the number of landslides that occur in each level. The catchment level susceptibility map of Norway is presented in Figure 9 (NVE, 2020a).

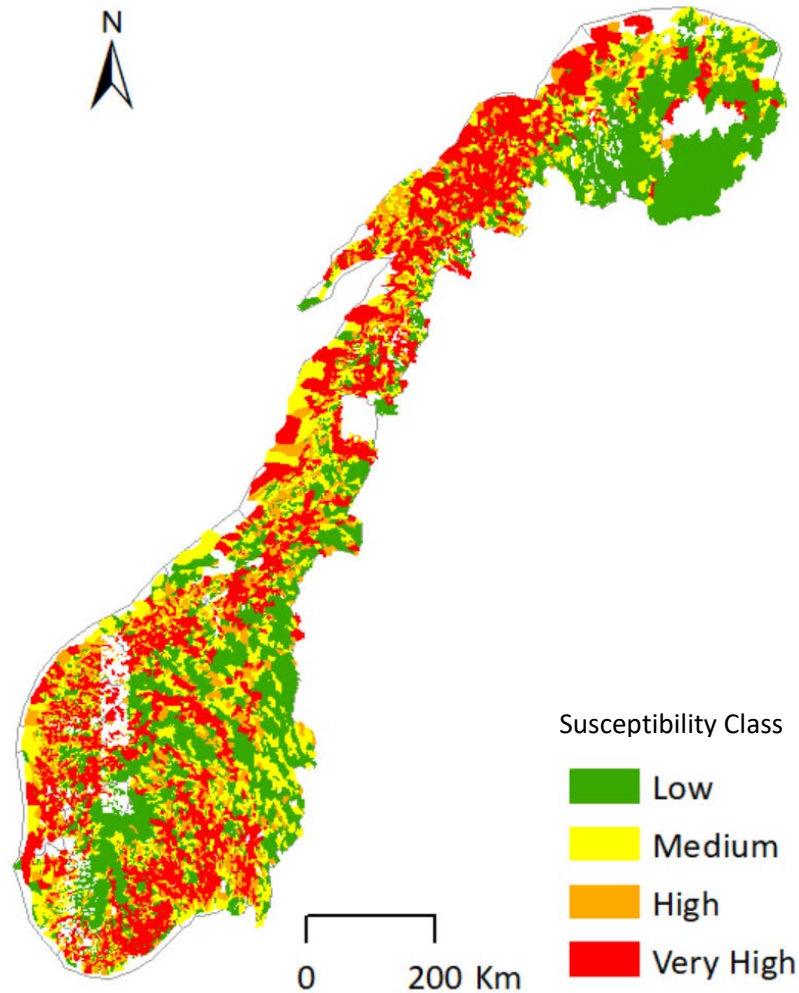


Figure 9. Catchment level susceptibility map of Norway, figure made using NVE data (NVE, 2020a)

The susceptibility level of each of the registered landslide points and the polygons mapped with  $\delta$ NVDI are recorded. A histogram of these intersections is calculated indicate their usefulness in predicting the location of landslides.

### 3.3.3 Quaternary Geology Mapping

Quaternary geology shapefiles mapping the quaternary geology of Norway were downloaded from NVE ([www.atlas.nve.no](http://www.atlas.nve.no)) at a scale of 1:1,000,000 and from NGU ([www.ngu.no](http://www.ngu.no)) at a scale of 1:250,000, hereafter named large and small scale, respectively. The latter is the map used in the development of the susceptibility map presented in Section 3.3.2. The large-scale quaternary geology map is illustrated in Figure 10.

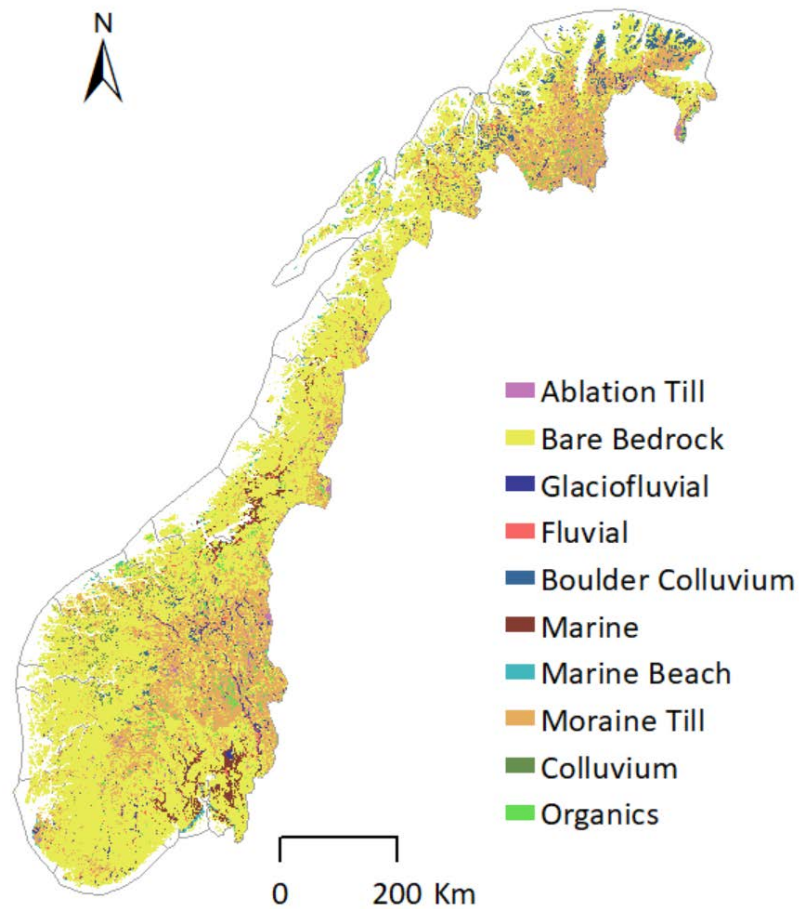


Figure 10. Quaternary geology map of Norway, figure made using NVE data (NVE, 2020c)

For the Norwegian case studies, the landslides registered in the NVE database will be mapped as points on the quaternary geology maps to determine the soil type that they are located in. The point location is not altered from the database. For the polygons mapped using remote sensing techniques, the soil types that they intersect are recorded. Each polygon can therefore have several intersections. The quaternary geology types that are most likely to have a shallow soil landslide are then determined, and these results interpreted. This interpretation aids in determining if the use of large- and small-scale geology maps helps or hinders landslide forecasting. A comparison of the two scales is made.

### 3.3.4 Weather

#### 3.3.4.1 Data

Rainfall and snowmelt data are collected at two different scales: 1) point data from weather stations, and 2) area data from an interpolated model, seNorge v2.0. Both data sources are retrieved for the three days prior and the day of each selected landslide event. The two scales are used to compare how well they each relate to landslide initiation.

The first data source is from the MET weather stations. Rain gauge with 1-hour precipitation data nearest the landslides for each event is selected using xgeo.no. When available, a gauge at a high

elevation is chosen to represent precipitation in the area of initiation. Unfortunately, most gauges are located near communities, in valleys at low elevations. 1-hour precipitation, undercatch corrected by MET, and 1-hour temperature data are collected for each from seklima.met.no (Meteorologisk institutt, 2020b). The mean annual precipitation (MAP) for each rain gauge is retrieved for all years on record. 24-hour snowmelt from the NVE Snow Map Model was retrieved from xgeo.no at the weather station.

The second data source is an interpolated dataset. seNorge v2.0 is a 1 km square gridded dataset of 1-hour precipitation and 1-hour temperature based on observations which are used to simulate a 3-hour equivalent snowmelt (Lussana, et al., 2018). seNorge v2.0 is based on a dataset of over 30 years and is considered sufficiently long to statistically capture rare events (Lussana, et al., 2018). The average and maximum grid values over the area of each case study were provided by NVE and are available online (senorge.no) (NVE, 2020a). Neither the average nor the maximum represents a physical value, but they serve as useful indicators of how concentrated precipitation fell and an approximate upper bound of each parameter.

Additional weather indicators were collected using xgeo.no. Modelled values including frost depth compared to normal, groundwater level compared to normal, and the degree of soil saturation data (volumetric as a percentage of maximum) are collected from a grid cell at one of the registered landslides. All values are compared relative to that day and location average across 1981-2010 value. All xgeo.no data retrieved is owned by NVE.

#### 3.3.4.2 Normalized Water Supply

The water supply required to initiate landslides has been found by others to be relative to the precipitation in the region, as discussed in Section 2.1.2. Water supply, calculated as the cumulative precipitation and snowmelt, from both data sources, weather stations and seNorge v2.0, are normalized using the average annual precipitation values from rain gauges, for consistency. Normalized 24-hour water supply for landslide initiation is calculated using the following equation, presented as a percentage of mm/24-hrs:

*Equation 3-2. Normalized water supply for landslide initiation*

$$\text{Normalized Water Supply mm/24hr \%} = \frac{24\text{hr Precipitation} + 24\text{hr Snowmelt}}{\text{Mean Annual Precipitation}} \times 100$$

#### 3.3.4.3 Return Periods

Return periods are another common expression of landslide initiation thresholds. Return periods of 1-, 12-, and 24-hour precipitation are determined using intensity-duration-frequency (IDF) curves taken from the nearest long-term and verified station (all greater than 10 seasons). IDF curves are downloaded from klimaservicesenter.no (Meteorologisk institutt, 2020a). Return periods are calculated as:

*Equation 3-3. Return period of a given water supply*

$$\text{Return Period [yrs]} = \frac{1}{\text{Probability of water supply in any one year}}$$

#### 3.3.4.4 Weather Categorization

With the use of the precipitation data collected, calculations of normalized water supply, return periods, and weather radar from xgeo.no, weather that triggered each event is categorized. Average and maximum seNorge v2.0 precipitation and snowmelt over the entire area studied are used as indicators of the concentration of water (i.e. even widespread rain or intense local rain). Loosely based on weather systems commonly associated with landslides and floods in Norway by (Roald, 2008), categories of weather are defined, herein, as:

- A: Remnants of tropical cyclone: occur from August to November bring warm and humid air from the Atlantic, Caribbean Sea, or Gulf of Mexico causing heavy rainfall as they hit Norway due to orographic lifting.
- B: Intense concentrated rainstorm: common in late summer and autumn and may be convective rain.
- C: Heavy widespread rainstorm: high magnitude rainfall common in late summer and autumn from moisture swept off the Atlantic that falls on the coast due to orographic lifting.
- D: Rapid spring melt: warm spring air temperatures cause intense melting and a partially frozen ground induce high runoff and high surface water levels.
- E: Wet antecedent conditions and moderate rain: warm spring air temperatures cause wetter than usual antecedent conditions including groundwater levels and soil saturation followed by moderate rain.
- F: Rain on snow: Mild and humid air across the Atlantic in the winter cause rain and snow and widespread snowmelt, often for long durations and at high intensities. May cause slushflows at high elevations that turn into debris flows and floods. Two subcategories include:
  - F1: With frost present
  - F2: Heavy rain
  - F3: Heavy rain and with frost present

#### 3.3.5 HYDMET Model

The observed daily HYDMET model results from NVE are made publicly available on xgeo.no (NVE, 2020c). The online interactive map was used to extract HYDMET results for the multiple landslide event case studies across Norway. Each pixel of the square grid has an indexed hazard level. Using the defined area of the 21 case studies, the maximum hazard level and the most common hazard level (mode) of the pixels are recorded. This process is completed by visual inspection in the absence of a more quantifiable method. It should be noted that these are the model results using weather observations, rather than forecasts, whereas the landslide forecaster only had the benefit of weather forecasts.

#### 3.3.6 Landslide Warnings

##### 3.3.6.1 Published Warnings

The hazard level published for each day of the year from 2013-2019 are recorded and were provided by NVE. A histogram of the number of days at each hazard level is calculated.

For each case study, landslide warnings are retrieved from NVE ([www.varsom.no](http://www.varsom.no)) for six days in the county in which the event took place, including three days prior, the main day of the event, and the two subsequent days.

### 3.3.6.2 NVE Warning Evaluation

Daily internal notes are provided by NVE that include a daily retrospective correction of what hazard level should have been warned. These corrections are partially quantitative, taking into account of landslides registered as of the end of day, but also have a subjective component that is challenging to reproduce. The corrected hazard levels were collected from NVE for the date of each case study in the appropriate county.

### 3.3.6.3 Quantitative Warning Evaluation

Quantitative thresholds are useful as they are reproducibly and objective. Two quantitative thresholds defined by others are used to compare to NVE evaluations. The first threshold is based strictly on the number of reported landslides within the defined event area, with intervals from the NVE hazard level definitions (NVE, 2020a). It is simple and reproducible but does not consider the volume, area, or damages of the landslides. The second threshold uses the normalized 24-hour water supply at weather stations, with intervals defined in a previous study of debris flow thresholds by Meyer et al., 2012. Hazard levels will be determined for the 21 case studies based on the two proposed thresholds. The intervals for each hazard level are presented in Table 4.

Table 4. Quantitative thresholds for landslide warning hazard levels

Hazard Level	Landslides per 10-15,000 km <sup>2</sup> (NVE, 2020a)	Normalized 24-hr Rainfall & Snowmelt at Weather Station (%) (Meyer, Dyrddal, Frauenfelder, Etzelmuller, & Nadim, 2012)
1 - Green	0	<2.18
2 - Yellow	1-5	2.18-4.14
3 - Orange	6-19	4.15-8.65
4 - Red	≥20	≥8.66

### 3.3.6.4 Proposed Area Thresholds

Rain gauge data is reliable, but it is accurate only for only one location. The selected landslides each had their own water supply that in most studies is collected as point data from an interpolated grid to develop initiation thresholds. Landslide warnings are, however, published for large areas and not points, requiring a landslide forecaster to interpret a grid of point data.

In this study, area thresholds, rather than traditional point thresholds, are proposed in order to capture the appropriate regional landslide hazard level. This experimental approach will be tested by assigning thresholds for each hazard level, assigning a level based on the average and maximum water supply over the entire area studied, and comparing these values with the landslide warnings of each case study.

While this water supply value is not a representation of a physical parameter, it is an index of water supply over the entire area. It is hypothesized that an average value could be more representative of the total consequences over the warning area. Landslide warnings in Norway are not predicting the likelihood of any one given slope having a landslide, but rather, they forecast the total consequences over the area. This “area” threshold attempts to account for the spatial and intensity uncertainty of weather forecasts and represent the regional nature of warnings. Threshold levels are defined by hazard level using average and maximum normalized seNorge v2.0 24-hr precipitation and snowmelt in the defined case study areas.

## 4 Results & Discussion

### 4.1 Case Studies

#### 4.1.1 Norway

A total of 25 extreme multiple landslide events were recorded in the NVE landslide database from July 2015 through December 2019. In three cases, events took place on subsequent days and were merged. Two events were rejected because they were too widespread and did not have a cluster of five landslides. Only one event was recorded north of Trøndelag (case 8). For geographic representation of the whole of Norway, one event was added in Northern Norway (case 20) that had only six landslides on one date, rather than ten, but fulfils all other criteria. The 21 Norwegian case studies are detailed in Table 5 and illustrated in Figure 11. The case studies are made up of 416 landslides registered in the NVE database, which are included in Appendix B.

Table 5. Norwegian multiple landslide event case studies

ID	Date(s) YYYYMMDD	County	Landslides in Database on Date	Landslides in Event Area	Event Area (km <sup>2</sup> )	Season
1	20150917	Vestfold	12	5	2022	Autumn
2	20151126/27	Sogn og Fjordane	36	11	8275	Autumn
3	20151205/06	Rogaland	36	7	3988	Winter
4	20161125	Møre og Romsdal	11	5	2605	Autumn
5	20161204/05	Trøndelag	35	11	6434	Winter
6	20161230	Sogn og Fjordane	19	9	6964	Winter
7	20170120	Møre og Romsdal	11	9	5576	Winter
8	20170126	Nordland	17	5	3770	Winter
9	20170518	Hedmark	11	9	1295	Spring
10	20170724	Oppland	13	10	2593	Summer
11	20171002	Vest Adger	29	7	4314	Autumn
12	20171123	Hordaland	11	8	4126	Autumn
13	20171207	Hordaland	23	21	7570	Winter
14	20171223	Hordaland	30	9	3338	Winter
15	20180418	Oppland	22	7	3596	Spring
16	20180926	Hordaland	12	6	4712	Autumn
17	20190104	Trøndelag	11	8	6724	Winter
18	20190606	Oppland	12	9	2346	Summer
19	20190730	Sogn og Fjordane	42	30	3100	Summer
20*	20191204	Troms og Finnmark	6	5	2205	Winter
21	20191229	Sogn og Fjordane	17	8	4843	Winter

\* Event was selected for geographic representation in Northern Norway, despite not meeting selection criteria



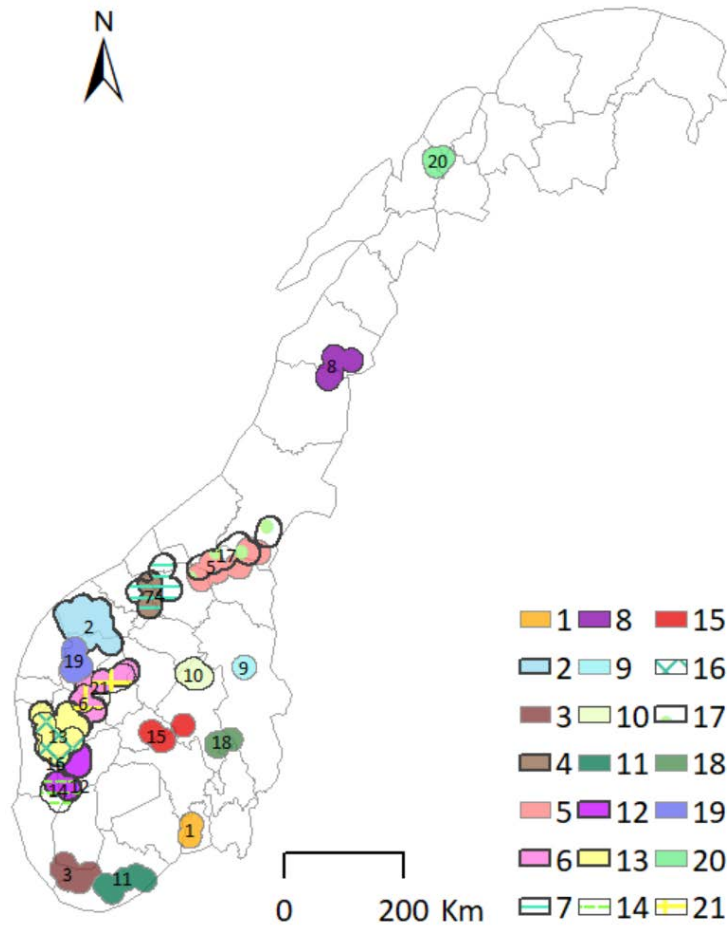


Figure 11. Map of selected case studies in Norway

It is evident that multiple landslides events are most frequent in Western Norway, even with the geographic variety selection bias. This is owed to high mean annual precipitation and orographic lifting when moist air from the Atlantic reaches the Norwegian coast. Extreme multiple landslide events are likely rare in Northern Norway due to stable winter temperatures with fewer freeze thaw events and a larger proportion of precipitation falling as snow.

A notable result from this analysis are the high proportion of autumn and winter events, with two events in spring, three in summer, six in autumn, and ten in winter.

#### 4.1.2 International

Four international multiple landslide events were used to test landslide mapping with the  $\delta$ NDVI and SAR methods in various conditions. Test sites A, B, and C and information about each were chosen from 'The Landslide Blog' ([www.blogs.agu.org/landslideblog/](http://www.blogs.agu.org/landslideblog/)) (Petley D. , 2020a). Site D was chosen specifically to test remote sensing methods in the high north and information was retrieved from (Christiansen, et al., 2016). Details of these events are included in Table 6 and a location map is included in Figure 12.

Table 6. International  $\delta$ NDVI landslide mapping test sites

ID	Location	Date DD-MMM-YY
A	Nyempundu, Burundi	04-Dec-19
B	Wenchuan, China	17-Aug-19
C	Baixada Santista, Brazil	03-Mar-20
D	Longyearbyen, Svalbard	15-Oct-16



Figure 12. Map of international test sites

## 4.2 Landslide Inventory

### 4.2.1 SAR

Acquired Sentinel-1 images have an average of five and three of days before and after the selected landslide events, respectively. This short time frame is short enough to be used for emergency response in extreme circumstances, but not in day to day response protocols. A list of Sentinel-1 images used are included in Appendix C.

There is a total of 415 landslides registered in the 21 Norwegian case studies. Of those 415, 23 are duplicates and 246 are not covered in the Sentinel-1 satellite images chosen. The remaining 150 landslides were analyzed and coded as follows:

- 20% are coded Y, detectable and mappable with high certainty without knowing their location,
- 25% are coded M, detectable and mappable with low certainty knowing their location, and
- 55% are coded N, not detectable.

Landslides coded Y and M are grouped together and termed “detectable” for simplicity. Only 10% of all landslides are detectable, with 90% undetectable even knowing their location. Table 7 is a summary of the scoring of the 150 analyzed landslides organized by case study using SAR.

*Table 7. Sentinel-1 SAR landslide mapping results for Norwegian case studies*

ID	Landslides in Database in Search Area (including duplicates)	Database Landslides Detected	% Detected (excluding duplicates)	Landslides Mapped	Season	Trigger (R = rain, S = snowmelt)
1	5	0	0	0	Autumn	R
2	12	2	17	0	Autumn	R&S
3	7	0	0	0	Winter	R&S
4	5	0	0	0	Autumn	R&S
5	7	0	0	0	Winter	R&S
6	8	2	25	0	Winter	R&S
7	6	0	0	0	Winter	R&S
8	7	0	0	0	Winter	R&S
9	9	0	0	0	Spring	R&S
10	2	0	0	0	Summer	R
11	6	0	0	0	Autumn	R
12	7	1	14	0	Autumn	R&S
13	18	0	0	0	Winter	R&S
14	3	0	0	0	Winter	R&S
15	8	0	0	0	Spring	S
16	3	0	0	0	Autumn	R
17	7	0	0	0	Winter	R&S
18	10	0	0	0	Summer	R
19	22	6	35	1	Summer	R
20	4	0	0	0	Winter	R&S
21	14	3	21	0	Winter	R&S

Case 19 had the best conditions for SAR of the case studies selected, likely due to the magnitude of landslide area. Even in these conditions, only six of the 22 landslides analysed in this event are detectable. Figure 13 illustrates case 19 SAR intensity, phase, and coherence.

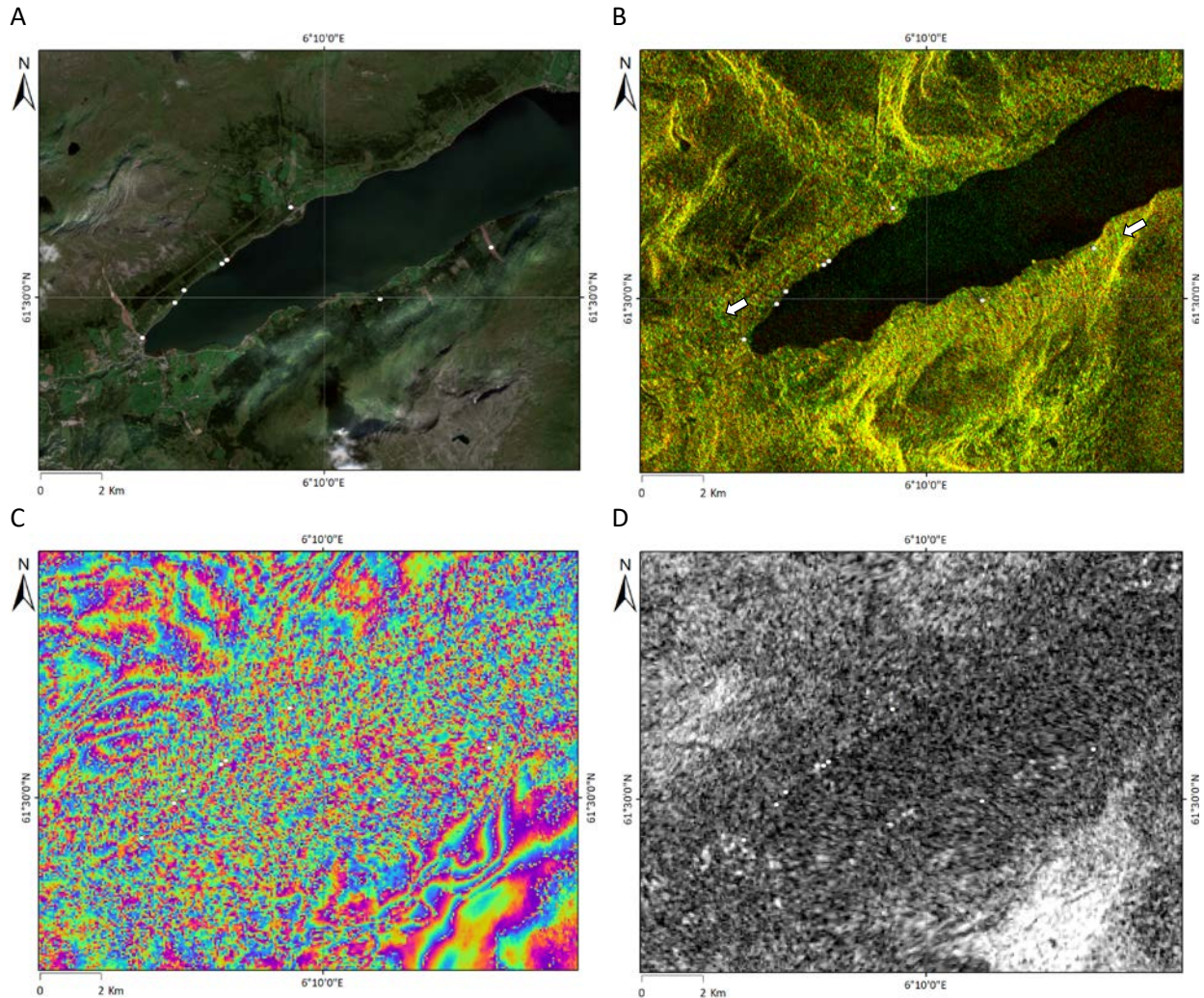


Figure 13. Comparison of A: Sentinel-2 natural colour image and Sentinel-1 SAR with registered landslides identified with white points and detectable landslides identified with white arrows on B: intensity, C: phase, and D: coherence interferograms (case 19, July 30, 2019, Sogn og Fjordane)

Both phase and coherence show no clear indication of landslides in any of the selected cases. In a weather induced landslide event, it is likely that the surrounding change has undergone too much change for small landslides to stand out. Figure 13C and D show the lake and surrounding area show the most change (in speckled rainbow and black, respectively) and the least change at the mountain tops (in striped rainbow and white, respectively). The landslides are likely too shallow (<1 m deep) and small (<0.1 km<sup>2</sup>) to be identified, even knowing their location.

Intensity, a function of soil moisture and ground roughness, is the most reliable tool for landslide detection of selected cases using SAR. Within the landslide scar, the vegetation has been removed, thus substantially changing both roughness and moisture. The most clear and distinct landslide of all selected cases is a debris flow with an area of approximately 0.06 km<sup>2</sup> that occurred on a forested northwest facing slope in case 19. In this example, intensity increases due to an increase of moisture content despite the decrease in intensity due to the decrease in roughness. A few days later this landslide is likely not detectable as the moisture content would have decreased. Additionally, if the scar was flooded, which it may have been initially, the intensity would have been reduced. This is the only

landslide, of the 150 analysed, that is clear enough to be coded “Y” and is confidently mapped using SAR. The optical Sentinel-2 image is shown in comparison with the SAR intensity of the Sentinel-1 image in Figure 14.

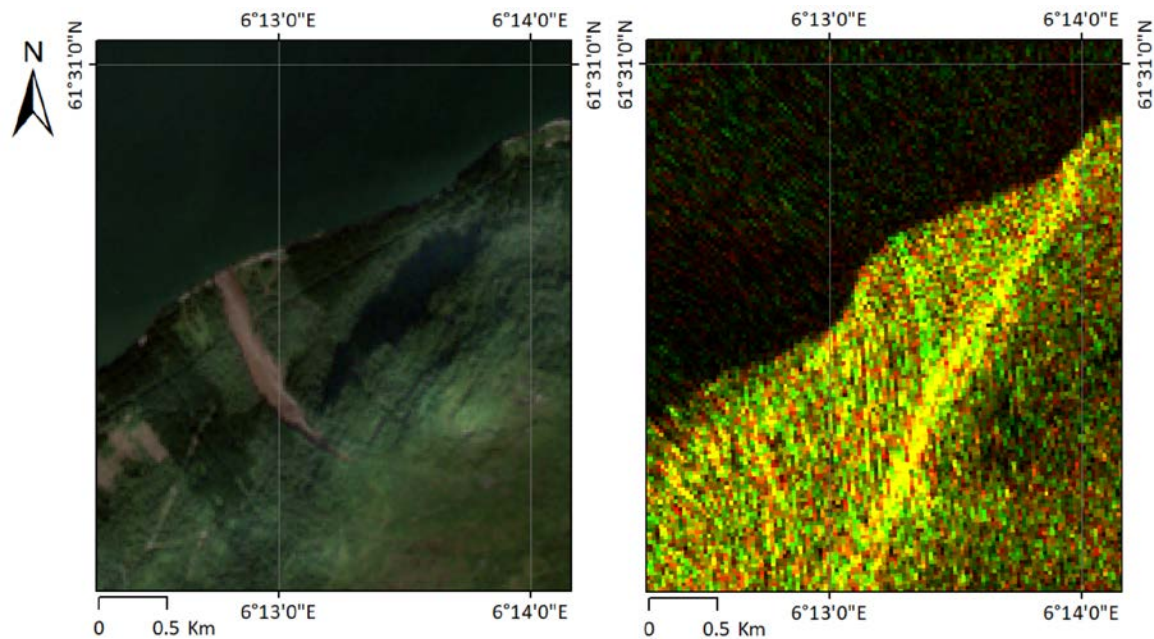


Figure 14. A: Optical image and B: SAR intensity of a debris flow with an approximate area of 0.06 km<sup>2</sup> (case 19, July 30, 2019, Sogn og Fjordane)

The main issues with using SAR to map landslides in the selected case studies is the deformation of their shape and location, the landslide depth and area being too small, and the overall terrain change being too significant for landslides to stand out.

#### Deformation

When detectable, landslides are distorted in both orientation and shape due to the acquisition mode and reference system conversion. Distortion could be to the steep slopes and narrow valleys in the chosen acquisition orbit, where ascending is the favourable orbit for west facing landslides and descending the favourable for east facing landslides (and equal for north and south facing). If a landslide is on a west facing slope, it will be foreshortened (will appear shorter than it is) in an ascending acquisition mode, when the antenna is facing right. This is the case in case 19. Note the clear signature of the landslide scar in Figure 14, above, and the deformation of shape and location compared to the optical image. Using SAR, it is mapped over 400 m away from its actual ground location, using the same reference system. Ideally, both ascending mode and descending mode should have been analysed for each case study due to the variety of slope exposures in each.

#### Landslide Size

The small magnitude of area of landslides in the selected cases, as is typical in Norway, hinders their detection using SAR. A study of rapid landslides around the world using SAR amplitude changes found that larger landslides were easier to detect, with those cases under 0.001 km<sup>2</sup> not detectable or only detectable if their location is known (Mondidi, et al., 2011). In the selected cases, the landslides detected with SAR intensity, phase, and coherence are all estimated to be greater than 0.01 km<sup>2</sup>.

Table 8. Sentinel-1 SAR change detection landslide mapping results by landslide type (Y = mappable, M = mappable if location is known, N = not detected, Y/M = detectable)

		% of analyzed landslides			
		Y	M	N	Y/M
Landslide Type	All	0.7	9	90	10
	140	0.0	3	97	3
	142	0.0	15	85	15
	144	1.5	6	92	8
	133	0.0	22	78	22

#### Moisture Increase and Snowmelt Noise

There is not enough confidence in detected landslides to attempt mapping. The primary issue with mapping landslides in the selected case studies is the noise in surrounding areas. There is no clear landslide signature because the surrounding terrain appears significantly changed in intensity, phase, and amplitude. Coherence of forested areas is not sufficient level of coherence, even for a weeklong interval, and the resulting interferogram are therefore distorted by noise. In summer events, vegetation is too significantly changed, and in winter, the snow cover is too significantly changed. Coherence values can also be affected by local weather, including rain, strong winds, and hot weather (ESA, 2007). Weather is likely causing noise in many cases, as the majority of cases had rain when the pre-event image was acquired. Freeze and thaw of the ground surface also causes coherence changes and noise in interferograms.

The selected landslides differ greatly from other mass movements that are easily mapped using SAR, such as snow avalanches in sub-zero temperatures (i.e. no snowmelt), rock landslides where the surroundings are stationary and easily referenceable, or deep-seated soil landslides that are not triggered by torrential rainfall.

Despite unavoidable coherence noise, the selection of Sentinel-1 imagery is likely not ideal in many cases, and this would ideally be reconsidered and chosen more careful, rather than prioritizing a short temporal window. Additionally, a DEM with higher resolution would improve results. The pre-processing steps used should all be more carefully re-visited for conditions in Norway to ensure they are optimized.

#### 4.2.2 $\delta$ NDVI

On average, pre- and post-event images are 36 days before and 35 days after the landslides took place, respectively, excluding the two events where an image was taken the summer before and after. A complete list of the pre- and post-event Sentinel-2 satellite images chosen for the 21 case studies is included in Appendix D.

There is a total of 415 landslides registered in the 21 Norwegian case studies. Of those 415, 24 are duplicates and 231 are not covered in the Sentinel-2 satellite images chosen. The remaining 160 landslides were analyzed and coded as follows:

- 20% are coded Y, detectable and mappable with high certainty without knowing their location,
- 25% are coded M, detectable and mappable with low certainty knowing their location, and
- 55% are coded N, not detectable.

Landslides coded Y and M are grouped together and termed “detectable” for simplicity. Table 9 is a summary of the scoring of the 160 analyzed landslides organized by case study.

*Table 9. Sentinel-2  $\delta$ NDVI landslide mapping results for Norwegian case studies*

ID	Landslides in Database in Search Area (including duplicates)	Database Landslides Detected	% Detected (excluding duplicates)	Landslides Mapped	Season	Trigger (R = rain, S = snowmelt)	Primary Reason for Non-detection
1	5	1	33	1	Autumn	R	Clouds
2	20	9	53	73	Autumn	R&S	Clouds
3	14	1	11	1	Winter	R&S	Landslide size
4	0	3	60	4	Autumn	R&S	Snow
5	5	3	50	5	Winter	R&S	Landslide size
6	6	2	50	2	Winter	R&S	Snowmelt
7	4	1	14	2	Winter	R&S	Snowmelt
8	7	2	40	2	Winter	R&S	Snowmelt
9	8	0	0	0	Spring	R&S	Landslide size
10	9	6	60	43	Summer	R	Landslide size
11	10	3	75	3	Autumn	R	Shadows/clouds
12	5	4	57	11	Autumn	R&S	Snowmelt
13	7	0	0	0	Winter	R&S	Clouds/Snow
14	9	1	20	19	Winter	R&S	Snowmelt
15	5	3	50	3	Spring	S	Snowmelt
16	7	4	100	23	Autumn	R	N/A
17	4	1	17	1	Winter	R&S	Landslide size
18	7	0	0	0	Summer	R	Landslide size
19	8	23	96	137	Summer	R	N/A
20	30	1	25	1	Winter	R&S	Clouds/Snow
21	4	5	63	9	Winter	R&S	Clouds/Snow

Shallow soil landslides are found to have a significant change in NDVI but are only detectable in the correct conditions. When favourable conditions are combined, a success rate of up to 94% is achieved. These conditions include:

- landslide trigger, indicating if snow was present or not;
- the number of days between images, indicating cloud cover, lighting, and vegetation changes, and;
- landslide type, indicating the size of area affected.

Landslides of each condition are summed and presented as the percent detected. The overall detection rate of selected landslides is 45%. Success rates for conditions that were found to be the most significant are presented in Figure 15.

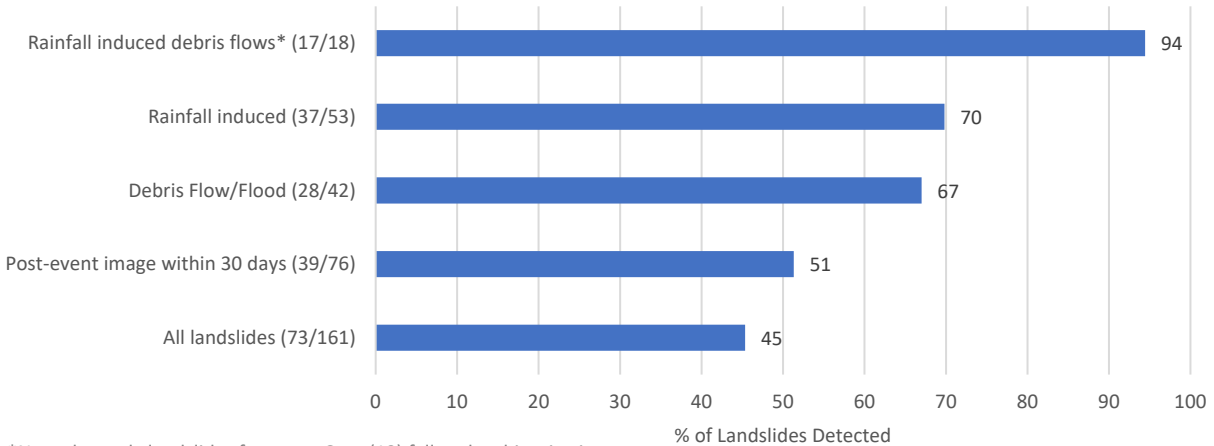


Figure 15. Sentinel-2  $\delta$ NDVI landslide detection success for various conditions as a percentage of landslides per category with the absolute number in brackets as (landslides detected/total landslides in category)

In seven cases conditions made it possible to map more landslides than were registered. In these cases (2, 10, 12, 14, 16, 19 and 21), the average increase of landslides mapped is 2.8 times the number registered.  $\delta$ NDVI images with all mapped polygons are included in Appendix D for these seven cases. Case 19 had the best conditions, taking place in summer, with relatively large rainfall induced landslides, mostly debris flows/floods/avalanches. Figure 16 illustrates the Sentinel-2 image in natural colours, false colour infra-red, and  $\delta$ NDVI with and without mapped polygons. While some landslides are obvious in all images, others reveal themselves clearly in  $\delta$ NDVI only. In the first two images it is challenging to differentiate bare bedrock and old landslide scars from new landslides, but they stand out clearly in  $\delta$ NDVI.



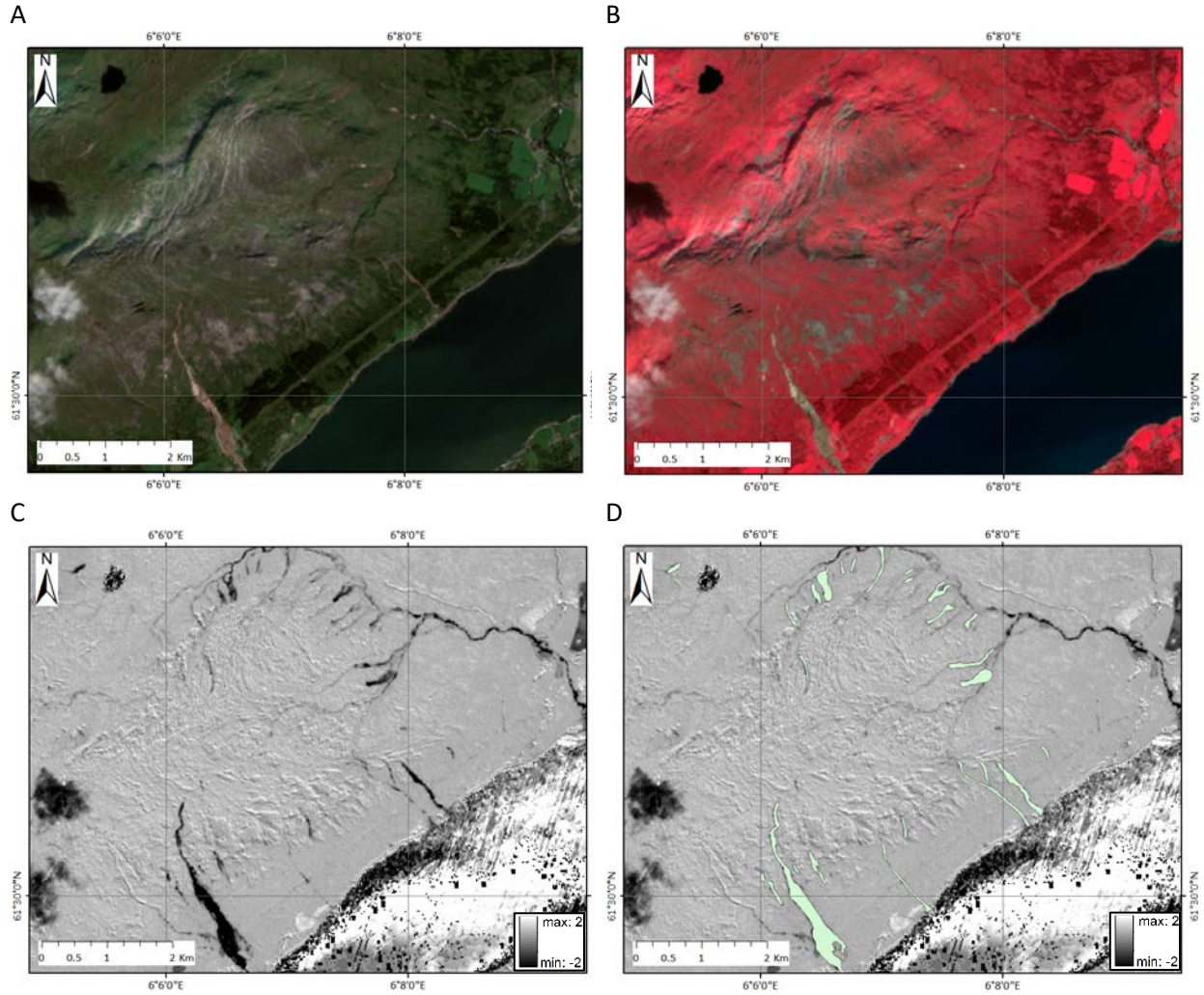


Figure 16. Comparison of satellite image with A: natural colours, B: false colour infra-red, C:  $\delta$ NDVI, and D:  $\delta$ NDVI with landslides mapped in case 19 (July 30, 2019, Sogn og Fjordane)

Three cases had snow present (12, 14, 21) making it challenging to map the extents of the landslides with certainty and requiring judgement to differentiate snowmelt from landslides. Extents of landslides are mapped with high confidence in the four events with no snow present (2, 10, 16, 19). Nearly all landslides mapped are less than 0.1 km<sup>2</sup> (100,000 m<sup>2</sup>) and over half are less than 0.01 km<sup>2</sup> (10,000 m<sup>2</sup>). The number of landslides mapped are listed by area in Table 10.

Table 10. Landslides mapped with  $\delta$ NDVI method, by area

Area (km <sup>2</sup> )	No. of Landslides	% of Landslides
<0.01	188	53
< 0.1 & > 0.01	162	46
> 0.1	6	2

Other processes and objects that have a significant change in NDVI can be challenging to differentiate from landslides. Changes in agriculture crops, snowmelt, elongated bodies of water, and clouds or cloud shadows can hide landslide scars or appear to be landslides, as illustrated in Figure 17. River erosion, flooding, and construction can also cause a significant change in NDVI.

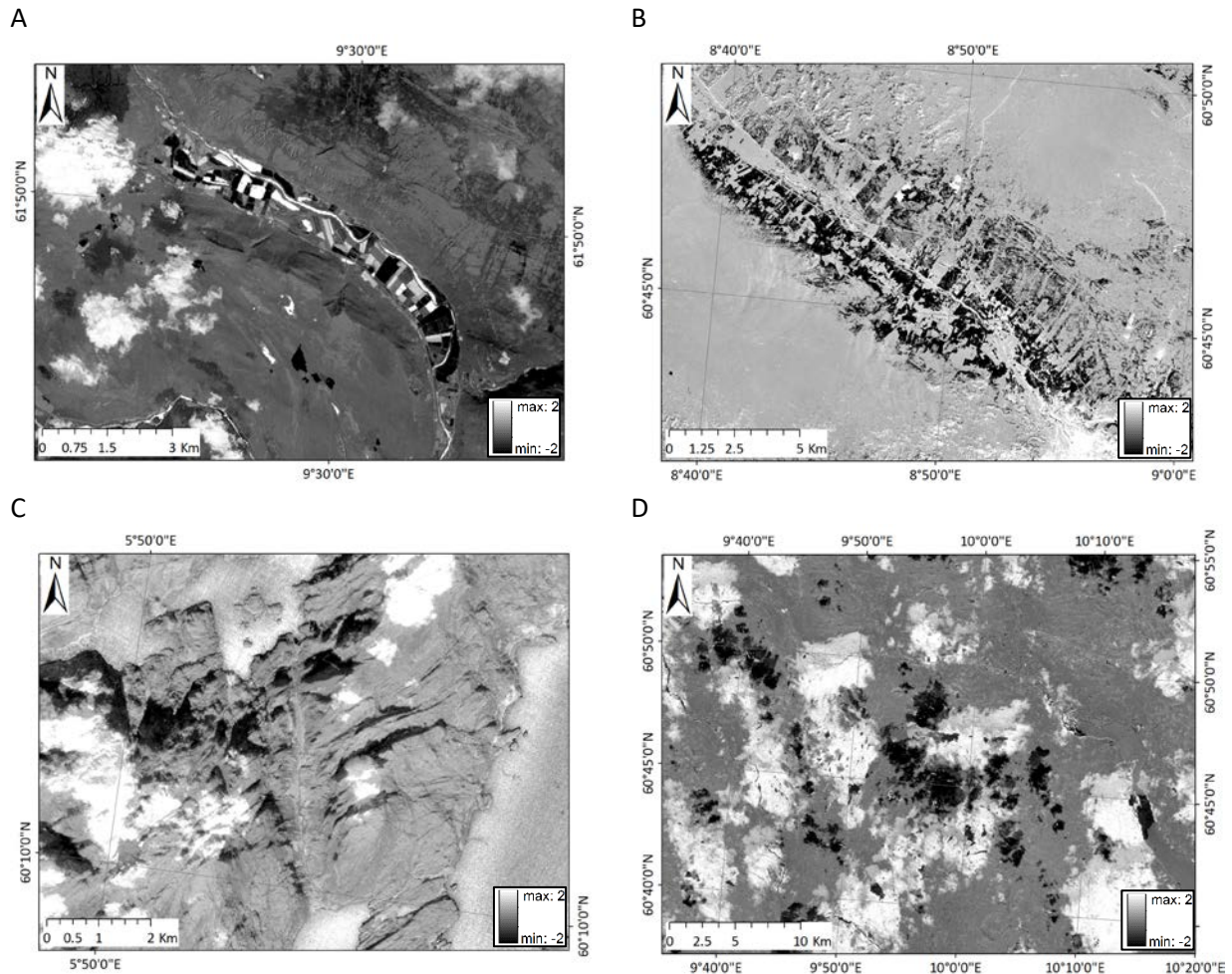


Figure 17. Processes and objects causing a significant change in NDVI obstructing landslide detection: A: agricultural crops (case 10, July 24, 2017, Oppland). B: snow melt (case 15, April 18, 2018, Oppland). C: elongated lakes and rivers (case 16, September 26, 2018, Hordaland). D: clouds (case 19, July 30, 2019, Sogn og Fjordane)

Three factors are found to be the main inhibitors of landslide detection using NDVI in Norway:

- Snow: widespread melt, altering the NDVI of a large area, or new snow covering landslide scars
- Cloud cover: result in a large window between before and after images, often with differing lighting and vegetation, or cloud shadows altering reflectivity
- Landslide size: not enough pixels exhibit a change in NDVI, and smaller landslides are therefore not detectable

The percentage of landslides detected by landslide type is presented in Table 11.

Table 11. Sentinel-2  $\delta$ NDVI change detection landslide mapping results by landslide type (Y = mappable, M = mappable if location is known, N = not detected, Y/M = detectable)

		% of analyzed landslides			
		Y	M	N	Y/M
Landslide Type	All	20	25	55	45
	140	7	35	58	42
	142	43	24	33	67
	144	15	18	67	33
	133	22	33	44	56

### Snow

The  $\delta$ NDVI method performs best for landslide detection when landslides occur in highly vegetated areas while the vegetation is green and healthy, typically in summer months. In cases with lush greenery before (around 0.6 to 0.8), the NDVI drops to just above zero (0.2 for bare soil or 0.1 for bedrock). In cases where landslides occurred when the ground was covered in snow, a landslide results in an increase of NDVI, from 0 to slightly above zero (0.2 for bare soil or 0.1 for bedrock). This small change in NDVI makes it extraordinarily difficult to detect landslides when snow is on the ground, as is the case for much of the year in Norway, and the majority of selected landslide events.

Slushflows are snow avalanches that have high velocity and power, entraining the underlying soil in the flow, creating geomorphological signatures similar to debris flows after the snow melts. Interestingly, slushflows (133 in Table 11, above) have a higher detection rate than unclassified landslides in soils or soil slides. This is likely owed to their size and long runout. They alter the NDVI only slightly, but over a large area, that is easier to detect. The size of landslide is, therefore, a more significant factor in detection than snow cover.

### Clouds and Daylight

Optical landslide detection relies on low-cloud or cloud-free days before and after the landslide, as close as possible to when it takes place. There is a relatively high number of days in Norway, with a mean annual cloud cover of 60-90% well spread throughout the year (see Figure 18) (Wilsom & Jetz, 2016).

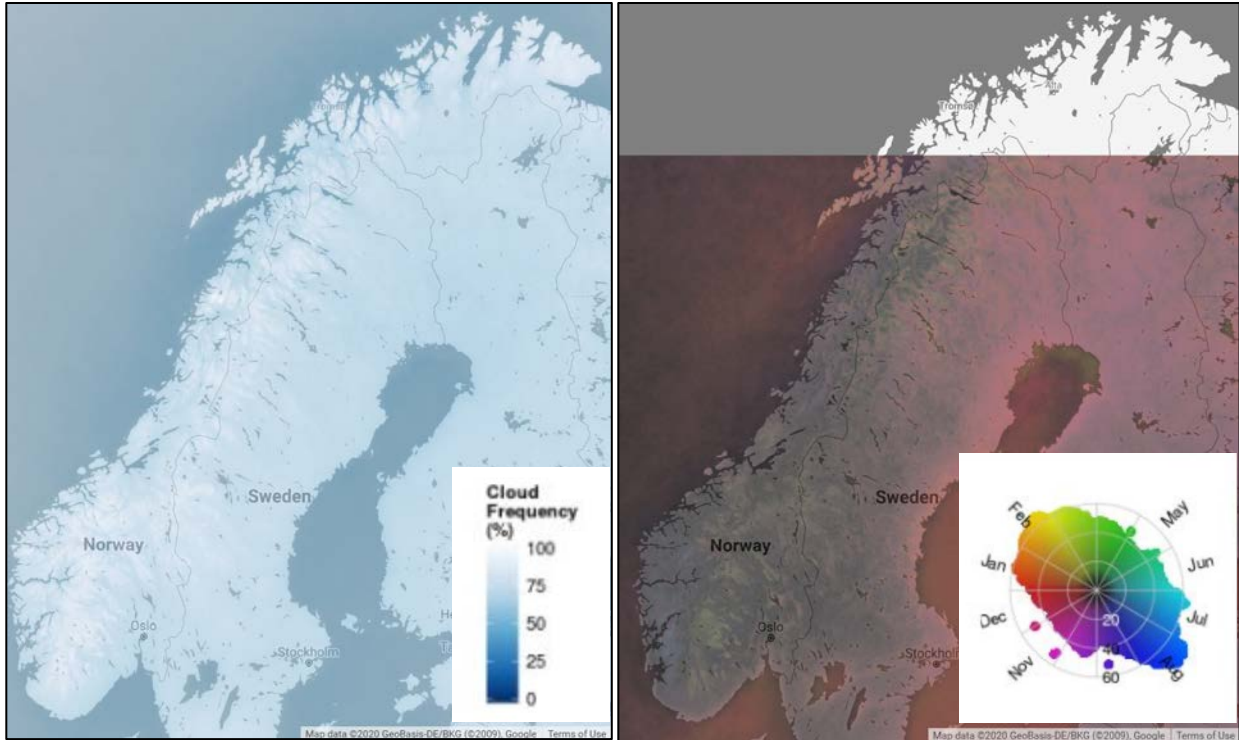


Figure 18. Norwegian cloud cover presented as mean annual frequency, ranging from 60-90% (left) and seasonality, slightly weighted to May through August (right), figure adapted from (Wilsom & Jetz, 2016).

For two events (cases 2 and 5), images from the summer before and after were chosen in the absence of cloud free images close to when the landslides took place and to avoid snow cover masking landslide scars.

Although using images one year apart makes it impossible to determine the date a landslide occurred or differentiate between two events in the same location, it proved to yield superior results than the nearest closest cloud free day due to shadows and snow in these two cases. It is unfortunately not possible to determine the exact date of the landslides in any case, and only that it occurred between the two image dates. Knowing the weather data and given a narrow window of images, an educated guess can be made for the date of occurrence, as soil slides are nearly always precluded by heavy rainfall. That being said, in five of the cases, the peak 24-hour rainfall occurred one to three days prior, and not the day of occurrence.

The spatial and temporal proximity and limited images due to cloud cover required that cases 4 and 7 and cases 12 and 14 use the same Sentinel-2 images, respectively. This makes it challenging to differentiate between events, highlighting that the exact time, let alone date, is not possible to determine using  $\delta$ NDVI and Sentinel-2 images. Even with satellite imagery with higher temporal resolution.

Norway is located geographically in a sub-polar region. The selected case studies are located between 58° and 70° North, and thus, have long daylight hours in the summer and short daylight hours in the winter. Cases that occur in dark periods of the year, with short or zero daylight hours and with very low sun angles causing long shadows, have obscured or no optical satellite images available. This may

explain the challenges in detecting even large landslides with no snow that take place in autumn and winter.

### Landslide Size

Due to the spatial resolution of the satellite imagery (10 m square pixels), the detection limit is found to be an area of approximately 1000 m<sup>2</sup> or 10 pixels. This limitation likely explains why debris flows/floods and slushflows have higher detection success than other landslide categorizations. A large number of landslides registered as uncategorized landslides in soils (140) are small erosional sluffs on roadside banks and are too small to detect. The percentage of landslides detected by landslide type is presented in Table 12.

Table 12. Sentinel-2  $\delta$ NDVI change detection landslide mapping results by landslide type (Y = mappable, M = mappable if location is known, N = not detected, Y/M = detectable)

		% of analyzed landslides			
		Y	M	N	Y/M
Landslide Type	All	20	25	55	45
	140	7	35	58	42
	142	43	24	33	67
	144	15	18	67	33
	133	22	33	44	56

### 4.2.3 International Test Sites

Four international test sites were used to test various conditions. All four were rainfall triggered debris flow events with over 20 landslides in a concentrated area. The climate, geography, and vegetation of the four sites are summarized in Table 13.

Table 13. Climate, geography, and vegetation of international test sites

ID	Climate	Geography	Vegetation
A	Hot, humid, equatorial climate	Metamorphic mountains with mafic intrusions	Deforested agricultural land
B	Monsoon summers and cold cloudy winters	Sedimentary mountains, Tibetan plateau	Mixed forests disturbed from past geohazards
C	Tropical rainforest climate	Urbanized coastal hills, residual soils	Urbanized lush rainforest
D	Dry arctic climate	Sedimentary mountains, tundra, and continuous permafrost	Moss and small shrubs

#### 4.2.3.1 SAR

Sentinel-1 satellite images chosen for the four international sites are included in Appendix C with the images of the intensity SAR processed images. Similar to the Norwegian cases, the terrain has likely been altered too much for landslides to stand out. Just one landslide was detectable, but only knowing its location, of all the landslides in the four sites, and its shape was not mappable (see Figure 19).

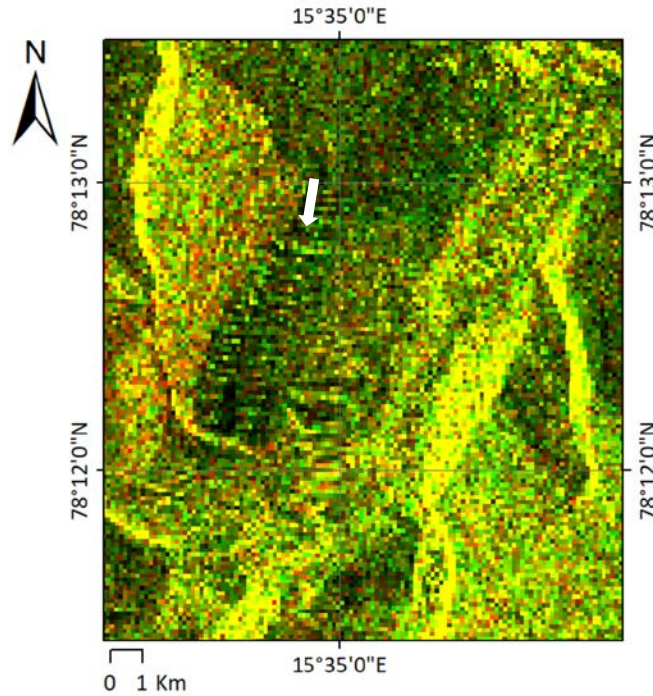


Figure 19. Detectable landslide, knowing its location, marked by the white arrow, using SAR intensity, at site D (October 15, 2016, Longyearbyen, Svalbard)

It is possible that if the exact location of landslides were known, it would have made it possible to detect more. These test sites demonstrate that SAR has limited potential for small rainfall induced landslides in the conditions tested.

#### 4.2.3.2 $\delta$ NDVI

Pre- and post-event Sentinel-2 satellite images chosen for the four test sites are included in Appendix D. Conditions in all four sites allowed for mapping an extensive landslide inventory. The number of landslides mapped and the challenges with using  $\delta$ NDVI for each are included in Table 14 and the mapped landslides on  $\delta$ NDVI images illustrated in Figure 20, Figure 21, Figure 22, and Figure 23.

Table 14. Number of landslides mapped and Sentinel-2  $\delta$ NDVI challenges for international test sites

ID	Landslides Mapped	Landslide Area (min-max km <sup>2</sup> )	Challenges with $\delta$ NDVI
A	237	0.0008 – 0.08	Cloud cover, agricultural changes
B	60	0.001 – 0.4	Cloud cover, other erosional processes present
C	68	0.0004 – 0.03	Urban environment
D	14	0.001 – 0.02	Low vegetation mass, low sun angle, cloud cover

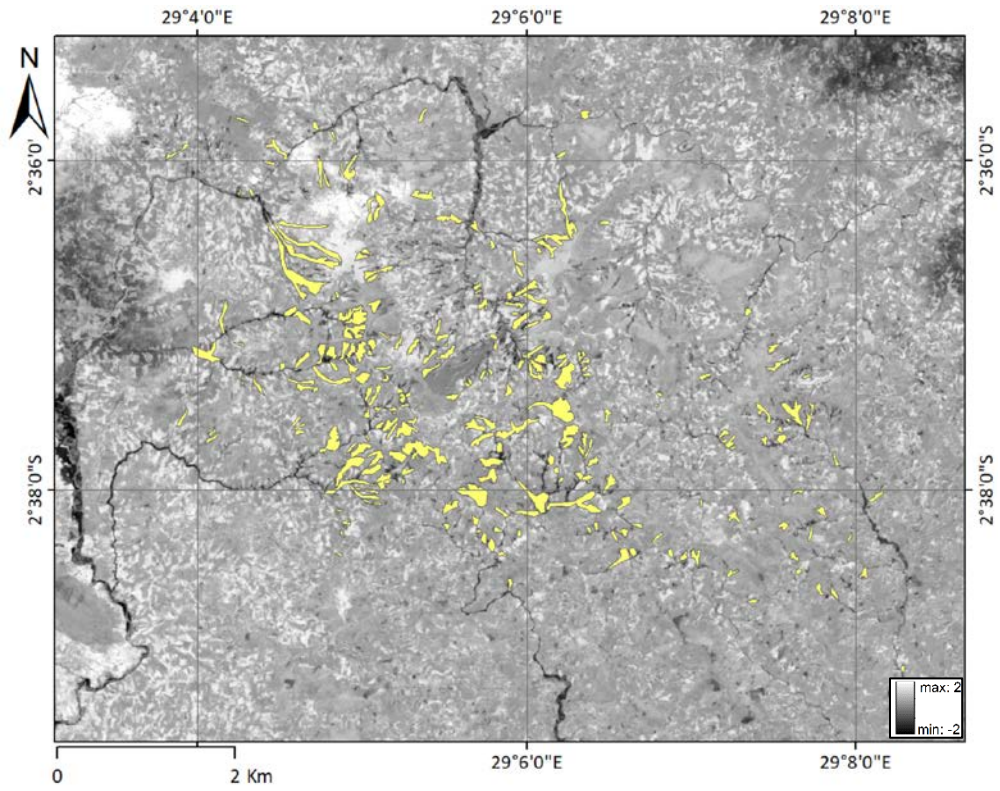


Figure 20.  $\delta$ NDVI images with mapped landslides at Site A (December 4, 2019, Nyempundu, Burundi)

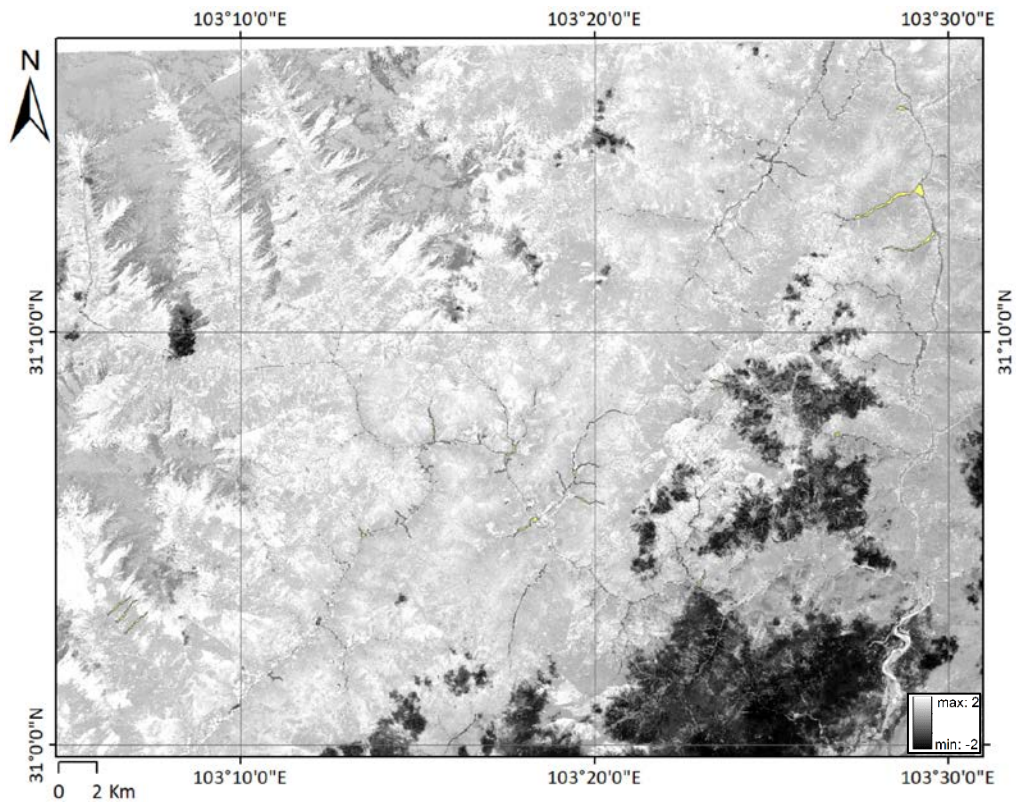


Figure 21.  $\delta$ NDVI images with mapped landslides at Site B (August 17, 2019, Wenchuan, China)

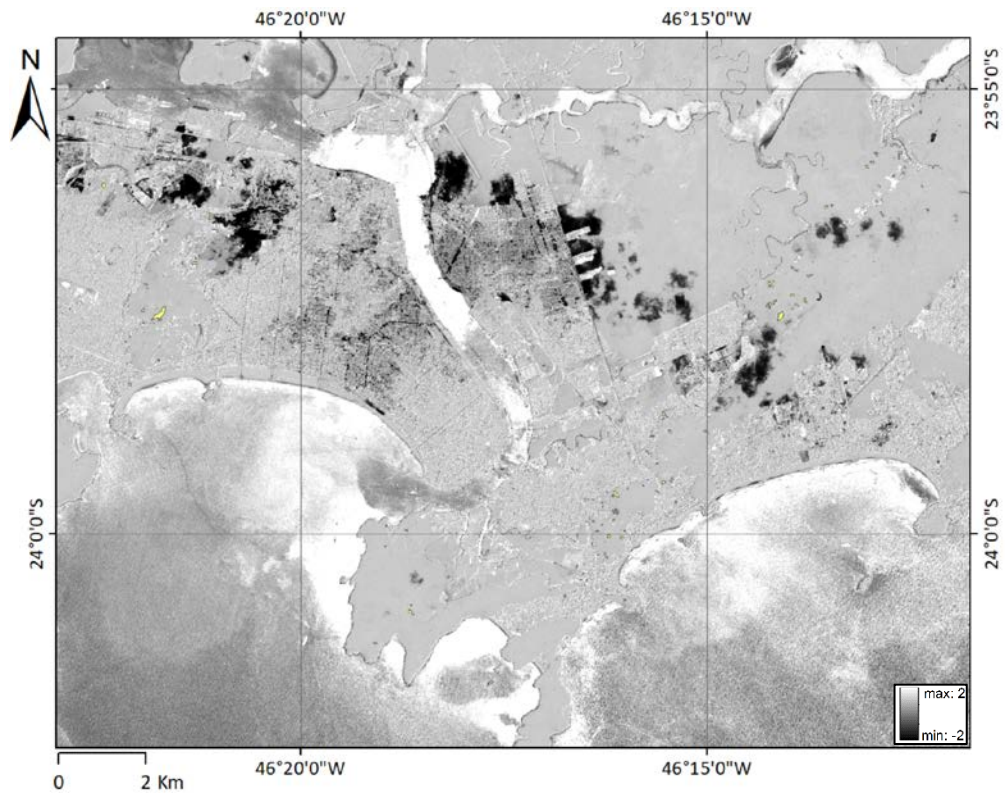


Figure 22.  $\delta$ NDVI images with mapped landslides at Site C (March 3, 2020, Baixada Santista, Brazil)

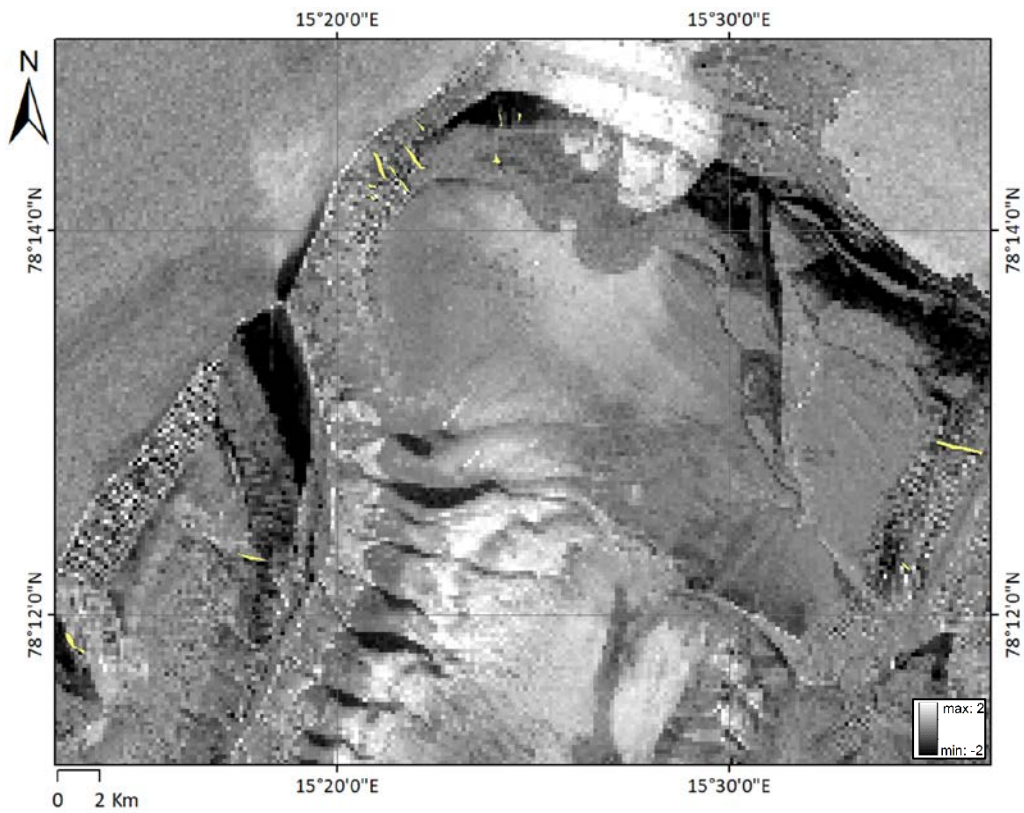


Figure 23.  $\delta$ NDVI images with mapped landslides at Site D (October 15, 2016, Longyearbyen, Svalbard)



## Clouds

Sites A and C have ideal conditions for  $\delta$ NDVI landslide mapping, with cloud free post-event images 10 and 4 days after, respectively. Site B in a region that is notoriously cloudy, boasting the least sunshine hours per year in the whole of China (Wilson & Jetz, 2016). It was therefore necessary to use a wide window for pre- and post-event images, making it impossible to differentiate between landslides that occurred on different dates. Site D occurred in a cloudy region, two weeks before the polar night began (24 hours of darkness) (Time and Date AS, 2020), making the window to acquire a cloud free image very narrow, so images from the summer before and after were used instead. On average, the pre-event images are taken 63 days before the event and the post-event images are taken 18 days after, excluding site D, or 98 days after including site D.

## Vegetation and Erosion

Sites A, B, and C had lush green vegetation, showing a clear landslide signature. In site B, it is challenging to differentiate river erosion from debris flows, but this shows the usefulness of  $\delta$ NDVI in mapping river, shoreline, or coastal erosion. On the slopes in site A, a large landslide appears fresh in false colour infra-red but is clearly differentiable as a previous event using change detection. The usefulness of  $\delta$ NDVI, rather than simply using false colour infra-red is illustrated clearly in this case, as seen in Figure 24.

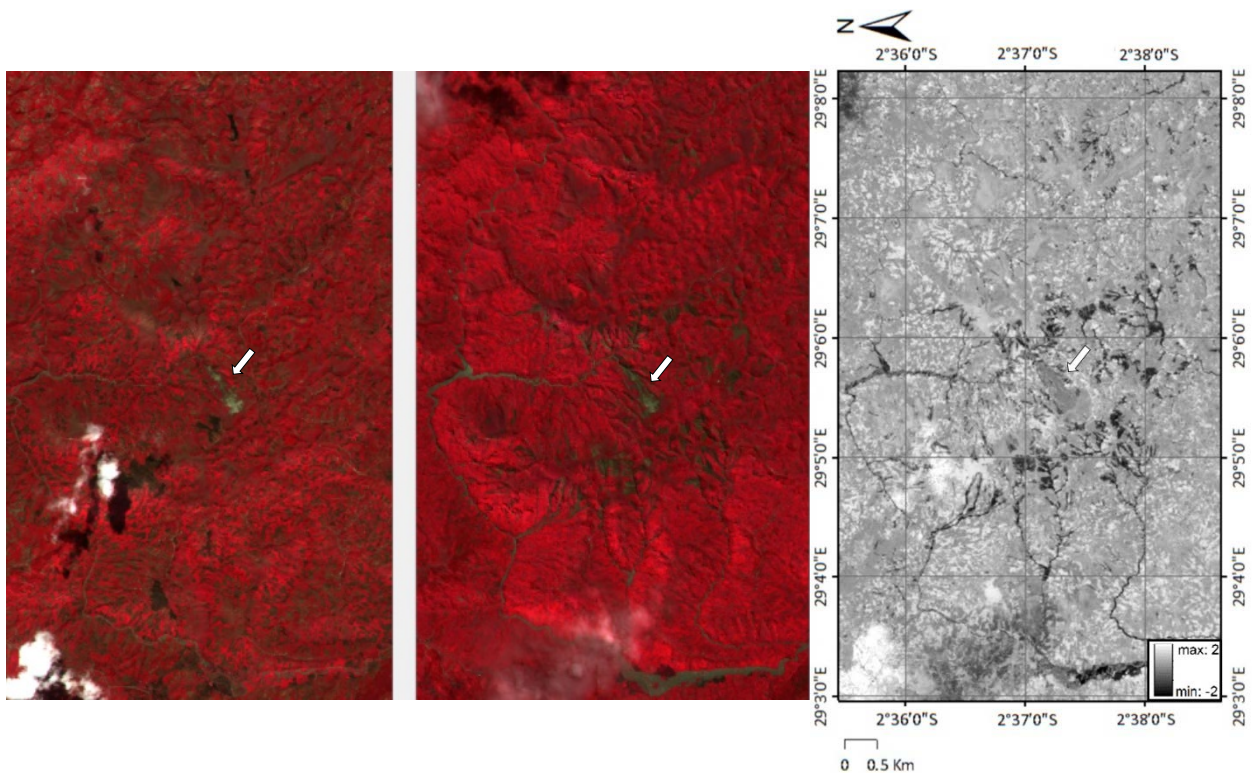


Figure 24. Comparison of false colour infra-red before and after, and  $\delta$ NDVI change detection, with arrows pointing to a large landslide scar from a previous event (Site A, December 4, 2019, Nyempundu, Burundi)

## Urban Environment

Urbanization was not found to be a significant obstruction in mapping site C, likely because the NDVI changed significantly in the path of the debris flow, removing all infrastructure in its path.  $\delta$ NDVI proves, in this case, to be highly successful in an urban environment. Sites A and B, while less densely urbanized, also had no hinderance from the urban environment.

## Arctic Conditions

Conditions in site D were moderate, despite obvious limitations of the arctic. The largest landslides are easily detectable using the  $\delta$ NDVI change detection method. Low vegetation mass, high cloud cover, and very low sun angles causing large shadows, make small landslides stand out less, but many advantages benefit the use of  $\delta$ NDVI in the Arctic. Slow vegetation regrowth on landslides scars, the evenness of the vegetation cover, and a moderate number of cloud free days in summer. The arctic is also relatively free from construction and man-made changes in landscape. This method shows high potential in the arctic due to the added benefits of remote sensing in regions with low population and access. As permafrost continues to thaw, and mild conditions bring a larger portion of precipitation as rain (NCSS, 2019), landslides are expected to be an increasingly common hazard in the arctic (Hestnes, et al., 2016).  $\delta$ NDVI could be used to create an inventory of landslides over arctic regions, and in turn calculate a landslide triggering threshold.

### 4.2.4 Method Comparison & Opportunities

$\delta$ NDVI has far superior landslide detection and mapping success compared to SAR in the 21 selected case studies and four international test sites. Despite SAR having a significantly shorter temporal window of image acquisition (5 days before and 3 days after, on average), being unaffected by cloud cover and lighting, it is able to detect only 15 of 150 landslides. SAR was not successful in any conditions, but results do indicate that larger landslides are more easily detected, but it is likely that typical soil landslides with shallow soil cover on steep slopes, are too shallow and small in area to be detected.  $\delta$ NDVI was able to detect 73 of 161 landslides, despite the relatively long temporal window of image acquisition (36 days before and 35 days after, on average). It performs poorly when snow is present, and it is significantly hindered by poor lighting, cloud cover, and if the size of landslide is extremely small ( $>1000 \text{ m}^2$ ).

In the best conditions for both methods, a relatively large landslide, in a forest, on a NW facing slope, with no snow present, a debris flow in case 19 was mapped using both methods. Figure 25 illustrates that SAR intensity is able to detect the landslide, but it is not able to accurately map the size or location, and  $\delta$ NDVI is able to accurately map the landslide scar in detail.

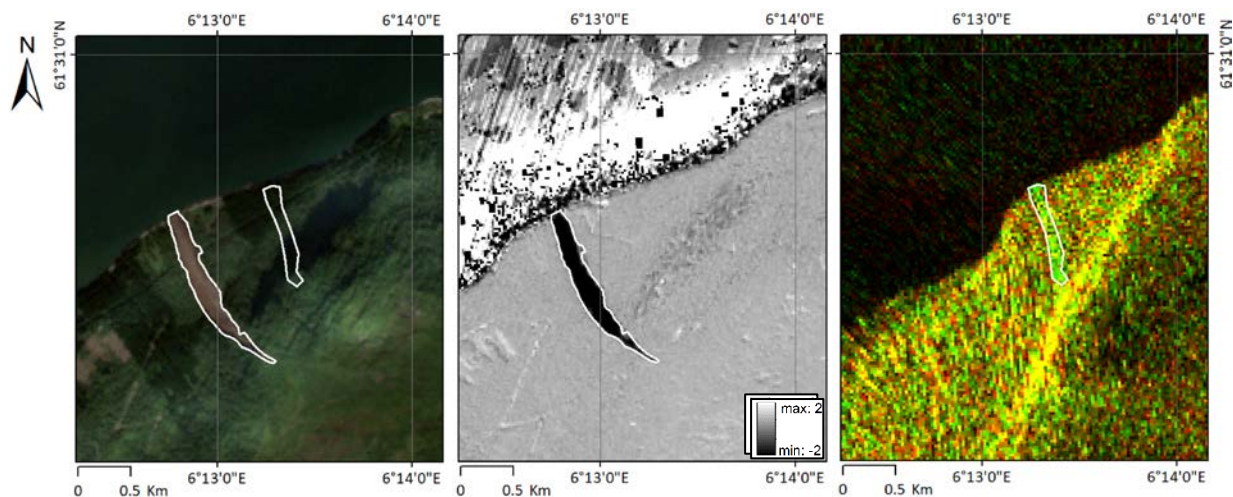


Figure 25. Comparison of  $\delta$ NDVI SAR mapped landslide (in white) on natural colour optical image (left),  $\delta$ NDVI (centre), and SAR intensity (right) in case 19

In remote or inaccessible regions, such as the arctic, war zones, or high alpine terrain, remote sensing has added value. Not only can it reduce costs, it can increase coverage compared to traditional mapping methods.  $\delta$ NDVI has been proven successful in a wide range of extreme conditions and could be used for landslide detection in essentially any inaccessible region.

The  $\delta$ NDVI technique is time consuming. The author found that it takes under one hour to download and process satellite data and identify a single landslide using a known location, but to download and map an entire satellite image tile (1500 km<sup>2</sup>), it takes approximately four to six hours. The time needed is lowest in cases with extremely clear landslide scars (such as case 19). This warrants the development of an automation process. A semi-automatic landslide inventory using  $\delta$ NDVI is deemed highly viable for rainfall induced soil landslides >1000 m<sup>2</sup> in Norway. The  $\delta$ NDVI value identifying landslide scars studied have an inexact signature that generally range between +0.2 to -1.0 in the studied cases. The  $\delta$ NDVI value based largely on the vegetation present before, the proportion of each pixel affected, and the time that has passed between images. By additionally using the shape of landslides mapped and overlaying slope, geology, and susceptibility maps, a more unique signature would be obtained. The automation process would be also improved with object identification, the removal of clouds and waterways. The landslides mapped in this study could be used as data input to train a machine learning model to detect landslides.

#### 4.2.5 NVE Landslide Database Limitations

While the Norwegian landslide database is advanced compared to those available in other regions of the world, it still has many limitations. Most notable limitations are a temporal bias, a spatial bias, and reporting errors or limitations.

##### 4.2.5.1 Temporal Bias

Recorded landslides are heavily weighted to the 21<sup>st</sup> century, with 70% of the inventory after the year 2000, although there are events registered that occurred hundreds of years ago. This is mostly due to the systematic approach to landslide records that have been introduced as well as the challenges of collecting non-digital records. The recency bias makes conclusions regarding trend analyses over time generally unreliable. It is challenging to address with the proposed remote sensing techniques due to the lack of satellite data.

##### 4.2.5.2 Spatial Bias

The inventory of landslides in the NVE database are primarily recorded by the Norwegian road and rail authorities. The landslides are consequently spatially biased to those visible from, or damage road and rail infrastructure, rather than proximity to population density or landslide severity. This spatial bias results in an incomplete landslide database for future landslide forecasting. A systematic record of all of Norway would greatly improve the usefulness of the database for landslide forecasting (Devoli, et al., 2017).

Landslides registered in the NVE database show a clear spatial bias to transportation routes. Of the landslides studied, 91% lie within 100 m of a road. Figure 26 is a road map with the landslides registered in the NVE database in case 2 in the county of Sogn og Fjordane, with a clear spatial bias to roads. It is therefore expected that recorded events represent only a fraction of the landslides that have occurred.

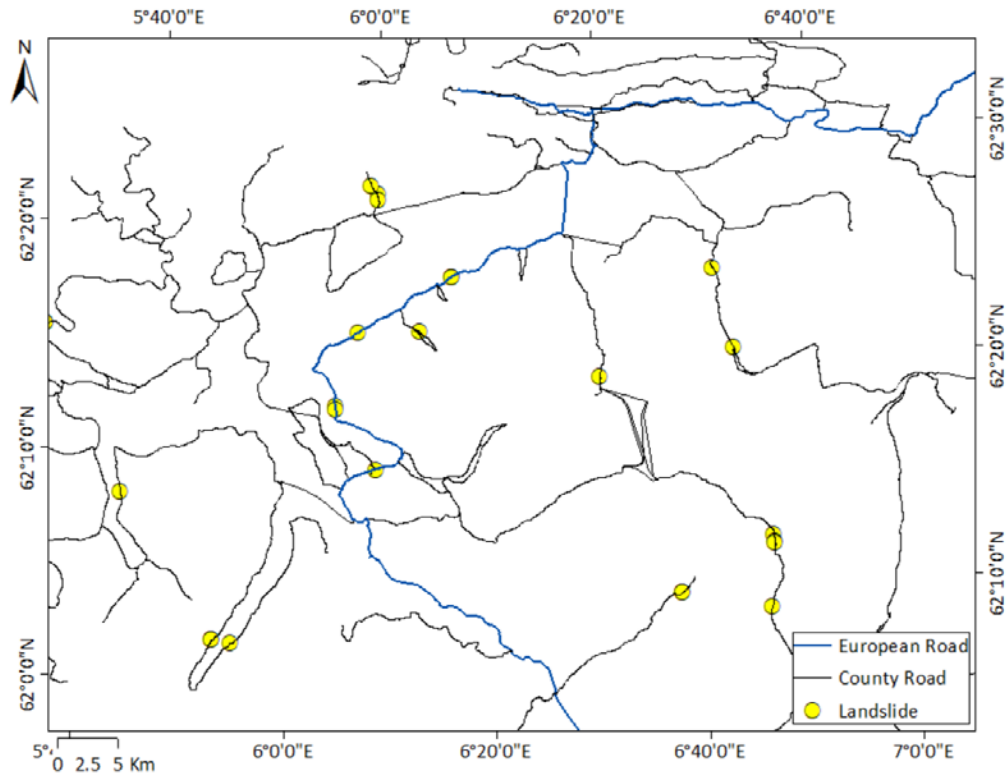


Figure 26. Road map with landslides registered in NVE landslide database in case 2 (November 26, 2015, Sogn og Fjordane) (road data downloaded from kartkatalog.geonorge.no (Kartverket, 2016))

In contrast, only 45% of the landslides mapped with  $\delta$ NDVI lie within 100 m of a road. In case 19, which had the best conditions for  $\delta$ NDVI mapping, just 16% were within 100 m of a road. These statistics indicate that the use of  $\delta$ NDVI mapping could substantially reduce the spatial bias of landslides to transportation routes. A histogram of landslides registered and mapped and their respective distance to a road is presented in Figure 27.

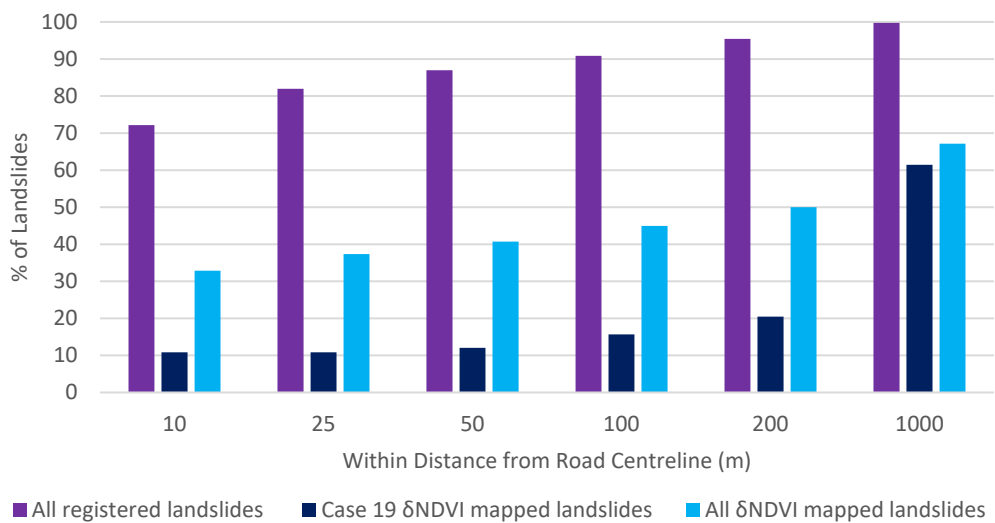


Figure 27. Distance of registered and  $\delta$ NDVI mapped landslides from road centreline

#### 4.2.5.3 Metadata

Each registry has 36 metadata of recorded information about the landslide. The landslide type, uncertainty of time and location of occurrence are inspected for information on potential difficulty in mapping incomplete or incorrect registries.

A third of the studied landslides are classified as type 140, an unspecified landslide in soil. While this is not in error, and superior to an erroneous classification, the use of an unspecified classification reduces the value of the database entry. It is challenging to make conclusions regarding landslide processes and triggers without proper classification. A summary of registered landslide types for the Norwegian case studies is included in Table 15.

Table 15. Landslide types in Norwegian case studies

ID	Mass Movement Type				Total No. of Landslides	Dominant Type
	Landslide in Soil, unspecified (140)	Debris Flow (142)	Soil Slide (144)	Slushflow (133)		
1	5	0	7	0	12	Soil Slide
2	15	7	12	2	36	Landslide in Soils
3	11	6	13	6	36	Soil Slide
4	2	6	1	2	11	Debris Flow
5	8	10	16	1	35	Soil Slide
6	9	4	4	2	19	Landslide in Soils
7	5	4	2	0	11	Landslide in Soils
8	10	0	7	0	17	Landslide in Soils
9	1	1	9	0	11	Soil Slide
10	9	2	2	0	13	Landslide in Soils
11	17	5	7	0	29	Landslide in Soils
12	4	0	1	6	11	Slushflow
13	10	3	10	0	23	Landslide in Soils
14	15	4	11	0	30	Landslide in Soils
15	4	0	15	3	22	Soil Slide
16	0	4	8	0	12	Soil Slide
17	0	0	11	0	11	Soil Slide
18	0	1	11	0	12	Soil Slide
19	1	23	18	0	42	Debris Flow
20	0	5	0	1	6	Debris Flow
21	0	12	4	1	17	Debris Flow

Registered landslides have fields for uncertainty of location and time of occurrence. Of the 418 selected registered landslides, 50 have an uncertainty of location of 100 m or greater, making it problematic to confirm their location when mapping. Fourteen of these were analyzed using  $\delta$ NDVI and nine (64%) were undetected. Notably, three are landslides in case 14. Another 33 have undocumented uncertainty in location, 24 (73%) of which were not detected using either mapping method. Documentation of the uncertainty of time of occurrence has only two events with uncertainty greater than one day. Eleven landslides had an undocumented uncertainty of time.

In conditions that allow  $\delta$ NDVI mapping, the uncertainty of location can be reduced entirely. The uncertainty of time, however, may worsen when using  $\delta$ NDVI alone, due to the long temporal window of pre- and post-event images. An estimate of landslide area could be automatically generated, as was completed in this study. With a known location, it is also much easier to classify the landslide type properly. Although landslides were not re-classified in this study, it is believed that all unspecified landslides could be recategorized when  $\delta$ NDVI mapping is possible. Improving landslide classification would make it possible to create thresholds for different types of landslides.

### 4.3 Landslide Prediction

#### 4.3.1 Landslide Database Trends

The 8490 registered shallow soil landslides in the NVE database are divided nearly equally by season. When considering only days that had ten or more landslides occur, there are significantly more events occurring in autumn and winter. Days with ten or more landslides have occurred, on average, 4.6 times per year for the past five years, over half of which occurred in winter and over three quarters in winter or autumn. Similarly, the majority of flood events in Norway occur from August to December as a result of intense rainfall from remnants of tropical storms, convective rainstorms, and snowmelt in mild temperatures (Roald, 2008). The seasonal distribution of landslides registered and days with >10 soil landslides that have occurred over the past two decades are illustrated in Figure 28. A comparison is made between those recorded in 2000-2014 and 2015-2019.

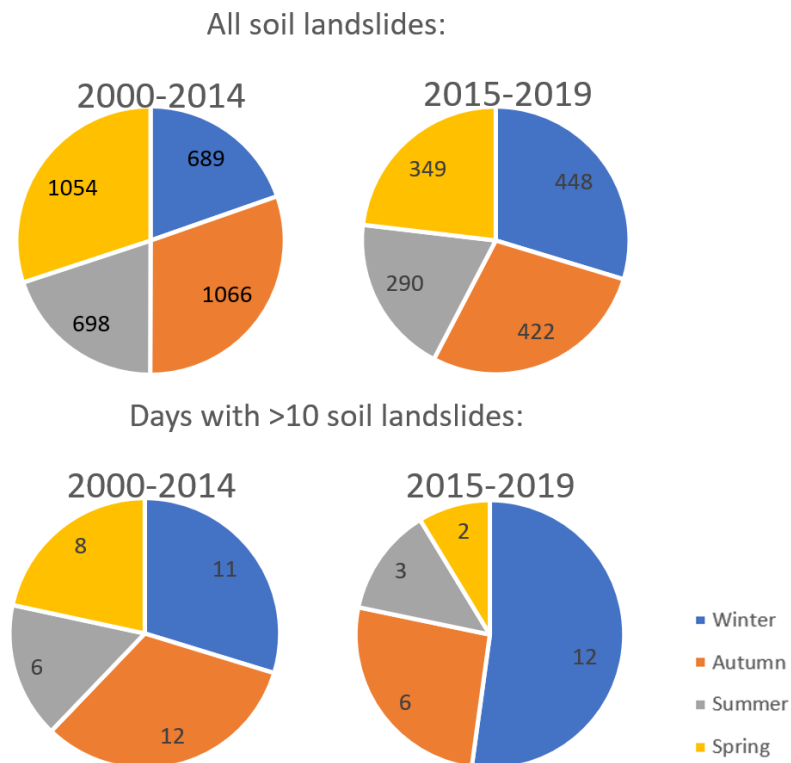


Figure 28. Seasonal distribution of landslides registered in the NVE landslide database from 2000-2019

An increased proportion of registered winter landslides is observed in 2015-2019 compared to 2000-2014. This is observed in and an even more substantial increase exists when looking only at days with

more than ten landslides. This increase could be attributed to external factors, such as an increase in reporting, but it is hypothesized that this change reflects recent climatic changes that increase the likelihood of landslides during colder months. There has been an increase of precipitation falling as rain in winter, milder winter temperatures, and warmer spring air temperatures resulting in warmer ground temperatures, shallower frost depth, shorter winters, and early melt (NCSS, 2019), all of which increase the probability of shallow soil landslides. Caution is taken in the conclusion that the increase of winter events is climate change related due to the recency bias discussed in Section 4.2.5.1.

Multiple landslide events also have spatial trends by season. An analysis of the 21 case studies illustrates that spring events are restricted inland, where temperatures are cold throughout the winter and springtime thaw combined with frontal precipitation trigger landslides. Summertime events occur all throughout Southern Norway and have the least spatial bias. Autumn events are restricted to the coast in southern Norway and are often storms that lose most of their moisture when they precipitate due to orographic lifting as they hit the west coast. Winter events are restricted to the west coast but are common across the length of Norway. Figure 29 illustrates the spatial distribution of the selected landslide case studies that occurred in each season.

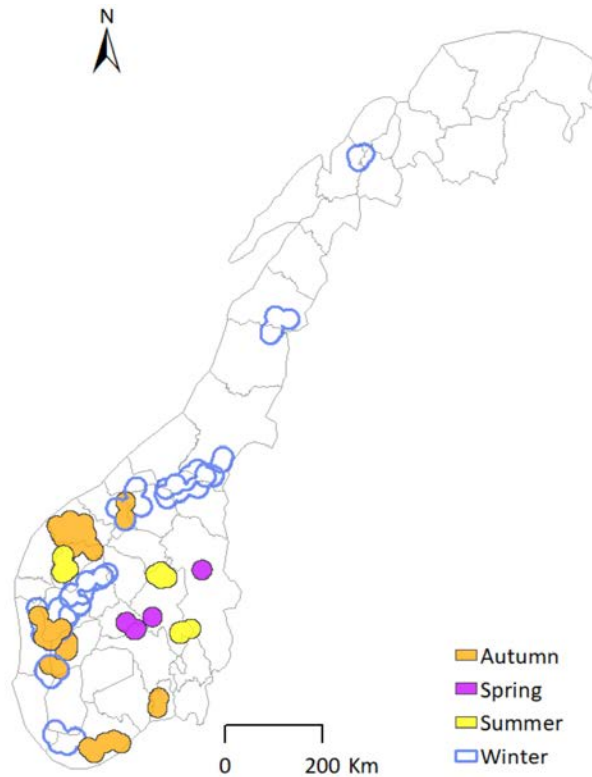


Figure 29. Spatial distribution of selected case studies, identified by season

#### 4.3.2 Susceptibility Mapping

Susceptibility classes of terrain in Norway are divided into thirds with very high (31%), high and medium (13% and 23%), and low (33%). For the Norwegian case studies, both the registered landslides and the  $\delta$ NDVI mapped polygons were mapped on the catchment level susceptibility map to quantify how much they can aid in predicting where landslides will occur. Figure 30 is a histogram of the number of

landslides falling into each of the four classes, showing that the large majority of landslides are in the very high susceptibility class.

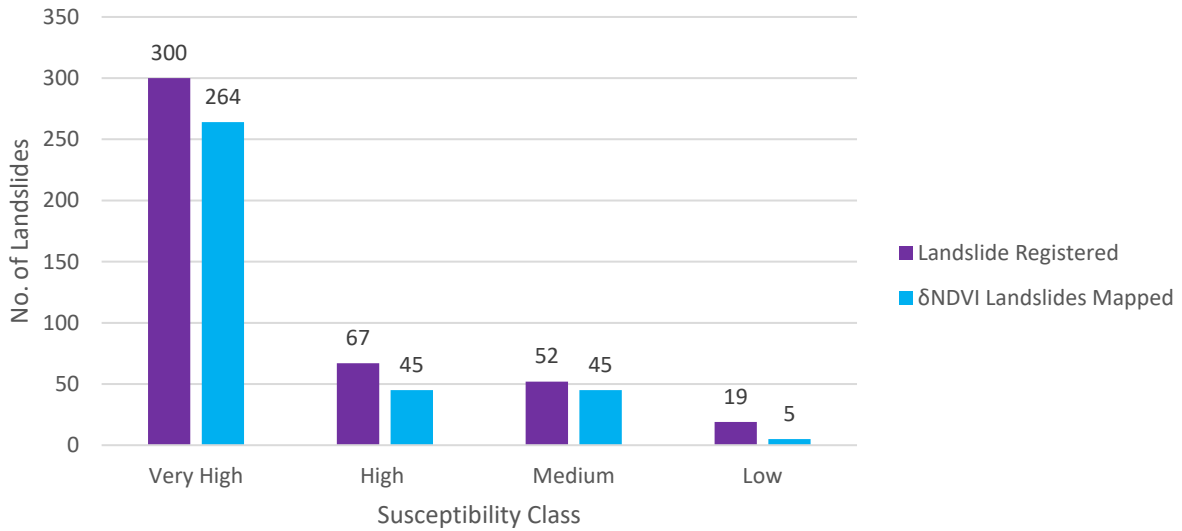


Figure 30. Histogram of landslides recorded and mapped in the catchment level landslide susceptibility classes

84% and registered landslides and 86% of  $\delta$ NDVI mapped landslides are located in zones mapped as high or very high. These results indicate that the catchment level susceptibility maps are extremely well calibrated and are a very useful tool for landslide forecasters, emergency responders, urban planning, and for education for the public.

#### 4.3.3 Quaternary Geology Mapping

Using the large-scale quaternary geology map, a similar ratio of the mapped landslides and registered landslide points fall into each classification. Surprisingly, over 50% of landslides are within bare bedrock polygons, indicating that soil mapping at this scale is not helpful to a landslide forecaster. The mapped polygons are 78% in bare bedrock polygons, and registered landslides points are 55% in bare bedrock polygons. The latter is lower as a consequence of the point location, which is most often on a road at the end of the runout, and more likely to have a thick soil cover. Bare bedrock suggests that a soil landslide could not be initiated. While the bedrock mapped could be deceiving, it does inform the forecaster of high runoff in these areas. Bare bedrock polygons, at this scale, should instead be understood as high runoff areas, with sufficient regolith for mass movement. Notably, the ratio of the entire map that is bare bedrock is exactly 50%. Till and colluvium are the second and third most common soil types landslides are mapped in large-scale, both having potential for a rapid increase in pore water pressures due to their fine-grained component.

The mapping may be correct at a large scale, a smaller scale would reveal a thin sporadic cover, often with enough volume to have large, high consequence, soil landslides. The small-scale map also had similar ratio of quaternary geology types between the mapped landslide polygons and registered landslide points, but these differ greatly from the large-scale map. With the added precision, till makes up nearly half of the intersections, followed by colluvium and bedrock at approximately one fifth each. The glaciofluvial and fluvial intersections make up a combined approximate 10-15%. This is likely an



indicator of terrain that is prone to landslides, rather than soil stability. It is, again, likely that the bedrock polygons have pockets of organics and till.

An example of a debris flow initiated in an area mapped as bare bedrock at both large and small scales is illustrated in Figure 31. Substantial pockets of moss covered till can be seen. This debris flow intersects colluvium and till at lower elevations, entraining significant material volume.



Figure 31. Debris flow initiation zone with quaternary geology mapped as bare bedrock at a scale of 1:250,000 (case 19, July 30, 2019, Sogn og Fjordane) (Photo credit: Lena Rubensdotter, NGU)

See Figure 32 for a complete histogram of the number of intersections of landslides with each soil type.

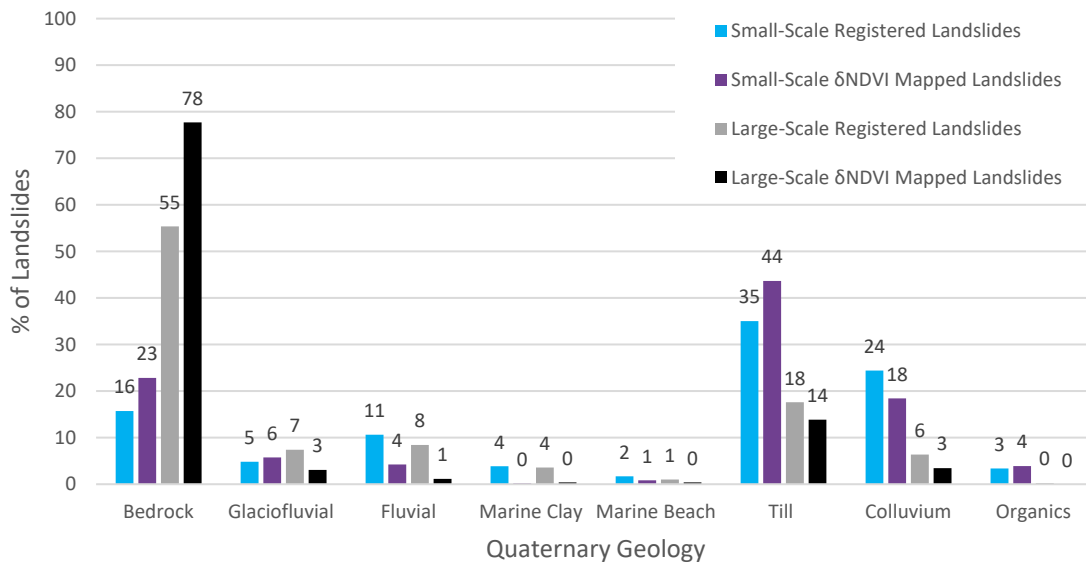


Figure 32. Large- and small-scales quaternary geology map intersections with registered and  $\delta$ NDVI mapped landslides

The analysis of large-scale quaternary geology maps shows limited usefulness, and rather, that they can be potentially misleading. In the absence of small-scale quaternary geology maps, which are often unavailable in remote or low populous areas, a large-scale map is little to no aid in landslide forecasting. Small scale geological mapping, that is often completed for more densely populated areas, should be a priority along infrastructure and low populous areas to improve susceptibility mapping, threshold models, and the resulting landslide forecasts. The 1:250, 000 scale maps clearly show that till and colluvium are the most landslide prone quaternary geology types, but the high proportion of landslide intersections with bare bedrock illustrates the need for more precise soil mapping.

#### 4.3.4 Weather

##### 4.3.4.1 Data

All 21 cases are induced by rainfall and/or snowmelt. Six cases are rainfall induced only and fourteen cases are rainfall and snowmelt induced. Case 15 is the only event with no rain (under 1 mm).

Rain gauge precipitation, snowmelt from the NVE Snow Map Model at the weather station, and mean annual precipitation for all years on record for the selected case studies are presented in Table 16, with information about the years on record and weather station location included in Appendix E.

*Table 16. Precipitation during event (1-, 3-, 24-hr) and mean annual precipitation from rain gauges (Meteorologisk institutt, 2020b)*

ID	Rain gauge (mm)			Weather Station	Mean Annual Precipitation (mm)	Snow Map Model
	1 hr	3 hr	24 hr			Snowmelt in equivalent water (mm)
1	7.5	15.9	53.3	Gvarv-Nes	841	0
2	6.5	17.7	88.6	Ørsta-Eitrefjell	1924	8
3	8.9	24.1	139.2	Elk-Hove	2596	10
4	7.1	14.2	41.9	Innerdalen	1396	10
5	4.5	9.9	29.2	Trondheim-Voll	851	10
6	8.1	23	90	Myrkdalen-Vetlebotn	1171	9
7	5	13.4	56	Innerdalen	1396	11
8	5.4	13.7	79.7	Glomfjord-Skihytta	1993	10
9	6.6	18.5	45.7	Rena-Ørnhaugen	687	3
10	10.5	29.5	52.4	Skåbu	692	0
11	11.7	31.9	75.9	Åseral	1684	0
12	10.6	18.8	83.9	Sauda	2164	6
13	9.1	25.1	82	Kvamskogen-Jonshøgdi	3128	7
14	11.3	29.3	125.7	Sauda	2164	15
15	1	2	2	Vest-Torpa II	860	19
16	15.7	45.7	138.8	Gullfjellet	3128	0
17	2.3	5.3	23	Trondheim-Voll	851	11
18	15.1	25.5	35.6	Hamar II	1154	0
19	22.8	43.6	113.6	Haukedal	2157	0
20	4	7.6	37.6	Malangen-Pålfinnmoen	1064	10
21	5.3	12	76.2	Vangsnes	1171	10

Snowmelt, when present, is a small proportion of water supply. It plays an important role, however, hence its presence in two thirds of cases. Snowmelt causes widespread pore water pressures to rise,

generates high overland flow and surface water, and leads to increased erosion. The contribution of mid-winter thaw events, and the role of snowmelt to the initiation of landslides is difficult to quantify with water supply alone. Further study of this concept is required.

The mean annual precipitation, for all years on record, and the absolute water supply, the sum of precipitation and snowmelt, at selected weather stations, are illustrated in a map of Norway in Figure 33.

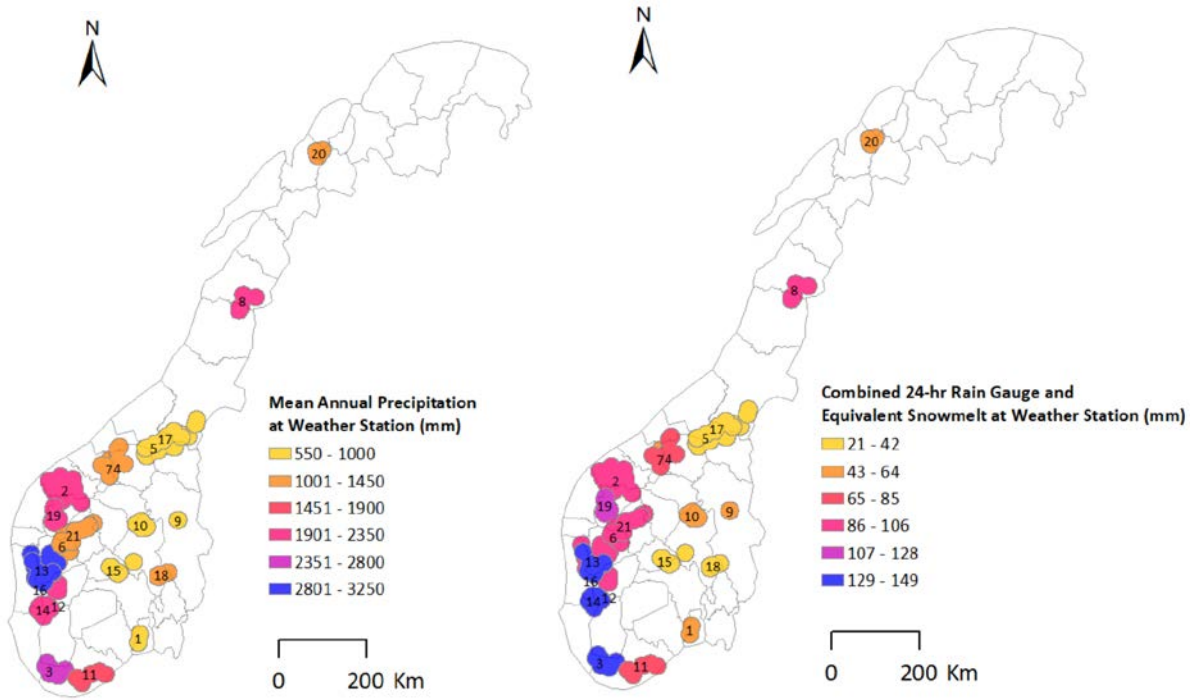


Figure 33. Mean annual precipitation at weather station for all years on record (left) and 24-hour water supply at weather station from rain gauge and snowmelt model (right)

A clear correlation of initiation water supply to the mean annual precipitation can be seen (i.e. the west coast has higher MAP and 24-hour precipitation than the east, and vice versa). This indicates that absolute water supply required to induce landslides is relative to the local precipitation. The combined precipitation and equivalent snowmelt from the seNorge v2.0 model results are presented in Table 17.

Table 17. seNorge v2.0 24-hr precipitation and equivalent snowmelt maximum and mean of grid over case study area data from (NVE, 2020a)

ID	seNorge v2.0 24-hr Combined Precipitation and Equivalent Snowmelt	
	Mean (mm)	Maximum (mm)
1	62	112
2	61	140
3	112	187
4	33	88
5	30	89
6	22	107
7	26	101
8	55	143
9	30	60
10	47	97
11	123	196
12	30	121
13	72	164
14	101	187
15	17	29
16	75	153
17	22	71
18	23	81
19	33	168
20	15	67
21	45	146

These values are mean and maximum of all pixels in the defined case study area. Areas are as illustrated in Section 4.1.1. The mean ranges from 15-123 mm and the maximum ranges from 29-196 mm. This wide range suggests that absolute values cannot be used as thresholds for landslides in Norway due to the variety in conditions. It is expected that had point values been taken for each landslide, as is done in threshold studies, the results would be more narrow.

Other weather and hydrological conditions recorded for each event are included in Table 18.

*Table 18. Weather and hydrological factors recorded for Norwegian case studies from a selected case study landslide on xgeo.no relative to reference years 1981-2010*

<b>ID</b>	<b>Degree of Soil Saturation</b>	<b>Groundwater level compared to normal</b>	<b>Frost depth compared to normal (depth)</b>
<b>1</b>	>90%	Very high	No frost
<b>2</b>	70-80	Very high	No frost
<b>3</b>	>90%	Very high	No frost
<b>4</b>	70-80	High	No frost
<b>5</b>	80-90	Very high	No frost
<b>6</b>	80-90	Very high	No frost
<b>7</b>	80-90	Very high	Normal (Shallow)
<b>8</b>	>90%	Very high	No frost
<b>9</b>	>90%	Very high	No frost
<b>10</b>	<60%	Very high	No frost
<b>11</b>	>90%	Very high	No frost
<b>12</b>	70-80	High	No frost
<b>13</b>	>90%	Very High	Normal (Shallow)
<b>14</b>	>90%	Very high	Normal (Partly frozen)
<b>15</b>	>90%	Very high	Deep (Moderate)
<b>16</b>	70-80	High	No frost
<b>17</b>	80-90	Very high	No frost
<b>18</b>	60-70	Very High	No frost
<b>19</b>	<60%	Very High	No frost
<b>20</b>	60-70	High	Normal (Shallow)
<b>21</b>	>90%	Very High	Shallow (Partly frozen)

Degree of soil saturation varies but is generally high and above 80%. Soil saturation is challenging to accurately estimate and may not be reliable. It is, however, an extremely important variable in landslide prediction. As soil saturation rises, friction between particles is reduced by water in the pores, and the effective strength of the soil is reduced. For fine grained and poorly draining soils, such as the till that is smeared on many slopes in Norway, pore water pressures rise rapidly and are slow to drain. This indicates, again, that geological mapping is of high importance for landslide forecasting. In the absence of reliable soil saturation estimates, instruments to measure soil saturation at the slope scale could be used to calibrate regional models or monitor vulnerable areas.

Groundwater level compared to normal for that day of the year is an extremely strong predictor, given that it is High for four cases and Very High for seventeen cases. Groundwater levels can reliably be measured where piezometers are installed and are directly related to surface water measurements and may be a reliable indicator of landslide susceptibility.

Frost is only present in seven cases, despite snow being present in fifteen. In those cases that frost is present, the ground is only partly frozen or shallow in all but one. It is surprising that soil landslides can occur at all when frost is present, and even more surprising given the number of landslides triggered. It is possible, given the shallow depth of frost, that the failure plane is located below the frost, and that the frozen layer acts as a cap to saturate the water below. Frost may play an important role and more attention should be given to landslides that occur when the ground is frozen.

#### 4.3.4.2 Normalized Water Supply

Absolute values for landslide initiation water supply in the selected case studies vary widely. Normalized water supply is therefore calculated to determine if it has a closer relationship with landslides. The normalized water supply values of both point values at the weather stations and area values taken across the case studies, mean, maximum, and difference between mean and maximum, are presented in Table 19.

Table 19. Normalized 24-hr Water Supply from weather stations points and mean and maximum seNorge v2.0 areas

ID	Normalized Combined 24-hr Rain Gauge and Equivalent Snowmelt (point data) (%)	Normalized seNorge v2.0 24-hr Combined Precipitation and Equivalent Snowmelt (area data)		
		Mean (%)	Maximum(%)	Maximum-Mean (%)
1	6.3	7.3	12.6	5.3
2	5.0	3.3	6.7	3.4
3	5.7	4.1	7.2	3.1
4	3.7	2.9	6.3	3.4
5	4.6	3.6	10.5	6.8
6	8.5	3.9	9.1	5.2
7	4.8	3.2	7.2	4.1
8	4.5	3.6	7.2	3.5
9	7.1	4.3	8.7	4.4
10	7.6	6.9	13.4	6.5
11	4.5	7.1	11.1	4.0
12	4.2	2.4	5.6	3.2
13	2.8	2.2	5.2	3.0
14	6.5	4.9	8.6	3.8
15	2.4	2.0	3.4	1.4
16	4.4	2.3	4.6	2.3
17	4.0	2.3	8.3	6.1
18	3.5	2.2	6.7	4.5
19	5.3	1.6	7.3	5.6
20	4.5	2.7	6.3	3.6
21	7.4	5.4	12.5	7.1
<b>Range</b>	2.4 – 8.5	1.6 – 7.3	3.4 - 13.4	1.4 – 7.1

The point data value is between the mean and maximum values in the large majority of cases (19/21). The two cases that it does not (case 1 and 11) demonstrate the importance of not relying on point data for water supply, as they not only don't capture the peak, they don't even capture the average. Interpolated datasets, such as seNorge v2.0, take into account all available point data to create a smoothed grid.

It is possible, however, that the peak of the storm is not captured in either data source. For example, a weather station at the base of a valley would not capture the additional snowmelt on south facing slopes compared to north facing slopes, nor would it capture the rainfall shadow on the leeward side of a mountain peak. These factors can be captured by a weather model, but in highly concentrated rainstorms, the peak can be missed. This is especially possible in convective rainfall, where rainfall is highly concentrated. The difference between the maximum and mean water supply, included in Table 19, is an indicator of how the spatial concentration of water supply. Values higher than five are considered "concentrated", those less than 3.5 are considered "even".

Calculated normalized water supply from point source at weather station and the mean and maximum over the case study areas are illustrated in Figure 36. The scales have the same number of equal divisions with different values to illustrate that the values differ but are mostly in the same relative order and thus colour.

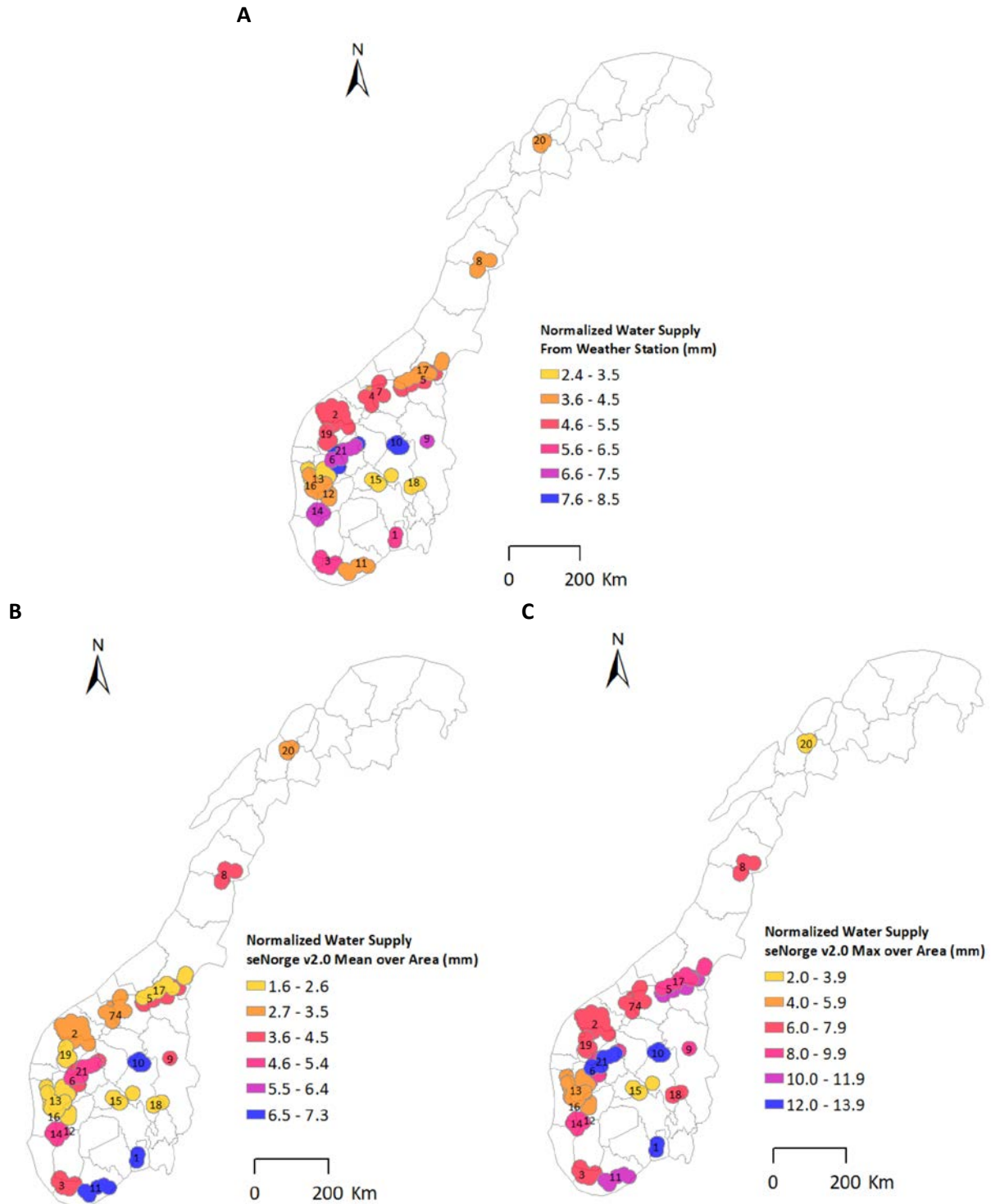


Figure 34. Normalized 24-hr initiation water supply from A: weather station rain gauge and modelled snowmelt B: mean seNorge v2.0 and C: maximum seNorge v2.0

Normalized 24-hour precipitation, calculated as a percentage of the annual mean precipitation, has a clear relationship with landslide occurrence. Three cases (13, 15, and 18) have very low normalized 24-hour water supply and stand out as outliers in their initiation threshold, and thus more challenging to forecast. Cases 15 and 18 occurred in the spring in Eastern Norway, and despite having low 24-hour precipitation and snowmelt, can be better explained by having a high water table, elevated from the spring melt, which occurs more seldom through the year. These are challenging to forecast as they were induced by insignificant absolute and relative water supply. It is expected that many landslides in Eastern Norway are induced by very low absolute water supply and the region would have many false alarms if thresholds were reduced to accommodate them. Regional thresholds have been implemented in some regions to account for these differences (Krøgli, et al., 2018). Case 13 had an especially high antecedent rainfall and snowmelt. It occurred in December and had a 3-day antecedent water supply over twice in magnitude than the 24-hour water supply.

Previous studies found the correlation of relative rainfall stronger than absolute rainfall (Meyer, et al., 2012) and that absolute rainfall severely underestimated landslides (Groenemeijer, et al., 2016). 24-hour precipitation is found to be the strongest correlating weather factor by others (Devoli, et al., 2017). Both of these results are confirmed in this study. Snowmelt is an important factor, but rainfall has a much more significant role. Antecedent conditions, particularly groundwater level relative to normal, is a very strong indicator, and is high or very high in all selected cases. Absolute water supply for initiation has an extremely wide range in these cases, and while normalized water supply is more indicative, it is not always exceptionally high. This result indicates that rainfall and snowmelt alone cannot predict landslides, despite a strong correlation in the majority of selected cases.

#### *4.3.4.3 Return Period*

Return periods of the combined rain gauge rainfall and equivalent snowmelt model are obtained for 1-, 3-, and 24-hour durations, and the highest value is selected. These show that not all case studies experienced extreme intense rain or snowmelt. Five cases have return periods 200 years or more, but thirteen cases have return periods of five years or less. The return periods of all case studies are included in Table 20 and IDF curves are included in Appendix E.



Table 20. Return period of rainfall and snowmelt of case studies

ID	Return Period of combined rainfall and snowmelt (years)
1	2
2	100
3	50
4	5
5	<2
6	2
7	25
8	>200
9	25
10	200
11	5
12	<2
13	5
14	10
15	<2
16	>200
17	<2
18	2
19	>200
20	>200
21	2

Due to the fact that IDF curves are found to be strongly correlated to landslide initiation in other studies, these results are deemed unreliable. It is expected that the weather stations chosen to collect precipitation and snowmelt are too far or have dissimilar conditions to the IDF curves used. Many weather stations have too few years on record (minimum ten years) to capture extreme highs and lows to create a reliable IDF. The reference IDF's chosen were deemed the most reliable data available but illustrate that an IDF curve should be used with caution. In theory, an IDF cannot not be interpolated further than the number of years used to build it, and they should not be extrapolated regionally unless conditions are consistent.

#### 4.3.4.4 Weather Categorization

Weather is grouped into six main categories, as defined in Section 3.3.4.4. The categorizations for the Norwegian case studies are presented in Table 21.

Table 21. Weather categorization and storm name for Norwegian case studies

ID	Storm Name	Weather Code	Weather Categorization
1	Petra	B	Intense concentrated rainstorm
2		F2	Heavy rain on snow
3	Synne	F2	Heavy rain on snow
4	Urd	F2	Rain on snow
5		F2	Rain on snow
6		F2	Heavy Rain on snow
7	Following Vidar	F2	Rain on snow
8	Following Vidar	F2	Heavy rain on snow
9		E	Wet antecedent conditions and moderate rain
10		B	Intense concentrated rainstorm
11	Remnants of tropical cyclones Maria and Lee	A	Remnant of tropical cyclone
12	Ylva	F	Rain on snow
13	Aina	F1	Rain on snow with frost
14	Birk	F3	Heavy Rain on snow with frost
15		D	Rapid spring melt
16		C	Heavy widespread rainstorm
17		F2	Heavy rain on snow
18		E	Wet antecedent conditions and moderate rain
19		B	Intense concentrated rainstorm
20		F3	Heavy rain on snow with frost
21		F3	Heavy Rain on snow with frost

The most common weather type is F: rain on snow, accounting for 13/21 cases. These are subcategorized into those with intense rain, those with frost, and those with both. Only one event is a known A: remnant of a tropical cyclone, although there may be more that are not identified. The spring/early summer events are notably different and are categorized into D: rapid snowmelt and E: wet antecedent conditions and moderate rain. D is a rare event, as ground frost is still present, and the soil is relatively strong. For such an event to trigger landslides, extremely intense snowmelt must occur. E is the more common spring landslide case, in which the soil is vulnerable to even moderate rainfall due to extremely wet antecedent conditions leading to high runoff volumes. Rain can be C: evenly distributed or B: concentrated, both leading to different challenges in landslide forecasting. Even events require a large area to be on alert whereas concentrated events are difficult to predict accurately. Convective rainstorms are known to be highly concentrated and challenging for landslide forecasting. The eye of the storm can cause devastating consequences (e.g. Kvam 2014, Utvik 2017, Jølster 2019), but is relatively unpredictable.

The weather categorizations vary immensely between cases and demonstrate that many weather types can cause multiple landslide events. Those that are most challenging to predict for landslide forecasters will be identified in Section 4.3.6.

A reverse analysis, considering days that reach a threshold water supply, to evaluate if they induce landslides, was not completed. It is expected, based on return periods and normalized water supply that water supply thresholds are frequently exceeded without triggering landslides. It would be valuable to

consider days with specific weather types and how often they induce landslides. Of particular interest are days with rain on snow, which occur seldom in some areas, and are the most frequent weather type to induce the selected landslide events.

#### 4.3.4.5 *Landslides in a Changing Climate*

Projected climatic changes are predicted to increase the frequency of landslides in Norway, primarily due to an increase in total rainfall and rainfall intensity (Jaedicke, et al., 2008). An increase in air temperature results in the ability of air to carry more moisture, with the potential to induce heavier rainfall. Heavy rainfall is projected to increase in both magnitude and intensity in most of Norway, with the highest percent increases to be seen in the driest parts of the country (inland) (Sorteberg, et al., 2018). These changes in rainfall in could result in landslides in new locations.

Relative to 1971-2000, there has been shorter and milder winters, an increase of precipitation falling as rain in winter (rather than snow), more freeze thaw events, rain on snow events, and warmer spring resulting in warmer ground temperatures, reduced frost penetration, and early melt (NCSS, 2019). These trends are all predicted to continue under climate scenarios RCP 8.5 (business as usual), and RCP 4.5 (reduction of greenhouse gas emissions after 2040) (NCSS, 2019). Shallow soil landslides are therefore expected to increase in the winter months, with the largest changes projected in Northern Norway (Jaedicke, et al., 2008). Although a decrease in avalanches is projected, due to a decrease of snow, an increase of slushflows is anticipated due to rain on snow (Jaedicke, et al., 2013).

One study of extreme weather in northern Scandinavia projected that in climate change scenario RCP 8.5, a 10-yr return period event will have a return period of 2-3-yr (i.e. occur over three times more frequently) (Groenemeijer, et al., 2016). They also concluded that extreme precipitation will increase by 6-7% in intensity in RCP 8.5 due to the higher moisture capacity of warmer air but have no increase in duration. In the Norwegian case studies, a direct relationship of landslide initiation water supply to the local MAP is observed. This observation suggests that landslide occurrence may temporarily increase but should eventually decrease to background levels. The threshold to initiate landslides, should thus, increase. Based on this conclusion, threshold values should continuously be adjusted to adapt to current conditions.

In Norway, the majority of soil landslides are of glacial origins, meaning the sediment budget, from erosion and transportation, is likely not in equilibrium with mass wasting from landslides. Increased precipitation may only lead to a surge of landslide occurrence, that eventually return back to historical background levels, due to the lack of available soil. This pattern has been recorded in other parts of the world. Landslides in Nepal show a cyclicity of occurrence that mirrors that of monsoon strength in SE Asia and an overall upward trend of occurrence from 1978-2005 (Petley, et al., 2007). A spike in landslides are similarly recorded at the end of the Little Ice Age in Western Norway, associated with an increased sediment budget (Grove, 1972). Additionally, it is possible that post deforestation of Norwegian slopes is largely responsible for a current period of higher landslide occurrence rates, as is found to be the case in New Zealand (Glade, 2003).

#### 4.3.5 HYDMET Model

The maximum and modal (i.e. most common) hazard level over the defined area for the 21 case studies areas are presented in Table 22.

Table 22. HYDMET Model Results (data from xgeo.no)

ID	HYDMET Geo Model Results (xgeo.no)	
	Maximum	Mode
1	3	3
2	3	2
3	3	2
4	3	2
5	3	2
6	4	2
7	2	1
8	1	1
9	3	3
10	1	1
11	1	1
12	1	1
13	3	2
14	3	2
15	3	1
16	1	1
17	3	1
18	1	1
19	3	1
20	1	1
21	4	3

Images of the model results are included in Appendix F. The HYDMET Model results from Case 2 are illustrated in Figure 35 as an example.

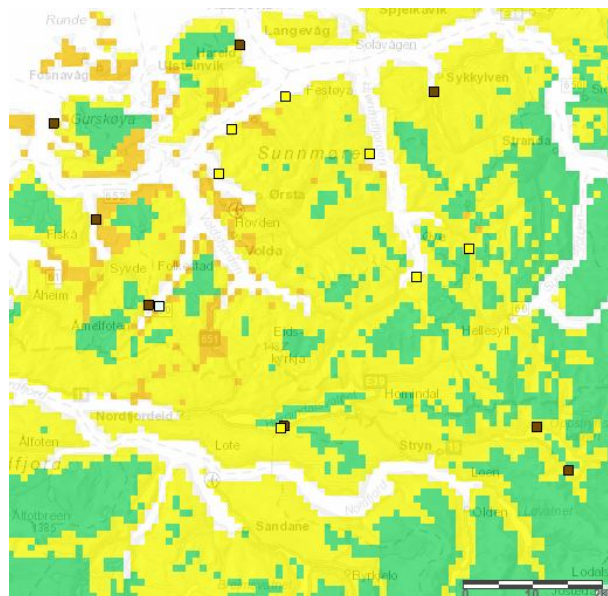


Figure 35. HYDMET Model results for case 2 (November 26, 2015, Sogn og Fjordane) where maximum hazard level is orange and the modal hazard level is yellow

It is clear that using the mode of the HYDMET model over an area would significantly underestimate hazard levels. Using the maximum reveals that seven cases would still have been missed altogether (i.e. are entirely green). Thresholds used in the HYDMET model produced many false alarms in the first two years of operation (8.5% and 14.5% of days in 2013 and 2014, respectively) and have since been adjusted (Krøgli, et al., 2018). The thresholds can therefore not simply be increased, as the hydro-meteorological conditions that exist when landslides take place are reached too frequently, resulting in no landslides.

#### 4.3.6 Landslide Warnings

##### 4.3.6.1 Published Warnings

A summary of the landslide hazard levels published for all days by NVE over the duration of the NLEWS is included in Table 23. Note that only one red warning has been issued and it was in the first year of operation.

Table 23. Percentage of days with landslide hazard levels warned in 2013-2019, data from (NVE, 2020a)

		Hazard Level			
		Green (1)	Yellow (2)	Orange (3)	Red (4)
Year	2013	81.7	16	2	0.3
	2014	83	15	2	0
	2015	90.4	8.5	1.1	0
	2016	93	7	0	0
	2017	89.8	8	2.2	0
	2018	86.6	13.2	0.3	0
	2019	86.6	12.3	1.4	0
	2013-2019	87.3	11.4	1.3	0

Surveys have been conducted in 2009, 2013, and 2019 with positive results (Colleuille & Engen, 2020). Respondents were predominantly emergency responders. While the NLEWS is designed for emergency responders and transportation authorities, it is also publicly available to the public. The system functions well for its target audience, but more emphasis on how warnings are perceived by the public is recommended to assess the NLEWS performance. Education on landslides and how they can affect the public has proven in other locations around the world to decrease vulnerability by empowering communities to make educated decisions on risk (Kelman, 2020). Improving public education on the NLEWS would also increase the capacity of citizen science. This could increase the number of landslides reported by members of the public on regobs.no. By extension, it could also increase the number of private weather stations (e.g. Netatmo) (Netatmo, 2019), which in past cases have had the nearest precipitation observations to estimate landslide initiation water supply (Meteorologisk institutt, 2019).

For the 21 Norwegian case studies, the collected warnings published by NVE are included in Table 24. In three of the events the landside hazard level was not lifted from a green (1) warning, meaning the event was missed altogether. There was no level red (4) warnings and just three orange (3) warnings, with the remaining fifteen events being level yellow (2) warnings.

Table 24. Published landslide warnings by NVE for Norwegian case studies (data from www.varsom.no)

ID	County Warning				
	3 days before	2 days before	1 day before	Day of Event	1 day after
1	1	1	2	2	1
2	1	1	1	1	2
3	1	1	2	3	3
4	1	1	1	2	1
5	1	1	1	2	1
6	1	1	1	2	1
7	1	1	2	2	1
8	1	1	3	2	1
9	1	1	1	1	1
10	1	1	1	1	1
11	1	3	3	2	1
12	1	1	2	2	1
13	1	3	3	2	2
14	1	1	3	3	1
15	1	1	2	2	2
16	1	1	2	2	2
17	1	1	2	2	1
18	1	1	1	2	2
19	1	1	1	2	2
20	1	1	2	2	1
21	1	1	1	3	2

High hazard level warnings cause large disruptions, evacuations, and economic loss from closing roads and railways. Landslide warnings are published on a regional level, further causing a reluctance to increase the hazard level without a high degree of uncertainty. Unfortunately, days with high uncertainty often result in high consequences. The hazard levels issued, included in Table 24 above, strongly suggest a reluctance to over-warn. As these are some of the most challenging days to forecast, it would be useful to include a degree of uncertainty with landslide warnings. The uncertainty could be communicated similar to the percent chance of precipitation in a weather forecast, giving the user an additional piece of information to make educated decisions. Uncertainty in landslide forecasting is largely due to uncertainty in weather forecasts, and thus, could explicitly carry this information to the user. It is also suggested that warnings be issued for smaller regions to promote issuing higher hazard levels.

#### 4.3.6.2 NVE Warning Evaluation

The landslide warnings published on the date of each date were collected and compared to the observed HYDMET model and the corrected hazard level according to an NVE evaluation. To visualize the comparison, the hazard levels of each are plotted together in Figure 36.

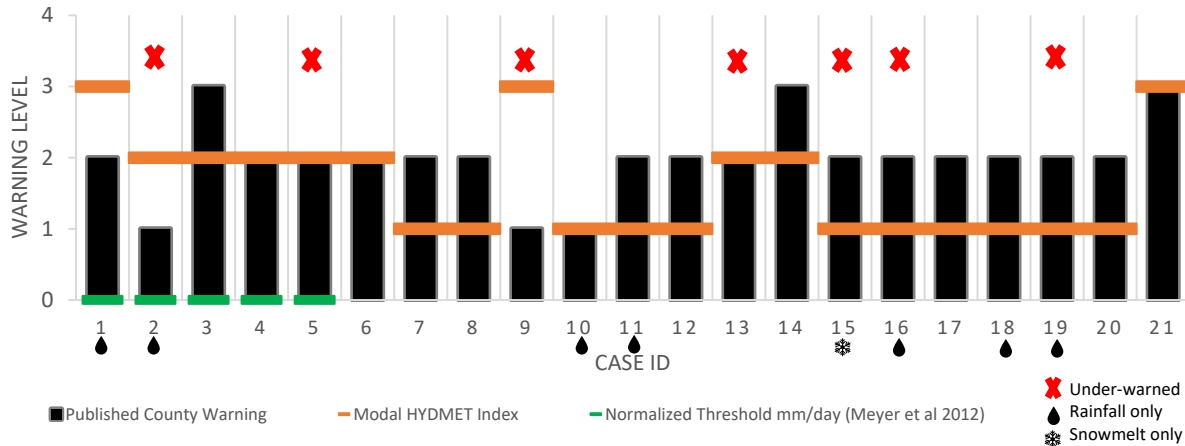


Figure 36. Landslide warnings from model results, published results, and corrections based on NVE and number of landslides

This comparison reveals that the mode of the HYDMET model is lower than the published warning in over half of cases (12/21), under the corrected warning in two thirds of cases (14/21), and over the corrected warning in only two cases. It is therefore essential with the current model for a landslide forecaster to use their judgement to increase the hazard level from the model. The same comparison with the maximum pixel HYDMET model hazard level, rather than the modal, shows that there are seven cases where not even one pixel warranted a landslide warning above a green (1) level and resulted in a yellow (2) or orange (3) level events. The requirement of a human component in landslide forecasting lacks objectivity and reproducibility. It also relies on highly trained individuals and is vulnerable to changes in staff. Continued improvements to objective indicators to determine warning hazard levels are needed to reduce the unreliability of human decision making.

One third of all events were under-warned based on the NVE post event evaluation and not a single event was over-warned. The warnings are semi-qualitative, but they do not directly consider losses. The two events with highest consequences are case 13 and 19. One death was recorded in each with 23 and 42 landslides registered in the NVE database, respectively, but in neither were re-evaluated as a red warning. This is evidence of a reluctance to alert a red warning. In fact, a summer rainstorm in 2013 is the only red warning that has ever been alerted in the NLEWS (Krøgli, et al., 2018).

A further analysis of the under-warned events shows that there are no clear trends of why these were missed. They vary by season, region, and weather. They vary largely in magnitude and intensity of water supply both in absolute and relative values and in their respective return periods. Previous studies have found that west facing slopes of the Norwegian mountain ranges have a hydro-meteorological regime that makes landslides more likely to be missed by water supply thresholds (Meyer, et al., 2012). While that is the case of some events, it is not determined to be a significant trend, and most events have landslides on slopes in all aspects. Details of these seven under-warned events are included in Table 25.

Table 25. Details of selected case studies that were under-warned according to NVE post-event evaluations

ID	Date	County	Season	Return Period (yrs)	Trigger (R = rain, S = snowmelt)	Weather Categorization
2	20151126/27	Sogn og Fjordane	Autumn	100	R&S	Heavy rain on snow
5	20161204/05	Trøndelag	Winter	<2	R&S	Rain on snow
9	20170518	Hedmark	Spring	25	R&S	Wet antecedent conditions and moderate rain
13	20171207	Hordaland	Winter	5	R&S	Rain on snow with frost
15	20180418	Oppland	Spring	<2	S	Rapid spring melt
16	20180926	Hordaland	Autumn	>200	R	Heavy widespread rainstorm
19	20190730	Sogn og Fjordane	Summer	>200	R	Intense concentrated rainstorm

Surprisingly, the weather categorizations of all seven under-warned cases differ. The only two case studies that occurred in Spring were under-warned. These case studies (9 and 15) are located in Eastern Norway where fewer landslides take place. Rainstorms with high return periods ( $\geq 100$  years) also have a high percentage of under-warned events (case 2, 16, and 19). Thresholds are determined using historical landslide events, therefore, it is hypothesized that the less frequent landslides occur, by location, season, or return period, the less likely they are to be predicted.

#### 4.3.6.3 Quantitative Warning Evaluation

Using two quantitative thresholds, the hazard levels for each case study were determined and compared to the NVE evaluations. All three evaluations agree in six cases. Strictly using number of reported landslides results in a higher hazard level than the NVE evaluation in eleven cases, lower in none, and agrees in ten. Using the water supply correction thresholds, the level is over the NVE evaluation in eight cases, under in two cases, and agrees in nine. Below, in Figure 37, the NVE corrected hazard levels are compared to the two quantified thresholds.

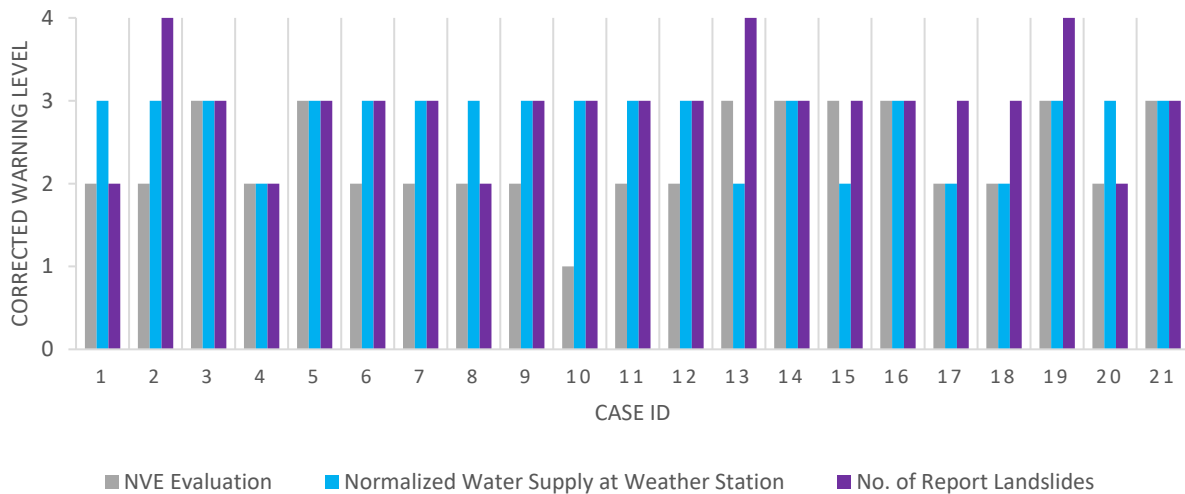


Figure 37. Corrected hazard levels based on NVE evaluation, reported landslides, and average water supply as a percent of annual average precipitation

The water supply thresholds again confirm that weather is indicative of vulnerability but that it alone cannot predict landslides. Even with observed water supply, rather than weather forecasts, the water



supply thresholds disagree with the NVE evaluations, both too high and too low. If the water supply were directly from the landslide initiation point and not a nearby weather station, these evaluations may be more similar.

Three cases warranted a red warning based on the number of landslides reported. Many landslides are reported the day after or in some cases, several days later. It is likely that if the warnings were re-evaluated well after the event, rather than the day of, the NVE evaluations would be higher. This could explain why the NVE evaluations are consistently lower than the evaluation based on number of landslides alone.

#### 4.3.6.4 Proposed Area Thresholds

The proposed area thresholds are based upon the mean and maximum normalized seNorge v2.0 precipitation and snowmelt presented in Table 19. The defined intervals, as defined herein, corresponding to hazard levels are presented in Table 26.

Table 26. Proposed area water supply thresholds using seNorge v2.0

Hazard Level	Normalized mean Area Threshold	Normalized Max Area Threshold
1	<1.5	<3
2	1.5-3.9	3.0-7.9
3	4.0-6.9	8.0-11.9
4	>7.0	>12

The area thresholds yield hazard levels that differ more from the NVE evaluation than simply using weather stations, and more importantly, over-warn in the wrong cases. Using the mean, the hazard level agrees with the NVE evaluation in twelve cases. Using the maximum, it agrees in ten cases. The calculated hazard levels for the Norwegian case studies are included in Table 27.

Table 27. Hazard level based on proposed area thresholds

ID	Hazard Level based on Mean Normalized 24-hr seNorge v2.0 Water Supply	Hazard Level based on Maximum Normalized 24-hr seNorge v2.0 Water Supply
1	4	4
2	2	2
3	3	2
4	2	2
5	2	3
6	2	3
7	2	2
8	2	2
9	3	3
10	3	4
11	3	3
12	2	2
13	2	2
14	3	3
15	2	2
16	2	2
17	2	3
18	2	2
19	2	2
20	2	2
21	3	4

This exercise is deemed unfavourable compared to the existing HYDMET model grid as using weather statistics over the area reduces the information available to the landslide forecaster at no benefit. This method intended to simplify hazard levels in a similar fashion as avalanche or forest fire hazard levels while capturing the regional hazard. Instead, they are found to over-simplify a complex problem. Overall, Area thresholds would produce hazard levels that are more challenging to disseminate.

## 5 Conclusions

Events with multiple landslides can cause major damage, loss of life, and economic costs. Early warnings greatly benefit emergency responders in mitigating damage. Rare, high consequence landslide events are challenging to forecast. This study aimed to (1) improve the landslide inventory and (2) analyse forecasting tools and warnings given for past events with multiple landslides, in order to assist in issuing more reliable warnings in the future. The following main conclusions are drawn:

- Road and rail authorities report the majority of landslides in Norway. Consequently, the NVE landslide database registries are biased to transportation routes. 72% of the landslides studied are within 10 m of a road. The database is also temporally biased, with 70% of the inventory occurring after the year 2000. Uncertainty exists in landslide categorizations and time and location of landslides. Improvements to the database are essential in the development of more reliable thresholds and many limitations could be reduced using remote sensing techniques.
- $\delta$ NDVI could dramatically improve the Norwegian landslide inventory for rainfall induced soil landslides  $>1000\text{m}^2$ . The method is hindered by snow cover, size of landslide ( $<1000\text{m}^2$ ), cloud cover, daylight hours and sun angle. Change detection of SAR intensity, phase, and coherence have little potential in the cases studied due to detection limits of size and depth landslides and the amount of noise present in the surrounding terrain. Similar results were found in Norwegian case studies and international test sites.
- In Norway over the past five years, over half of days with  $\geq 10$  soil landslides occurred in December and January. They are widespread across the country but are most common in Western Norway and rare in Northern Norway. They have occurred nearly five times per year, on average.
- Forecasting tools for the selected cases revealed varied usefulness. The HYDMET model underestimated hazard levels in 67% of cases. 84% of registered landslides occurred in locations accurately mapped as very high or high susceptibility levels, highlighting the value of susceptibility maps. At both 1:1,000,000 and 1:250,000 scales, registered landslides occur most commonly in areas mapped as till, colluvium, and bedrock, but at vastly different ratios (18%, 6%, 55% and 44%, 18, 16%, respectively). These results illustrate the value of small-scale quaternary geology mapping for landslide forecasting.
- Selected Norwegian case studies are all induced by rainfall or snowmelt, and over half by a combination of both. 24-hour rainfall is the strongest predictive factor, but snowmelt plays an important role. 11/21 Norwegian case studies had water supply return periods of  $\leq 5$  years. This result suggests that the water supply at the landslide initiation may not be observed or modelled, and, moreover, that weather alone cannot predict landslides.
- 1/3 of cases are under-warned, 2/21 of which were missed (i.e. warned at green (1) level). If strictly considering the number of landslides, 2/3 of cases are under-warned, 3/21 of which were missed. Under-warned and missed cases are highly varied by season, trigger, location, and return period. The most challenging forecasting conditions are 1) uncertain high return period rainstorms and 2) spring melt with wet antecedent conditions. Notably, both conditions are rare, and therefore contribute less to thresholds.

## 5.1 Landslide Inventory

21 Norwegian and four international case studies were selected to test the potential of two remote sensing techniques to improve landslide inventories. Norwegian case studies are days with ten or more registered soil landslides with a geographic cluster of five or more. International case studies are events with over ten debris flows in varied regions, including arctic, urban, tropical, and monsoon influenced conditions. Remote sensing techniques using Sentinel-1 (SAR) and Sentinel-2 ( $\delta$ NDVI) satellite images are tested with mixed results.

Results in mapping soil landslides with SAR show little potential. Although change detection of SAR intensity, phase, and coherence have proven useful in other studies for landslide mapping, and many other geohazard applications, this study found only 10% of landslides analyzed are detectable, and only one out of 150 landslides is mappable. SAR intensity has the most clear landslide signature, and SAR phase and coherence interferograms have too much noise for landslides to stand out. The studied landslides are likely too shallow and small in area to be identified using SAR. Noise in the surrounding terrain caused by vegetation, freeze and thaw, local weather, and changes in moisture, renders landslides ambiguous. Sentinel-1 images were chosen to reduce the temporal window of pre- and post-event images; however, the window is likely too long for emergency response use (on average 5 days before and 3 days after), and the acquisition mode is found to be a much more important factor. Landslides are best identified on east and west facing slopes in descending and ascending mode, respectively, in order to reduce foreshortening. SAR is limited in detecting landslides on north and south facing slopes due to the pole to pole orbit of Sentinel-1 satellites, on which the instrument antenna is directed to the right. Images and DEM should be more carefully selected for each event to ensure they are optimized. In all case studies, more than one slope aspect is present, and it is therefore recommended to analyse images in both ascending and descending acquisition modes.

$\delta$ NDVI using Sentinel-2 images has promising results. Optical satellite landslide detection is often impeded by cloud cover, shadows, and short daylight hours. This is especially true in regions, like Norway, at high latitudes with a high concentration of cloud cover. For this reason, optical landslide detection methods have been overlooked as a promising technique in such regions. This study uncovers the potential of  $\delta$ NDVI using Sentinel-2 images in a cloudy region that is frequently plagued by landslides. Sufficiently sized landslide scars ( $>1000\text{m}^2$ ), can be detected with an image acquisition window of over a year with the same lighting conditions and no snow cover, despite long cloudy periods. Of the 161 landslides analysed in Norway, 45% are detectable using  $\delta$ NDVI. If only considering rainfall induced debris flows/floods, however, the detection rate increases to an impressive 94%. The main factors affecting the effectiveness of this method, in order of significance, are snow cover, size of landslide ( $<1000\text{ m}^2$ ), cloud cover, daylight hours and sun angle. Noise caused by agriculture, waterways/higher water levels, construction, and other mass movements can hinder landslide detections and increases directly with time between images.

In seven cases, conditions allowed for landslide mapping in addition to those registered in the database. Nearly three times the number of landslides registered are mapped, indicating that in proper conditions, landslide inventories in Norway could be drastically improved using  $\delta$ NDVI with Sentinel-2 satellite imagery. The time required to download, process, and map a Sentinel-2  $1500\text{ km}^2$  image tile using  $\delta$ NDVI and the method described herein, is approximately four to eight hours, warranting the development of an automated process. A semi-automatic landslide inventory using  $\delta$ NDVI is deemed

highly viable for rainfall induced soil landslides  $>1000 \text{ m}^2$  in Norway. The automation process would be improved with object identification to remove clouds and waterways and the use of a DEM and susceptibility maps.

With the availability of free Sentinel-2 satellite imagery, even at a spatial resolution of 10 m, the use of  $\delta\text{NDVI}$  images show great promise in inexpensive landslide mapping across the globe. Various conditions were tested, including continuous permafrost arctic tundra, a tropical urban centre, a cloudy mountainous monsoon influenced region, and an equatorial climate plagued by frequent mass movements. All test sites were successful in mapping a large landslide inventory. The arctic case proved that  $\delta\text{NDVI}$  can be successful even with low vegetation mass and long dark winters due to the slow regrowth in landslide scars and infrequent human alteration of the terrain (e.g. construction, agriculture, forestry). At a reduced cost and increased coverage, compared to more traditional methods,  $\delta\text{NDVI}$  could be a valuable tool to build landslide inventories in remote and inaccessible locations.

Temporal, spatial, and data limitations were identified in the Norwegian landslide database. In the studied Norwegian cases, a clear spatial bias of registered events to transportation routes was confirmed. 91% of the studied registered landslides lie within 100 m of a road. In comparison, only 16% of the mapped landslides are within 100 m of a road in the case which had the best conditions for mapping a complete inventory with  $\delta\text{NDVI}$  (case 19). This bias could be significantly reduced using  $\delta\text{NDVI}$  in proper conditions. Many key metadata, including uncertainty of location, landslide size, and landslide type could be improved using  $\delta\text{NDVI}$ . Conversely, the uncertainty of time, may worsen. Precise time or even date cannot be acquired using  $\delta\text{NDVI}$  alone. Additionally, in the event that many landslides follow the same path, they will not be accounted for. The NVE database is also limited by a recency bias which cannot be addressed with the proposed remote sensing techniques.

## 5.2 Landslide Forecasting

A statistical temporal and spatial analysis of days with  $\geq 10$  soil landslides registered in the NVE database over the past five years in Norway revealed that over half occurred in December and January. The highest density of such days is in Western Norway due to a tempered climate and high precipitation. They occur rarely north of Trondelag due to lower mean annual rainfall and stable winter temperatures. Of selected case studies in Norway, those that occur from April to June are predominantly inland, those that occur from September to January are restricted to the coast, and events in June to August are all located in Southern Norway.

Of the 21 case studies, six are rainfall induced, one was triggered by snowmelt, and fourteen are induced by combined rainfall and snowmelt. Rain is nearly always present in these events, but snowmelt is also a major contributing factor. Snowmelt causes widespread pore water pressures to rise, generates high overland flow and surface water, and leads to increased erosion. The water supply needed to trigger the selected landslide events is found to be proportional to the amount of annual precipitation. Some events were triggered by short, intense rainfall ( $<24$  hours), while others had moderate rainfall and snowmelt over a long duration (1-15 days). Normalized water supply ranges from 2.4% and 8.5% of mean annual precipitation, agreeing with the range of thresholds of debris flows in Norway calculated by Meyer et al. (2012), but return periods of 1, 3, and 24-hour water supply are lower than expected, with  $\leq 5$  years in 11 cases and  $\geq 100$  years in six cases. This suggests that initiation water supply may not be observed, and that weather alone is insufficient in predicting shallow soil landslides.

Climate change projections are uncertain, but the projected trends increase the likelihood of landslide activity in Norway. Western Norway currently has the highest density of extreme landslide events and is projected to have a minor increase in landslide activity, despite increases in intensity and duration of extreme rainfall. The greatest increase of landslide activity is expected to be in Northern Norway, where more mild winters will bring a greater proportion of precipitation as rain and more frequent freeze-thaw, and in Eastern Norway, the driest part of the country, where the greatest increase of precipitation is projected (Jaedicke, et al., 2008). Western Norway will continue to host the most frequent landslides.

In over half of the case studies, basing the landslide warning on the mode (i.e. most frequent) hazard index alone would have resulted in a level green warning. In a third of the cases, using the maximum pixel in the area would also yield a green warning. These results illustrate that while threshold models are useful, they are insufficient to warn of extreme landslide events alone. Landslide forecasters drastically improve the accuracy of hazard levels of warnings for the selected landslide events compared to the HYDMET threshold model. The mode of the hazard levels of the HYDMET Model in the area of the landslide was less than the published value in 12/21 cases and over the NVE evaluation value in just 2/21 cases. Even still, one third of all events were under-warned based on the NVE post-event evaluation and not a single event was over-warned. When strictly considering the number of landslides, two thirds of events were under-warned, and none were over-warned.

A reluctance to issue false alarms or over-warn exists, despite clear internal messaging that false alarms are favourable to missed events. In the seven years of operation, the NLEWS has only once published a level red (4) warning, despite at least three events studied having severe damage and over 20 reported landslides. A decrease in the size of warning areas or communication of uncertainty may reduce under-warned events. Continued improvements to objective indicators to determine warning hazard levels are needed to reduce the inconsistency of human decision making.

### 5.3 Future Studies

Fields requiring more research based on the results of this study include the following:

- To test the full potential of  $\delta$ NDVI, a study should be completed exclusively on ideal conditions (i.e. rainfall induced debris flows and floods). The accuracy should also be tested by comparing to more traditional method (e.g. field mapping or photogrammetry with aerial photographs).
- The  $\delta$ NDVI signature of landslides mapped in this study, in addition to existing landslide indicators, such as slope angle, geology, susceptibility mapping, degree of soil moisture, and groundwater level, could be used as data input to train a machine learning model to automatically detect landslides for inventory building.
- Snowmelt and frost play an important role in triggering landslides that requires more research. Rain on snow events, which are becoming more frequent with climate change (Hannsen-Bauer, et al., 2017), are the most common trigger of days with more than 10 landslides in Norway.
- Suggested improvements to the NLEWS that should be further researched include a stronger focus on communication to the general public, adopting smaller warning regions to promote higher hazard levels in uncertain conditions, and communication of uncertainty in warnings.

## 6 References

- Bouvet, M. (2020). *GETASSE30 Elevation Model*. Retrieved from SeaDAS:  
<https://seadas.gsfc.nasa.gov/help/visat/GETASSE30ElevationModel.html>
- Brunetti, M., Xiao, Z., Komatsu, G., Peruccacci, S., & Guzzetti, F. (2015, November 1). Large rock slides in impact craters on the Moon and Mercury. *Icarus, Volume 260*, pp. 289-300.
- Caine, N. (1980). The rainfall intensity – duration control of shallow landslides and debris flows. *Geografiska Annaler Series A62*, pp. 23 – 27.
- Calvello, M. (2017). Early warning strategies to cope with landslide risk. *Riv. Ital. di Geot.*, 2, pp. 63–91.
- Calvello, M., & Piciullo, L. (2016). Assessing the performance of regional landslide. *Nat. Hazards Earth Syst. Sci.*, 16, 103–122.
- CCMEO. (2013). *Remote Sensing Fundamentals*. CCMEO - The Canada Centre for Mapping and Earth Observation (formerly Canada Centre for Remote Sensing).
- Cepeda, J., Høeg, K., & Nadim, F. (2010). Landslide-triggering rainfall thresholds: A conceptual framework. *Eng. Geol. Hydrogeol.*, 43, 69–84.
- Christiansen, H. H., Farnsworth, W., Gilbert, G. L., Hancock, H., Humlum, O., O'Neill, B., . . . Strand, S. M. (2016). *Report on the 14-15 October 2016 mass movement event in the Longyearbyen area*. Longyearbyen, Svalbard: The University Centre in Svalbard, UNIS.
- Clague, J., & Stead, D. (2012). *Landslides: types, mechanisms, and modeling*. Cambridge Univ. Press.
- Clark, R. (1999). Chapter 1: Spectroscopy of Rocks and Minerals, and Principles of Spectroscopy, in *Manual of Remote Sensing*. In *Remote Sensing for the Earth Sciences, Volume 3*. New York: John Wiley and Sons, Inc.
- Closson, D., & Milisavljevic, N. (2017). Chapter 6: InSAR Coherence and Intensity Changes Detection. In C. Beumier, *Mine Action - The Research Experience of the Royal Military Academy of Belgium* (pp. 155-176). IntechOpen.
- Colleuille, H., & Engen, K. (2020). *Brakerundersøkelse om flom- og jordskredvarslingen Utført høsten 2019, Rapport Nr. 6*. Retrieved from  
[http://publikasjoner.nve.no/rapport/2020/rapport2020\\_06.pdf](http://publikasjoner.nve.no/rapport/2020/rapport2020_06.pdf)
- Colleuille, H., Boje, S., Devoli, G., Krøgli, I., Engen, I., Sund, M., . . . Wirehn, P. (2017). *Jordskredvarslingen: nasjonal varslingstjeneste for jord-, sørpe- og flomskredfare*. Oslo: NVE.
- Corominas, J., Van Westen, C., Frattini, P., Cascini, L., Malet, J., Fotopoulou, S., . . . Smith, J. (2013). *Recommendations for the quantitative analysis*. Bull Eng Geol Environ.
- Devoli, G. (2019, November 7). Orange vs Red Warning Jolster. (E. Lindsay, Interviewer)
- Devoli, G., Bell, R., & Cepeda, J. (2019). *Susceptibility map at catchment level, to be used in landslide forecasting, Norway. Rapport Nr 1/2019*. Oslo, Norway: Norges vassdrags- og energidirektorat.

- Devoli, G., Jorandli, L., Engeland, K., & Tallaksen, L. (2017). Largescale synoptic weather types and precipitation responsible for landslides in southern Norway. *Proceeding 4th WLF 2017*, (pp. 159-167).
- Dowling, C. A., & Santi, P. M. (2014). Debris flows and their toll on human life: a global analysis of debris-flow fatalities from 1950 to 2011. *Natural Hazards*, 71, pp. 203-227.
- Endo, T. (1969). *Probable distribution of the amount of rainfall causing landslides, Annual Report 1968, Hokkaido Branch, For. Exp. Stn. Sapporo*.
- ESA. (2007). *InSAR Principles: Guidelines for SAR Interferometry Processing and Interpretation, TM-19*. Noordwijk, The Netherlands: ESA Publications. Retrieved from [https://www.esa.int/esapub/tm/tm19/TM-19\\_ptB.pdf](https://www.esa.int/esapub/tm/tm19/TM-19_ptB.pdf)
- ESA. (2020a). *RUS webinar: Rapid Landslide Detection with Sentinel-1 - HAZA07*. Retrieved from Youtube: <https://youtu.be/Eb9nEVU6Y8E>
- ESA. (2020b). *Sentinel 1*. Retrieved from European Space Agency Sentinel Online: <https://sentinel.esa.int/web/sentinel/missions/sentinel-1>
- ESA. (2020c). *Sentinel Image Retrieval Map*. Retrieved from Copernicus Open Access Hub: <https://scihub.copernicus.eu/dhus/#/home>
- ESA. (2020d). *Sentinel-2 MSI*. Retrieved from European Space Agency Sentinel Online: <https://sentinel.esa.int/web/sentinel/user-guides/sentinel-2-msi>
- ESA. (2020e). *SNAP 7.0 Software*. Retrieved from European Space Agency: <https://step.esa.int/main/download/snap-download/>
- ESRI. (2019). *ArcMap 10.7 Software*. Retrieved from ESRI Downloads: <https://support.esri.com/en/downloads>
- ESRI. (2020). *Python - Importing ArcPy*. Retrieved from ArcGIS Pro: <https://pro.arcgis.com/en/pro-app/arcpy/get-started/importing-arcpy.htm>
- Fiorucci, F., Ardizzone, F., Mondini, A., Viero, A., & Guzzetti, F. (2019). Visual interpretation of stereoscopic NDVI satellite images to map rainfall-induced landslides. *Landslides (2019) 16*, 165–174.
- Fjeld, M. (2018). *Detection of Landslides Using Optical Satellite Remote Sensing*. Trondheim, Norway: Norwegian University of Science and Technology.
- Foude, M., & Petley, D. (2018). Global fatal landslide occurrence from 2004 to 2016. *Natural Hazards Earth Science Systems*, 2161-2181.
- Glade, T. (2003). Landslide occurrence as a response to land use change: a review of evidence from New Zealand. *Catena, Volume 51, Issues 3-4*, 297-314.
- Groenemeijer, P., Vajda, A., Lehtonen, I., Kämäräinen, M., Venäläinen, A., Gregow, H., . . . Púčik, T. (2016). *Present and future probability of meteorological and hydrological hazards in Europe. RAIN - Risk Analysis of Infrastructure Networks in Response to Extreme Weather*. RAIN Project.



- Grove, J. (1972). The Incidence of Landslides, Avalanches, and Floods in Western Norway during the Little Ice Age. *Arctic, Antarctic, and Alpine Research, Volume 4*, 131-138.
- Guzzetti, F., Gariano, S., Peruccacci, S., Brunetti, M., Marchesini, I., Rossi, M., & Melillo, M. (2019). Geographical landslide early warning systems. *Earth-Science Reviews 200*.
- Guzzetti, F., Peruccacci, S., Rossi, M., & Stark, C. (2007). Rainfall thresholds for the initiation of landslides in central and southern Europe. *Meteorog Atmos Phys 98*, pp. 239–267.
- Guzzetti, F., Peruccacci, S., Rossi, M., & Stark, C. (2008). The rainfall intensity–duration control of shallow landslides and debris flows: an update. *Landslides 5(1)*, pp. 3-17.
- Hannsen-Bauer, I., Førland, E., Haddeland, I., Hisdal, H., Mayer, S., Nesje, A., & Nilsen, N. (2017). *Climate in Norway 2100 - a knowledge base for climate adaptation*. The Norwegian Centre for Climate Services (NCCS).
- Haque, U., da Silva, P., Devoli, G., Pilz, J., Zhao, B., Khaloua, A., . . . Glass, G. (2019). The human cost of global warming: Deadly landslides and their triggers (1995-2014). *Science of the Total Environment, 673-684*.
- Haque, U., da Silva, P., Lee, J., Benz, S., Auflič, M., & Blum, B. (2017). Increasing Fatal Landslides in Europe. *4th World Landslide Forum* (pp. 505-512). Ljubljana, Slovenia: Springer International Publishing.
- Hestnes, E. (1998). Slushflow hazard – where, why and when? 25 years of experience with slushflow consulting and research. *Ann. Glacial., 26*, pp. 370-376.
- Hestnes, E., Bakkehoi, S., & Jaedicke, C. (2016). Longyearbyen, Svalbard - Vulnerability and Risk Management of an Arctic Settlement under Climate Change. *International Snow Science Workshop 2016*, (pp. 363-370). Brackendale, Colorado.
- Hungr, O., Leroueil, S., & Picarelli, L. (2014). The Varnes classification of landslide types, an update. *Landslides 11*, 167-194.
- Jaedicke, C., Høydal, Ø., & Midtbø, K. (2013). Identification of slushflow situations from regional weather models. *International Snow Science Workshop*, (pp. 177-182). Grenoble, Chamonix Mont-Blanc.
- Jaedicke, C., Lied, K., & Kronholm, K. (2009). Integrated database for rapid mass movements in Norway. *Nat. Hazards Earth Systems*, pp. 469–479.
- Jaedicke, C., Solheim, A., Blikra, L., Stalsberg, K., Sorteberg, K., Aaheim, A. K., . . . Mestl, H. (2008). Spatial and temporal variations of Norwegian geohazards in a changing climate, the GeoExtreme Project. *Natural Hazards and Earth Science Systems*, 893-904.
- Kartverket. (2016, June 14). *VBase Download*. Retrieved from GeoNorge: <https://kartkatalog.geonorge.no/nedlasting>
- Kelman, I. (2020). *Disaster by Choice, How our actions turn natural hazards into catastrophes*. Oxford University Press.

- Kriegler, F. J., Malila, W. A., Nalepka, R., & Richardson, W. (1969). Preprocessing transformations and their effects on multispectral recognition. *Proceedings of the Sixth International Symposium on Remote Sensing of Environment* (pp. 97-131). Ann Arbor, Michigan: University of Michigan.
- Krøgli, I. K., Devoli, G., Colleuille, H., Boje, S., Sund, M., & Karin Engen, I. (2018). The Norwegian forecasting and warning service for rainfall- and snowmelt-induced landslides. *Natural Hazards and Earth System Sciences*, 1427-1450.
- Lopez-Martinez, C., Fabregas, X., & Pottier, E. (2005). A New Alternative for SAR Imagery Coherence Estimation. *AMPER-Application of Multiparameter Polarimetry in Environmental Remote sensing*.
- Lucchitta, B. (1979). Landslides in Valles Marineris, Mars. *Proceedings of the Second International Colloquium on Mars*, pp. 8097-8113.
- Lussana, C., Saloranta, T., Skaugen, T., Magnusson, J., Tveito, O., & Andersen, J. (2018). seNorge2 daily precipitation, an observational gridded dataset over Norway from 1957 to the present day. *Earth System Science Data*, 10, 235–249.
- Meteorologisk institutt. (2019). *Intense byger med store konsekvenser i Sogn og Fordane 30.juli 2019*. Bergen, Norway.
- Meteorologisk institutt. (2020a). *Nedbørintensitet*. Retrieved from Norsk Klima Service Senter: <https://klimaservicesenter.no/faces/desktop/idf.xhtml>
- Meteorologisk institutt. (2020b). *Observations and weather statistics*. Retrieved from Norsk Klima Service Senter: <https://seklima.met.no/observations/>
- Meyer, N., Dyrddal, A., Frauenfelder, R., Etzelmuller, B., & Nadim, F. (2012). Hydrometeorological threshold conditions for debris flow initiation. *Natural Hazards Earth Science Systems*, 3059-3073.
- Mondidi, A. C., Guzzetti, F., Reichenbach, P., Rossi, M., Cardinali, M., & Ardizzone, F. (2011). Semi-automatic recognition and mapping of rainfall induced shallow landslides using. *Remote Sensing of Environment* 115, 1743-1757.
- Nadim, F., Cepeda, J., Sandersen, F., Jaedicke, C., & Heyerdahl, H. (2009). Prediction of rainfall-induced landslides through empirical and numerical models. *Proceedings of the First Italian Workshop on Landslides (IWL 2009)*, (pp. 206—215). Naples, Italy.
- NCSS. (2019). *Climate in Svalbard 2100 - a knowledge base for climate adaptation. Report no. 1/2019*.
- Netatmo. (2019, November 28). *Weather Map*. Retrieved from <https://weathermap.netatmo.com/>
- NGU. (2013). *Quaternary Geology of Norway - Geological Survey of Norway Special Publication, 13*. Norges geologiske undersøkelse.
- NGU. (2019). *Maps and Data*. Retrieved from Norges Geologiske Undersøkelse: <https://www.ngu.no/emne/kart-og-data>

- Nichol, J., & Wong, M. (2005). Satellite remote sensing for detailed landslide inventories using change detection and image fusion. *International Journal of Remote Sensing* 26(9), 1913–1926.
- NTB. (2019, July 31). *Redningsaksjon på vent – geologer på vei inn i rasområdene i Jølster*. Retrieved from Uldresfiabifen: <https://www.adressa.no/nyheter/innenriks/2019/07/31/Redningsaksjon-p%C3%A5-vent-%E2%80%93-geologer-p%C3%A5-vei-inn-i-rasomr%C3%A5dene-i-J%C3%B8lster-19598351.ece?fbclid=IwAR3utYHPFtTcK9H5ZJf2S8X3DbFdm9O-dRBUZaLq1igHlVDq-tr2eXQj9Is>
- NVE. (2018). *Jordskred of flomskred varsling fakta 05*. Retrieved from [www.varsom.no/flom-og-jordskredvarsling](http://www.varsom.no/flom-og-jordskredvarsling)
- NVE. (2019a). *Awareness level for flood and landslide forecasting and warning*. Retrieved from Varsom.no: <https://www.varsom.no/en/flood-and-landslide-warning-service/awareness-level-for-flood-and-landslide-forecasting-and-warning/>
- NVE. (2019b). *Faresonekartlegging i Jølster kommune*. Oslo: NVE.
- NVE. (2020a). Catchment Level Susceptibility Maps, Yearly Summaries of Landslide Warning 2015, 2016, 2017, 2018, 2019, SeNorge v2.0, Metpp weather data. Oslo, Norway.
- NVE. (2020b). *Flom og Jordskredvarsling*. Retrieved from Varsom: <https://www.varsom.no/flom-og-jordskredvarsling/>
- NVE. (2020c). *Flood and landslides map data*. Retrieved from Varsom Xgeo: <http://www.xgeo.no/>
- NVE. (2020d). *Hvordan varsler NVE flom og jordskredfare?* Retrieved from Varsom: <https://www.varsom.no/flom-og-jordskredvarsling/hvordan-varsler-nve-flom-og-jordskredfare/?ref=mainmenu>
- Oishimaya, S. (2017, April 25). *Deadliest Landslides In Recorded History*. Retrieved from World Atlas: [worldatlas.com/articles/deadliest-landslides-in-recorded-history.html](http://worldatlas.com/articles/deadliest-landslides-in-recorded-history.html)
- Pecoraro, G., Calvello, M., & Cepeda, J. (2019). Using local monitoring data for regional forecasting of weather-induced landslides in Norway. *XVII European Conference on Soil Mechanics and Geotechnical Engineering 2019 Proceedings*. Reykjavik, Iceland: Geotechnical Engineering foundation of the future.
- Peebles, P. (1998). *Radar Principles*. John Wiley and Sons, Inc.
- Petley, D. (2020a). *The Landslide Blog*. Retrieved from <https://blogs.agu.org/landslideblog/>
- Petley, D. (2020b). *Zongling: an area of intense landslide activity in Guizhou Province, China*. Retrieved from The Landslide Blog: <https://blogs.agu.org/landslideblog/2020/04/22/zongling-1/>
- Petley, D., Hearn, G., Hart, A., Rosser, N., Dunning, S., Oven, K., & Mitchell, W. (2007). Trends in landslide occurrence in Nepal. *Natural Hazards* 43, 23–44.
- Piciullo, L., Calvello, M., & Cepeda, J. (2018). Territorial early warning systems for rainfall-induced landslides. *Earth-Science Reviews* 179, 228-247.

- Piciullo, L., Dahl, M., Devoli, G., Colleuille, H., & Calvello, M. (2017). Adapting the EDuMaP method to test the performance of the Norwegian early warning system for weather-induced landslides. *Natural Hazards and Earth System Sciences*, 817-831.
- Riedel, B., & Walther, A. (2008). InSAR processing for the recognition of landslides. *Advances in Geoscience*, 8, 189-194.
- Road, L. (2008). *Rainfall Floods and Weather Patterns Oppdragsrapport A 14*. Oslo, Norway: NVE.
- Rouault, C., Lindsay, E., Nordal, S., & Lohne, J. (2020). Jølster landslide event July 2019: predisposition, trigger and consequences. *NGF Abstracts and Proceedings, no. 1* (p. 184). Oslo, Norway: Geological Society of Norway.
- Rouse, J., Haas, R., Schell, J., & Deering, D. (1973). *Monitoring the vernal advancement and retrogradation (green wave effect) of natural vegetation*. College Station, Texas: Remote Sensing Center, Texas A&M University.
- Rubensdotter, L. (2019, October 25). Jølster Quaternary Geology and Geohazards Interpretations from October 2019 Field Visit. (C. Rouault, Interviewer)
- Sandersen, F., Bakkehøi, S., Hestnes, E., & Lied, K. (1996). The influence of meteorological factors on the initiation of debris flows, rockfalls, rockslides and rockmass stability. *Landslides*, 97–114.
- S-Cool. (2020). *GCSE, Geography, Weather and Climate, Rainfall Types*. Retrieved from S-Cool The Revision Website: <https://www.s-cool.co.uk/gcse/geography/weather-and-climate/revise-it/rainfall-types>
- Segoni, S., Piciullo, L., & Gariano, S. (2018). A review of the recent literature on rainfall thresholds for landslide occurrence. *Landslides* 15, 1483–1501.
- Sorteberg, A., Lawrence, D., Dyrødal, A., Mayer, S., & Engeland, K. (2018). *Climatic changes in short duration extreme precipitation and rapid onset flooding - implications for design values*. Norwegian Centre for Climate Services.
- Surendranath, M., Ghosh, S., Ghoshal, T., & Rajendran, N. (2008). Remote Sensing and GIS Technologies for Landslide Hazard Zonation in Darjeeling Himalayas: A Case Study on Integration of IRS and SRTM Data. *Monitoring and Prediction of Disasters*, 121–135.
- Time and Date AS. (2020). *Longyearbyen, Svalbard, Norway — Sunrise, Sunset, and Daylength, October 2016*. Retrieved from Time and Date: <https://www.timeanddate.com/sun/norway/longyearbyen?month=10>
- Torheim, Ø. (2019, August 9). *Veien åpnet like før bil ble tatt: Geolog vurderte rasfaren i Jølster på avstand*. Retrieved from Bergens Tidende: <https://www.bt.no/nyheter/lokalt/i/QoE1xJ/veien-aapnet-like-foer-bil-ble-tatt-geolog-vurderte-rasfaren-i-joelster?fbclid=IwAR27KEDIIirHTvKfB91Fb8mPcG9DKOszdjdEDSkpUVs-63kdd-AVnMPJS68>
- UNISDR. (2009). *Terminology on Disaster Risk Reduction*. Retrieved from [https://www.unisdr.org/files/7817\\_UNISDRTerminologyEnglish.pdf](https://www.unisdr.org/files/7817_UNISDRTerminologyEnglish.pdf)

- USGS. (2020). *Interferometric Synthetic Aperture Radar (InSAR)*. Retrieved from U.S. Geological Survey: [https://www.usgs.gov/centers/ca-water-ls/science/interferometric-synthetic-aperture-radar-insar?qt-science\\_center\\_objects=0#qt-science\\_center\\_objects](https://www.usgs.gov/centers/ca-water-ls/science/interferometric-synthetic-aperture-radar-insar?qt-science_center_objects=0#qt-science_center_objects)
- Wang, R., & Yunkai, D. (2017). Bistatic InSAR. In *Bistatic Sar System and Signal Processing Technology* (pp. 235-275). Beijing, China: Springer Singapore.
- Weirich, F., & Blesius, L. (2007). Comparison of satellite and air photo based landslide susceptibility maps. *Geomorphology*, 352–364.
- White, I., Mottershead, D., & Harrison, J. (1996). *Environmental Systems, 2nd edn*. Chapman & Hall, London.
- Wiesmann, A., Wegmüller, U., Honikel, M., Strozzi, T., & Werner, C. (2002). Hazard mapping with multi-temporal SAR and InSAR. *Third International Symposium on Retrieval of Bio- and Geophysical Parameters from SAR Data for Land Applications Proceedings* (pp. 133-138). Sheffield, UK: ESTEC Publishing Division .
- Wilsom, A. M., & Jetz, W. (2016). Remotely Sensed High-Resolution Global Cloud Dynamics for Predicting Ecosystem and Biodiversity Distributions. *PLoS Biol* 14(3): e1002415. doi:10.1371/journal.pbio.1002415" Data available on-line at <http://www.earthenv.org/>.

## Appendix A: Python Code

## Appendix A – Python Code

```
#Filter NVE Landslide Database
#Written by Christy Rouault, February 2020
import arcpy

arcpy.env.overwriteOutput = True
arcpy.env.workspace = r'C:\Users\crouault\Documents\4 NTNU\Thesis\Data\Landslide Database'

# filters for soil landslides and slushflows and events that occurred after 20150630 and before 20200101
ls_db_table = r'C:\Users\crouault\Documents\4 NTNU\Thesis\Data\Landslide Database\Export_DB_Filtered.shp'
outpath = r'C:\Users\crouault\Documents\4 NTNU\Thesis\Data\Landslide Database'

arcpy.MakeFeatureLayer_management(ls_db_table, 'ls_db_layer')
arcpy.SelectLayerByAttribute_management('ls_db_layer', "NEW_SELECTION", '"skredType" > 139')
arcpy.SelectLayerByAttribute_management('ls_db_layer', "SUBSET_SELECTION", '"skredType" < 150')
arcpy.SelectLayerByAttribute_management('ls_db_layer', "ADD_TO_SELECTION", '"skredType" = 133')
arcpy.SelectLayerByAttribute_management('ls_db_layer', "SUBSET_SELECTION", '"Date" > 20150630')
arcpy.SelectLayerByAttribute_management('ls_db_layer', "SUBSET_SELECTION", '"Date" < 20200101')
#arcpy.SelectLayerByAttribute_management('ls_db_layer', SWITCH_SELECTION)
arcpy.FeatureClassToFeatureClass_conversion('ls_db_layer', outpath, 'LS_filtered')

LS_filtered = r'C:\Users\crouault\Documents\4 NTNU\Thesis\Data\Landslide Database\LS_filtered.shp'

# Within selected features, further select only those events which occur on the same day as 10 other
landslides
def unique_values(table, field):
    with arcpy.da.SearchCursor(table, [field]) as cursor:
        return sorted({row[0] for row in cursor})
vals = unique_values("ls_db_layer", "Date")

ls_count = [0]*len(vals)
index = 0
Dates_of_interest = [0]

for i in vals:
    arcpy.MakeFeatureLayer_management(LS_filtered, 'selection', "" "Date" = {} {}.format(i))
    countS = str(arcpy.GetCount_management('selection'))
    ls_count[index] = int(countS)
    if ls_count[index] > 9:
        Dates_of_interest.append(int(i))
    index = index + 1

# add event from Troms
Dates_of_interest.append(int(20191204))
#Dates_of_interest.append(int(20161015))
print(Dates_of_interest)

# create shapefile with just the landslides with more than 10 events on a given day in the time period of
interest
arcpy.MakeFeatureLayer_management(LS_filtered, 'LS_filtered_layer')
for i in Dates_of_interest:
    arcpy.SelectLayerByAttribute_management('LS_filtered_layer', "ADD_TO_SELECTION", "" "Date" = {}
    {}.format(i))
arcpy.FeatureClassToFeatureClass_conversion('LS_filtered_layer', outpath, 'Landslide_Day_w10'.format(i))

print len(Dates_of_interest)
```

```
#Buffer Landslides selected
#Written by Christy Rouault, February 2020

import arcpy
import numpy as np

arcpy.env.overwriteOutput = True
arcpy.env.workspace = r'C:\Users\crouault\Documents\4 NTNU\Thesis\Data\Landslide Database'
```

## Appendix A – Python Code

```
Landslide_Day_w10 = r'C:\Users\crouault\Documents\4 NTNU\Thesis\Data\Landslide
Database\Landslide_Day_w10.shp'
arcpy.MakeFeatureLayer_management(Landslide_Day_w10, 'LS_Day_w10_layer')
outpath = r'C:\Users\crouault\Documents\4 NTNU\Thesis\Data\Landslide Database'

# Buffer areas of impact around landslides with more than 10 in a day with 20 km
landslides = 'LS_Day_w10_layer'
LSBuffer = "LS_Day_w10_buffer"
distanceField = 20000 #buffer radius in metres
arcpy.Buffer_analysis(landslides, LSBuffer, distanceField)

# Add an ID field to the landslides to group multi-day events
# arcpy.AddField_management(Landslide_Day_w10, "ID", "SHORT")
with arcpy.da.UpdateCursor(Landslide_Day_w10, ['Date', 'ID']) as ID_cursor:
    for x in ID_cursor:
        if x[0] == 20150917:
            x[1] = 1
        elif x[0] == 20151126:
            x[1] = 2
        elif x[0] == 20151127:
            x[1] = 2
        elif x[0] == 20151205:
            x[1] = 3
        elif x[0] == 20151206:
            x[1] = 3
        elif x[0] == 20161015:
            x[1] = 4
        elif x[0] == 20161125:
            x[1] = 5
        elif x[0] == 20161204:
            x[1] = 6
        elif x[0] == 20161205:
            x[1] = 6
        elif x[0] == 20161230:
            x[1] = 7
        elif x[0] == 20170120:
            x[1] = 8
        elif x[0] == 20170126:
            x[1] = 9
        elif x[0] == 20170518:
            x[1] = 10
        elif x[0] == 20170724:
            x[1] = 11
        elif x[0] == 20171002:
            x[1] = 12
        elif x[0] == 20171123:
            x[1] = 13
        elif x[0] == 20171207:
            x[1] = 14
        elif x[0] == 20171223:
            x[1] = 15
        elif x[0] == 20180418:
            x[1] = 16
        elif x[0] == 20180926:
            x[1] = 17
        elif x[0] == 20190104:
            x[1] = 18
        elif x[0] == 20190606:
            x[1] = 19
        elif x[0] == 20190730:
            x[1] = 20
        elif x[0] == 20191204:
            x[1] = 21
        elif x[0] == 20191229:
            x[1] = 22
        else:
            x[1] = 0
```



## Appendix A – Python Code

```
ID_cursor.updateRow(x)

# Within selected features, further select only those events which occur in the same event as 10 other
landslides
ID_vals = np.arange(1, 23)
ls_count = [0]*len(ID_vals)
index = 0
ID_of_interest = []
LS_in_envelope_count = []
LS_envelope_ID = []
for i in ID_vals:
    arcpy.MakeFeatureLayer_management(Landslide_Day_w10, 'selection', "" "ID" = {} "" ".format(i))
    countS = str(arcpy.GetCount_management('selection'))
    ls_count[index] = int(countS)
    if ls_count[index] > 9:
        ID_of_interest.append(int(i))
    index = index + 1
ID_of_interest.append(4) # add event from this date due for geographic coverage (Troms)
ID_of_interest.sort()

# selects only features that overlap with events in the same event using hand-drawn polygons
Cluster_PYG = r'C:\Users\crouault\Documents\4 NTNU\Thesis\Data\Landslide Database\Cluster_PYG.shp'
arcpy.MakeFeatureLayer_management(Cluster_PYG, 'Cluster_PYG_layer')
outpath = r'C:\Users\crouault\Documents\4 NTNU\Thesis\Data\Landslide Database\Results\LS_Polygons.shp'

for i in ID_vals:
    arcpy.MakeFeatureLayer_management(Landslide_Day_w10, 'Landslide_{}'.format(i))
    # arcpy.SelectLayerByLocation_management('Landslide_{}'.format(i), "INTERSECT", 'Landslide_{}'.format(i), "",
"NEW_SELECTION")
    # Create envelope around landslides that are overlapping if there are more than 4 events overlapping
    arcpy.SelectLayerByAttribute_management('Cluster_PYG_layer', "NEW_SELECTION", "" "ID" = {}
"".format(i))
    arcpy.MakeFeatureLayer_management('Cluster_PYG_layer', 'Cluster_PYG_layer_{}'.format(i))
    arcpy.SelectLayerByLocation_management('Landslide_{}'.format(i), "INTERSECT", 'Cluster_PYG_layer_{}'.format(i), "",
"NEW_SELECTION")
    count = str(arcpy.GetCount_management('Landslide_{}'.format(i)))
    count = int(count)
    if count > 3:
        landslides = 'Landslide_{}'.format(i)
        LSBuffer = "{}_Envelope".format(i)
        distanceField = 20000 #buffer radius in metres
        sideType = "FULL"
        endType = "FLAT"
        dissolveType = "LIST"
        dissolveField = "ID"
        arcpy.Buffer_analysis(landslides, LSBuffer, distanceField, sideType, endType, dissolveType,
dissolveField)
        LS_in_envelope_count.append(int(count))
        LS_envelope_ID.append(int(i))
    else:
        LS_in_envelope_count.append("None")
        LS_envelope_ID.append("None")

arcpy.Append_management(["1_Envelope.shp", "2_Envelope.shp", "3_Envelope.shp", "4_Envelope.shp",
"5_Envelope.shp", "6_Envelope.shp", "7_Envelope.shp", "8_Envelope.shp", "9_Envelope.shp",
"10_Envelope.shp", "11_Envelope.shp", "12_Envelope.shp", "13_Envelope.shp", "14_Envelope.shp",
"15_Envelope.shp", "16_Envelope.shp", "17_Envelope.shp", "18_Envelope.shp", "19_Envelope.shp",
"20_Envelope.shp", "21_Envelope.shp", "22_Envelope.shp"], outpath)
# TESTS
print ID_of_interest
print len(ID_of_interest)
print LS_in_envelope_count
print len(LS_in_envelope_count)
print LS_envelope_ID
print len(LS_envelope_ID)
print ID_vals
print len(ID_vals)
```

## Appendix A – Python Code

```
#Determine Susceptibility Class of landslides
#Written by Christy Rouault, March 2020

import arcpy
import numpy as np

arcpy.env.overwriteOutput = True
arcpy.env.workspace = r'C:\Users\crouault\Documents\4 NTNU\Thesis\Data\Landslide Database\Analysis'
outpath = r'C:\Users\crouault\Documents\4 NTNU\Thesis\Data\Landslide Database\Analysis'

S_CL_Map = r'C:\Users\crouault\Documents\4 NTNU\Thesis\Data\Geology\Catchment Level Susceptibility
Mapping\Norway_ls_susc_Regime_complete.shp'
#LS_points = r'C:\Users\crouault\Documents\4 NTNU\Thesis\Data\Landslide Database\Landslide_Day_w10.shp'
NDVI_pyg = r'C:\Users\crouault\Documents\4 NTNU\Thesis\Data\Landslide
Database\Results\S2_Polygons_Merge2.shp'
arcpy.MakeFeatureLayer_management(NDVI_pyg, 'NDVI_pyg_layer')
#arcpy.MakeFeatureLayer_management(LS_points, 'LS_points_layer')
classes = ['very high', 'high', 'medium', 'low']
arcpy.AddField_management('NDVI_pyg_layer', "Sus_C1", "TEXT")

# Check which points intersects catchment level susceptibility and add an attribute with L/M/H/VH
for x in classes:
    arcpy.MakeFeatureLayer_management(S_CL_Map, 'S_CL_Map_layer', "" "susc_class" = '{}' "" ".format(x))
    arcpy.SelectLayerByLocation_management('NDVI_pyg_layer', "INTERSECT", 'S_CL_Map_layer', "",
"NEW_SELECTION")
    arcpy.FeatureClassToFeatureClass_conversion('NDVI_pyg_layer', outpath, 'LS_susc_{}'.format(x))
    class_count = arcpy.GetCount_management('NDVI_pyg_layer')
    print class_count
    with arcpy.da.UpdateCursor('NDVI_pyg_layer', ['Sus_C1']) as S_cursor:
        for i in S_cursor:
            i[0] = '{}'.format(x)
            S_cursor.updateRow(i)
```

```
#Determine Geology of landslides
#Written by Christy Rouault, March 2020

import arcpy
import numpy as np

arcpy.env.overwriteOutput = True
arcpy.env.workspace = r'C:\Users\crouault\Documents\4 NTNU\Thesis\Data\Landslide Database\Analysis'
outpath = r'C:\Users\crouault\Documents\4 NTNU\Thesis\Data\Landslide Database\Analysis'

Geol_Map = r'C:\Users\crouault\Documents\4
NTNU\Thesis\Data\Geology\LosmasseN1000\LosmFlate_N1000_20200227.shp'
arcpy.MakeFeatureLayer_management(Geol_Map, 'Geol_Map_layer')
LS_points = r'C:\Users\crouault\Documents\4 NTNU\Thesis\Data\Landslide Database\Landslide_Day_w10.shp'
arcpy.MakeFeatureLayer_management(LS_points, 'LS_points_layer')
NDVI_pyg = r'C:\Users\crouault\Documents\4 NTNU\Thesis\Data\Landslide
Database\Results\S2_Polygons_Merge2.shp'
arcpy.MakeFeatureLayer_management(NDVI_pyg, 'NDVI_pyg_layer')
geology = [14, 0, 31, 50, 73, 41, 42, 11, 81, 90]
arcpy.AddField_management('NDVI_pyg_layer', "Geology", "TEXT")

# Check which poolygons intersects with geology map
print 'polygons'
for x in geology:
    arcpy.MakeFeatureLayer_management(Geol_Map, 'Geol_Map_layer', "" "jordart" = {} "" ".format(x))
    arcpy.SelectLayerByLocation_management('NDVI_pyg_layer', "WITHIN", 'Geol_Map_layer', "",
"NEW_SELECTION")
    #arcpy.FeatureClassToFeatureClass_conversion('NDVI_pyg_layer', outpath, 'Geol_{}'.format(x))
    class_count = arcpy.GetCount_management('NDVI_pyg_layer')
    print class_count
    #with arcpy.da.UpdateCursor('NDVI_pyg_layer', ['Geology']) as S_cursor:
    #    for i in S_cursor:
```

## Appendix A – Python Code

```
#      i[0] = {}.format(x)
#      S_cursor.updateRow(i)

# Check which pointss intersects with geology map
print 'points'
for x in geology:
    arcpy.MakeFeatureLayer_management(Geol_Map, 'Geol_Map_layer', "" "jordart" = {} "" ".format(x))
    arcpy.SelectLayerByLocation_management('LS_points_layer', "WITHIN", 'Geol_Map_layer', "",
"NEW_SELECTION")
    class_count = arcpy.GetCount_management('LS_points_layer')
    print class_count

#Determine distance from landslide to the nearest road
#Written by Christy Rouault, March 2020

import arcpy

arcpy.env.overwriteOutput = True
arcpy.env.workspace = r'C:\Users\crouault\Documents\4 NTNU\Thesis\Data\Landslide Database\Analysis'
outpath = r'C:\Users\crouault\Documents\4 NTNU\Thesis\Data\Landslide Database\Analysis'

Roads = r'C:\Users\crouault\Documents\4 NTNU\Thesis\Data\Landslide Database\Results\vbse_Road_Merge.shp'
arcpy.MakeFeatureLayer_management(Roads, 'Roads_layer')
LS_points = r'C:\Users\crouault\Documents\4 NTNU\Thesis\Data\Landslide Database\Landslide_Day_w10.shp'
arcpy.MakeFeatureLayer_management(LS_points, 'LS_points_layer')
LS_polygons = r'C:\Users\crouault\Documents\4 NTNU\Thesis\Data\Landslide
Database\Results\2_S2_Polygon.shp'
arcpy.MakeFeatureLayer_management(LS_polygons, 'LS_polygon_layer')

# Check if each landslide points intersects roads with a 10 m buffer

LS_count = arcpy.GetCount_management('LS_polygon_layer')
arcpy.SelectLayerByLocation_management('LS_polygon_layer', "WITHIN_A_DISTANCE", 'Roads_layer', "10
meters", "NEW_SELECTION")
Road_int_count = arcpy.GetCount_management('LS_polygon_layer')
print LS_count
print Road_int_count

arcpy.SelectLayerByLocation_management('LS_polygon_layer', "WITHIN_A_DISTANCE", 'Roads_layer', "25
meters", "NEW_SELECTION")
Road_int_count = arcpy.GetCount_management('LS_polygon_layer')
print Road_int_count

arcpy.SelectLayerByLocation_management('LS_polygon_layer', "WITHIN_A_DISTANCE", 'Roads_layer', "50
meters", "NEW_SELECTION")
Road_int_count = arcpy.GetCount_management('LS_polygon_layer')
print Road_int_count

arcpy.SelectLayerByLocation_management('LS_polygon_layer', "WITHIN_A_DISTANCE", 'Roads_layer', "100
meters", "NEW_SELECTION")
Road_int_count = arcpy.GetCount_management('LS_polygon_layer')
print Road_int_count

arcpy.SelectLayerByLocation_management('LS_polygon_layer', "WITHIN_A_DISTANCE", 'Roads_layer', "200
meters", "NEW_SELECTION")
Road_int_count = arcpy.GetCount_management('LS_polygon_layer')
print Road_int_count

arcpy.SelectLayerByLocation_management('LS_polygon_layer', "WITHIN_A_DISTANCE", 'Roads_layer', "1000
meters", "NEW_SELECTION")
Road_int_count = arcpy.GetCount_management('LS_polygon_layer')
print Road_int_count
```

## Appendix B: Landslide Database Selection

Appendix B – Landslide Database Selection

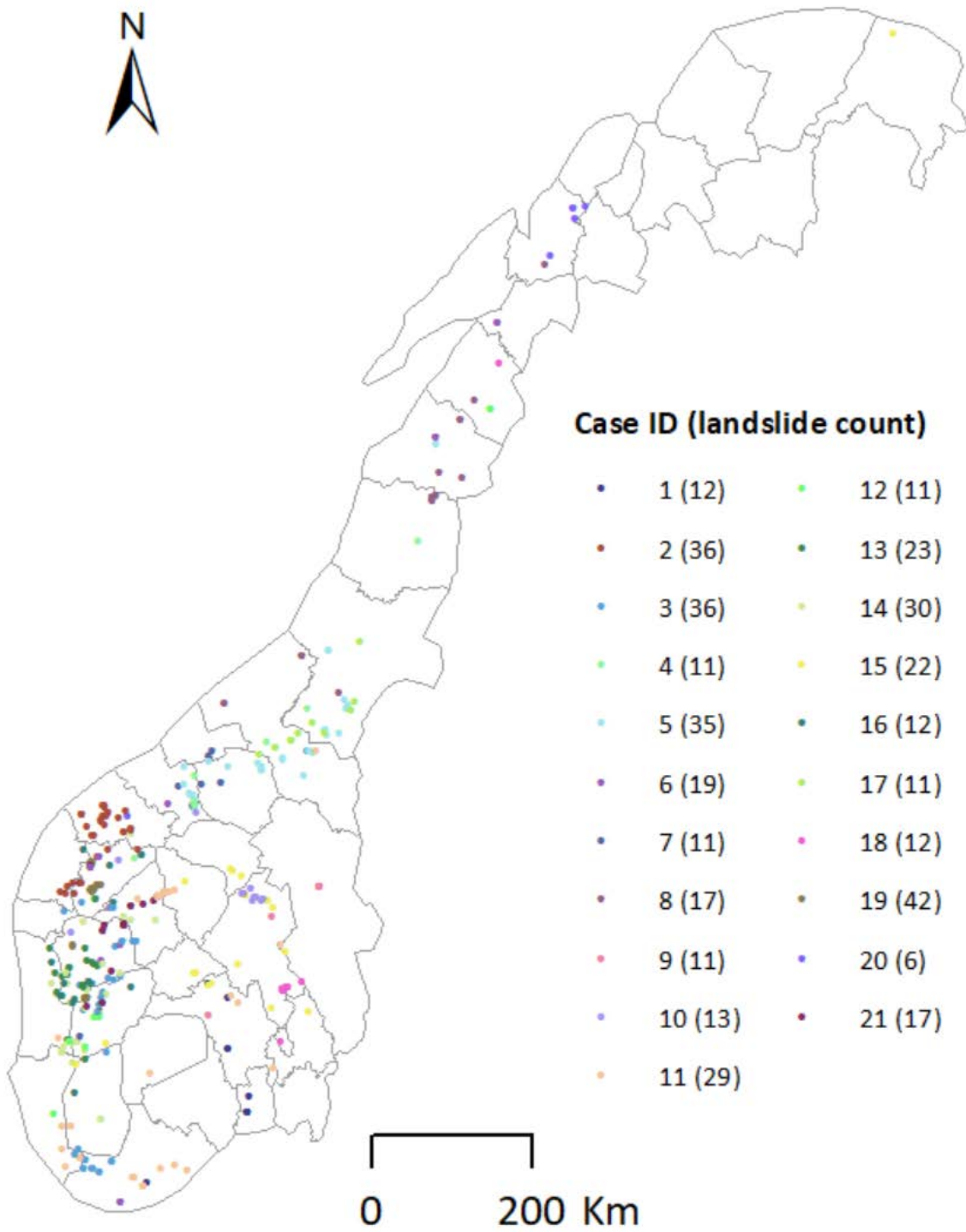


Figure A1. Landslides Registered in NVE database on dates of selected case studies, including those outside of clusters, identified by .











## Appendix B – Landslide Database Selection

Landslide ID	Type	Time	noyTidspkt	noyPosisjo	regStatus	ID	dNDVI	InSAR
A23823F2-18B6-4BC0-8116-	144	20190730170000	4 timer	250 m	Registrert	19	NA	NA
569B9C02-FB80-45F4-84C5-	144	20190730170000	4 timer	10 m	Registrert	19	NA	NA
CBDA30AD-BDF2-4374-8C40-	144	20190730170000	4 timer	10 m	Registrert	19	NA	NA
1F199ACE-C39D-4F3B-B923-	144	20190730170000	4 timer	100 m	Registrert	19	NA	NA
84CE9879-17F1-42E2-BDAE-	144	20190730170000	4 timer	250 m	Registrert	19	NA	NA
16C0208F-D631-4453-B2B4-	142	20190730160000	4 timer	Eksakt	Registrert	19	M	NA
32E92CE4-84DF-41D4-84F5-	142	20190730150000	12 timer	50 m	Registrert	19	M	NA
F02244E7-F213-4FD9-8B15-	142	20190730160000	12 timer	50 m	Registrert	19	M	NA
92E399D4-63F5-442B-8736-	142	20190730165300	1 time	500 m	Registrert	19	D	
3848BB80-BE80-472C-9420-	142	20190730160000	4 timer	Eksakt	Registrert	19	D	NA
986FED1B-4ADB-4ED8-AB76-	142	20190730163000	1 time	500 m	Registrert	19	D	
47414DA4-3125-4232-A82C-	142	20190730163000	30 min	Eksakt	Registrert	19	N	
850B3FD3-FE2C-4C51-9294-	142	20190730170000	30 min	Eksakt	Registrert	19	NA	NA
3D8180D9-8F8E-4985-8B37-	142	20190730170000	30 min	Eksakt	Registrert	19	NA	NA
6AC2A921-598C-41D1-A6DD-	142	20190730164000	4 timer	Eksakt	Registrert	19	Y	
0C475368-7F44-4727-A67D-	142	20190730150000	12 timer	Eksakt	Registrert	19	Y	
27055E63-3010-4A50-A32E-	142	20190730160000	4 timer	Eksakt	Registrert	19	Y	NA
BF78591E-9EF8-47E3-81FD-FF5EA706F16E	142	20190730165000	10 min	Eksakt	Registrert	19	Y	
CEFCAA5C-5D50-4293-9766-	142	20190730165300	12 timer	500 m	Registrert	19	Y	
05C8A39C-6902-41B6-900A-	142	20190730155800	12 timer	500 m	Registrert	19	Y	
2B876048-78C3-46D2-A947-	142	20190730164500	15 min	Eksakt	Registrert	19	Y	
5467BF2A-60F7-4CEC-A5B8-	142	20190730163000	30 min	Eksakt	Registrert	19	Y	
D63F6AAA-0F07-4F22-8D3C-	142	20190730163000	30 min	Eksakt	Registrert	19	Y	
185297FB-39F6-4A2B-9160-	142	20190730163000	30 min	Eksakt	Registrert	19	Y	
E43FF1F4-A2ED-4171-8BEB-	142	20190730160000	4 timer	Eksakt	Registrert	19	Y	NA
D22B3AC6-5F46-4F3F-8A97-	142	20190730160000	4 timer	Eksakt	Registrert	19	Y	NA
58A27DBD-0A22-4842-8798-	142	20190730160000	4 timer	Eksakt	Registrert	19	Y	NA
8EF78858-4F86-444E-8AB7-	142	20190730163000	1 time	Eksakt	Registrert	19	Y	
FF7CD9BF-E006-40E4-B1A3-	144	20190730204900	Eksakt	Eksakt	Registrert	19	Y	N
6C12E5EB-A0AE-4A20-A70D-	144	20190730164500	30 min	Eksakt	Registrert	19	Y	
EFAAD6B9-43B8-44D1-85B1-	144	20190730163000	30 min	Eksakt	Registrert	19	Y	
BE09ECA6-66EA-4D7E-8447-	144	20190730163000	1 time	500 m	Registrert	19	Y	
9769F4D6-00D9-454E-BC84-	144	20190730173000	15 min	50 m	Registrert	19	Y	
26044F99-1F06-4401-AE9C-	133	20191204070000	Ikke registrert	Eksakt	Registrert	20	NA	
EF786C32-DEDC-4784-9F0D-	142	20191204180000	Eksakt	Eksakt	Registrert	20	N	
0E255DDE-991C-4C4D-8274-	142	20191204200000	Eksakt	Eksakt	Registrert	20	N	
DD8765A1-94EE-4081-A050-	142	20191204160000	Eksakt	Eksakt	Registrert	20	N	
9C768FEB-FD59-4A91-8B40-	142	20191204095300	Eksakt	Eksakt	Registrert	20	NA	
6504985C-C092-46B5-8D8F-	142	20191204203600	Eksakt	Eksakt	Registrert	20	Y	
24D46E88-A176-4B53-BE00-	144	20191229170500	Eksakt	Eksakt	Registrert	21	M	
61DB054E-33ED-425A-8C03-	144	20191229000055	Eksakt	Eksakt	Registrert	21	NA	
83392C11-A403-4BB5-B902-	144	20191229200010	2 dager	Eksakt	Registrert	21	NA	
2486721E-61B5-4C6E-BD98-	144	20191229132600	Eksakt	Eksakt	Registrert	21	NA	
9F22B7B3-49DD-434E-A040-	142	20191229185533	1 dag	Eksakt	Registrert	21	M	
6382D3B3-F6C8-4665-B02D-	142	20191229181300	Eksakt	Eksakt	Registrert	21	M	
842B9580-2367-4E05-9B16-	142	20191229174100	Eksakt	Eksakt	Registrert	21	M	
ED105170-44FE-4BAD-A737-	142	20191229153923	1 dag	10 m	Registrert	21	N	
9733D24C-A0F0-44F7-BC9E-	142	20191229212500	Eksakt	Eksakt	Registrert	21	N	
0400D9D2-2C49-43FB-922F-	142	20191229120000	1 dag	1000 m	Registrert	21	N	
FD13FFCA-8329-4299-A597-	142	20191229095600	Eksakt	Eksakt	Registrert	21	NA	
DD26B900-EF7A-431E-9F74-	142	20191229114000	Eksakt	Eksakt	Registrert	21	NA	
1F0D7603-DCFB-4BE3-AAB5-	142	20191229112300	Eksakt	Eksakt	Registrert	21	NA	
275DCC8D-A823-450C-B102-	142	20191229201300	Eksakt	Eksakt	Registrert	21	NA	
3E1230FD-34BF-47D0-8A77-	142	20191229201300	Eksakt	Eksakt	Registrert	21	NA	
0B9E3A0E-F186-4036-82D3-	142	20191229090800	Eksakt	Eksakt	Registrert	21	NA	
FD17F67F-FF78-4D50-A7CE-	133	20191229165000	30 min	Eksakt	Registrert	21	M	

Appendix C: SAR Analysis

Appendix C – SAR Analysis

Table C1. Sentinel-1 images for SAR landslide mapping

ID	Track	Orbit	Pre-Event Image	Days Before Event	Post-Event Image	Days After Event
1	44	Ascending	S1A_IW_SLC__1SDV_20150909T170204_20150909T170231_007641_00A981_D46B	7	S1A_IW_SLC__1SDV_20150921T170204_20150921T170231_007816_00AE19_7B14	5
2	15	Ascending	S1A_IW_SLC__1SDV_20151118T171859_20151118T171926_008662_00C501_6E56	4	S1A_IW_SLC__1SDV_20151130T171858_20151130T171925_008837_00C9E7_50B8	4
3	15	Ascending	S1A_IW_SLC__1SDV_20151130T171805_20151130T171835_008837_00C9E7_D78B	5	S1A_IW_SLC__1SDV_20151212T171808_20151212T171835_009012_00CEC5_DFD2	7
4	44	Ascending	S1A_IW_SLC__1SDV_20161114T170306_20161114T170333_013941_016729_C815	11	S1A_IW_SLC__1SDV_20161126T170306_20161126T170333_014116_016C7A_E07A	1
5	37	Descending	S1B_IW_SLC__1SDV_20161202T054607_20161202T054634_003213_005787_39CE	2	S1B_IW_SLC__1SDV_20161214T054607_20161214T054634_003388_005C92_70D1	10
6	110	Descending	S1A_IW_SLC__1SDV_20161225T055533_20161225T055600_014532_01799C_08DC	5	S1B_IW_SLC__1SDV_20161231T055448_20161231T055515_003636_0063B9_B7D2	1
7	110	Descending	S1A_IW_SLC__1SDV_20170118T055506_20170118T055534_014882_01845F_D44C	2	S1B_IW_SLC__1SDV_20170124T055421_20170124T055449_003986_006E0F_4B8A	3
8	66	Descending	S1B_IW_SLC__1SDV_20170121T052839_20170121T052906_003942_006CC6_DCED	5	S1A_IW_SLC__1SDV_20170127T052932_20170127T052959_015013_018863_E910	1
9	37	Descending	S1A_IW_SLC__1SDV_20170513T054711_20170513T054738_016559_01B74F_9E04	5	S1B_IW_SLC__1SDV_20170519T054632_20170519T054659_005663_009EB2_B33B	1
10	146	Ascending	S1A_IW_SLC__1SDV_20170719T165428_20170719T165455_017543_01D56C_B8AA	5	S1B_IW_SLC__1SDV_20170725T165348_20170725T165415_006647_00BB10_393D	1
11	117	Ascending	S1B_IW_SLC__1SDV_20171003T170925_20171003T170953_007668_00D8A4_AB93	5	S1A_IW_SLC__1SDV_20170927T171016_20170927T171046_018564_01F4A1_98DE	1
12	15	Ascending	S1A_IW_SLC__1SDV_20171119T171851_20171119T171919_019337_020C5A_907D	4	S1B_IW_SLC__1SDV_20171125T171800_20171125T171827_008441_00EF3E_823B	2
13	117	Ascending	S1A_IW_SLC__1SDV_20171126T171046_20171126T171114_019439_020FA5_F713	11	S1A_IW_SLC__1SDV_20171208T171046_20171208T171114_019614_021518_88AA	1
14	15	Ascending	S1B_IW_SLC__1SDV_20171219T171749_20171219T171817_008791_00FA66_3F52	4	S1A_IW_SLC__1SDV_20171225T171850_20171225T171918_019862_021CB3_AF5C	2
15	37	Descending	S1A_IW_SLC__1SDV_20180414T054732_20180414T054759_021459_024F4B_12E1	4	S1B_IW_SLC__1SDV_20180420T054642_20180420T054709_010563_013434_84F7	2
16	15	Ascending	S1B_IW_SLC__1SDV_20180921T171807_20180921T171834_012816_017A90_B2FF	5	S1A_IW_SLC__1SDV_20180927T171901_20180927T171930_023887_029B6C_91D1	1
17	73	Ascending	S1B_IW_SLC__1SDV_20181230T164616_20181230T164643_014274_01A8D0_C78C	5	S1A_IW_SLC__1SDV_20190105T164658_20190105T164726_025345_02CE24_97EC	1
18	139	Descending	S1A_IW_SLC__1SDV_20190603T053931_20190603T053958_027511_031ABA_1E94	3	S1B_IW_SLC__1SDV_20190609T053841_20190609T053908_016615_01F45C_FF79	3
19	117	Ascending	S1B_IW_SLC__1SDV_20190725T171026_20190725T171053_017293_020856_0890	5	S1A_IW_SLC__1SDV_20190731T171108_20190731T171136_028364_033489_BE08	1
20	58	Ascending	S1B_IW_SLC__1SDV_20191130T160659_20191130T160727_019159_02429D_8F86	4	S1A_IW_SLC__1SDV_20191206T160735_20191206T160802_030230_0374B1_9052	2
21	110	Descending	S1A_IW_SLC__1SDV_20191222T055555_20191222T055622_030457_037C89_3B2C	7	S1A_IW_SLC__1SDV_20200103T055554_20200103T055621_030632_03828E_FA85	5
A	174	Ascending	S1A_IW_SLC__1SDV_20191202T162038_20191202T162105_030171_0372A2_9334	2	S1B_IW_SLC__1SDV_20191208T162000_20191208T162028_019275_024650_3E9B	4
B	62	Descending	S1A_IW_SLC__1SDV_20190808T230435_20190808T230502_028484_033836_FD0B	9	S1A_IW_SLC__1SDV_20190820T230436_20190820T230503_028659_033E4A_E468	3
C	53	Descending	S1A_IW_SLC__1SDV_20200228T083057_20200228T083127_031450_039EF4_BD1C	4	S1B_IW_SLC__1SDV_20200305T083024_20200305T083052_020554_026F33_3F26	2
D	14	Ascending	S1B_IW_SLC__1SSH_20161013T154442_20161013T154509_002490_00432B_FE5E	2	S1A_IW_SLC__1SSH_20161019T154524_20161019T154551_013561_015B59_27EA	4

Appendix C – SAR Analysis

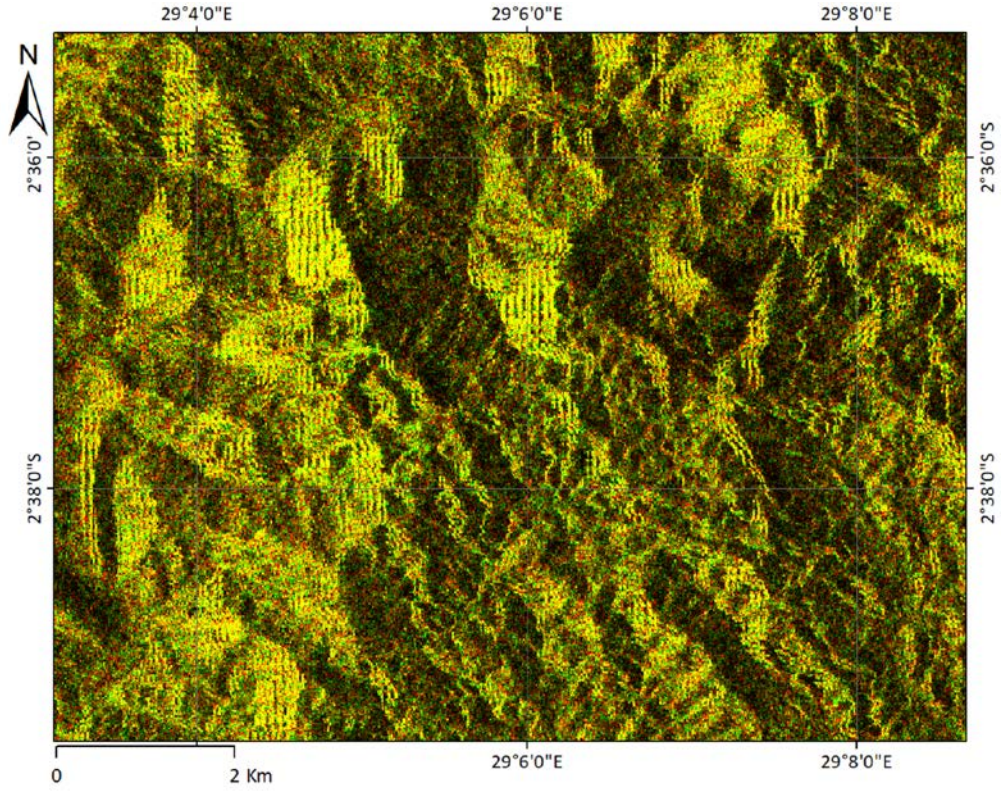


Figure C1. SAR intensity change detection at Site A, Burundi

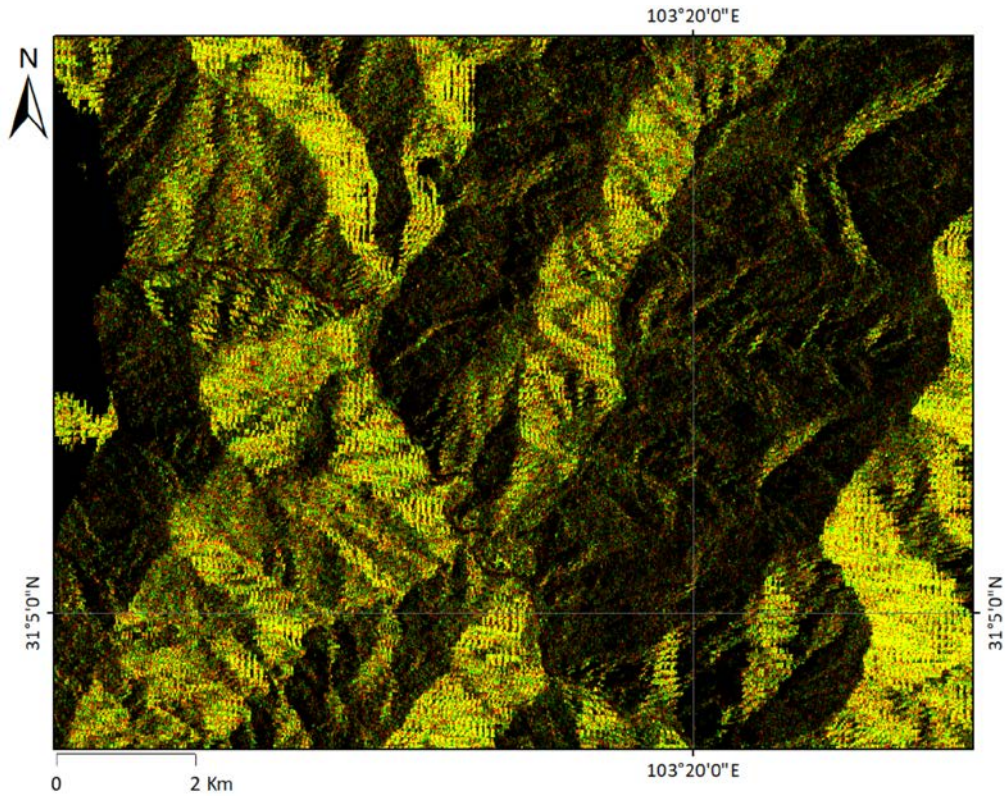


Figure C2. SAR intensity change detection at Site B, China

Appendix C – SAR Analysis

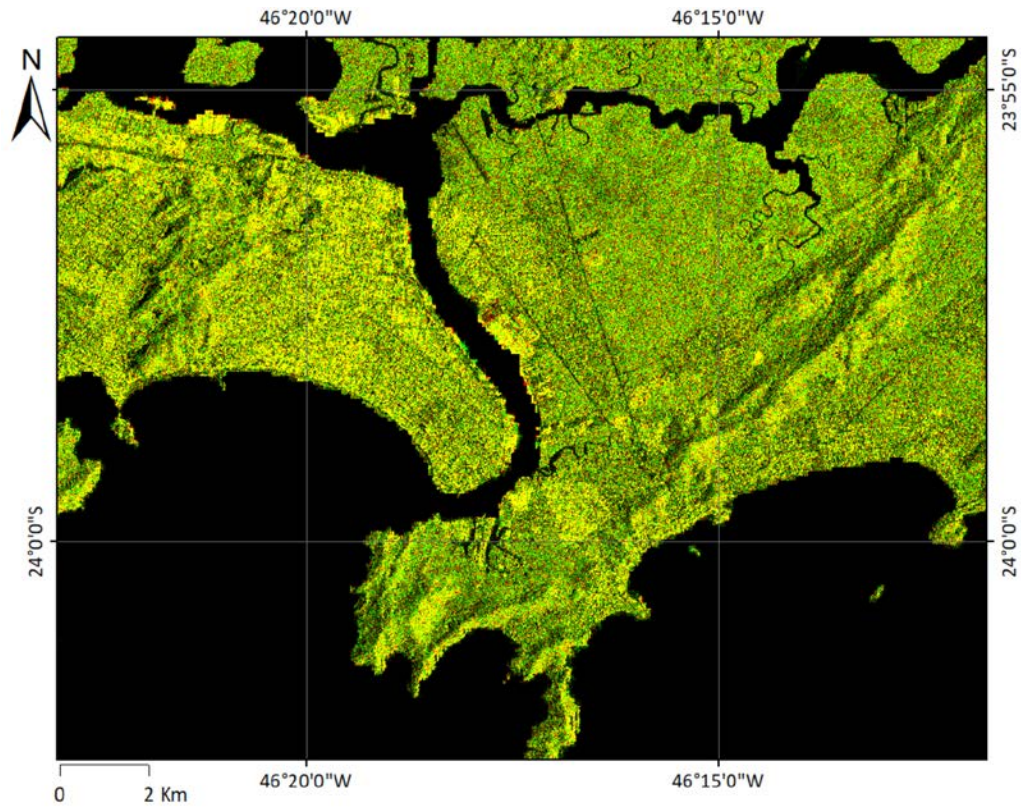


Figure C2. SAR intensity change detection at Site C, Brazil

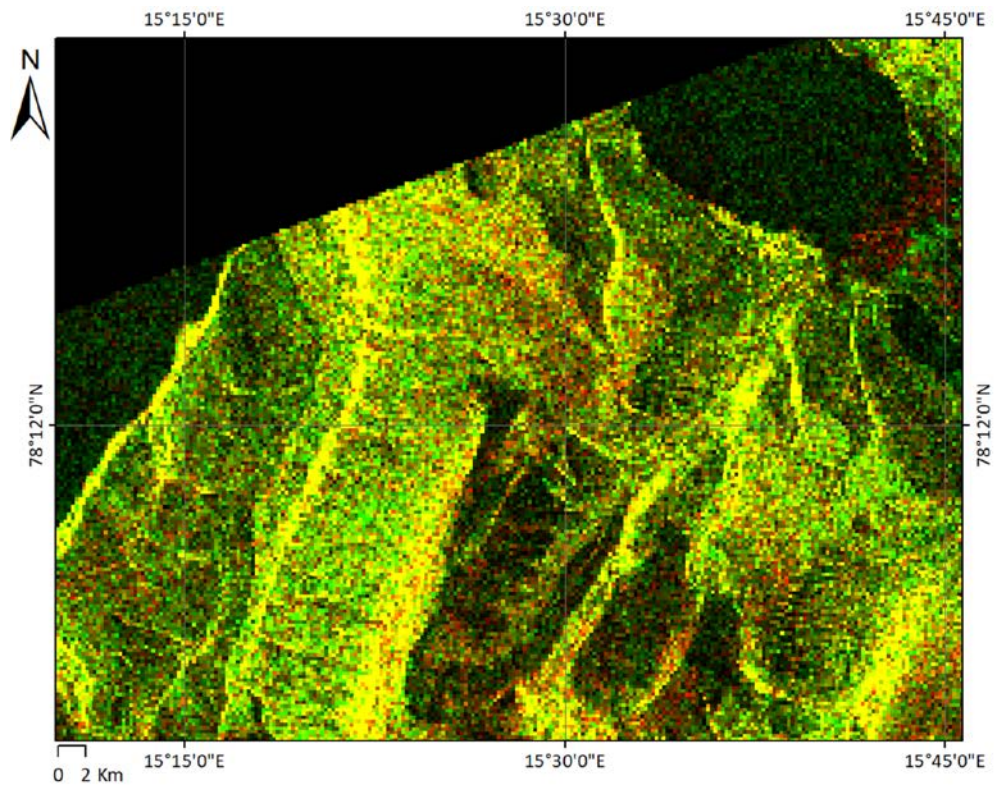


Figure B2. SAR intensity change detection at Site D, Svalbard

## Appendix D: $\delta$ NDVI Analysis

Appendix D –  $\delta$ NDVI Analysis

Table D1. Sentinel-2 images for  $\delta$ NDVI landslide mapping

ID	Pre-Event Image	Days Before Event	Post-Event Image	Days After Event
1	S2A_MSIL1C_20150911T104036_N0204_R008_T32VNL_20150911T104038	6	S2A_MSIL1C_20151113T105302_N0204_R051_T32VNL_20151113T105301	57
2	S2A_MSIL1C_20150821T111056_N0204_R137_T32VLP_20150821T111059	97	S2A_MSIL1C_20160822T105652_N0204_R094_T32VLP_20160822T105653	270
3	S2A_MSIL1C_20150904T105046_N0204_R051_T32VLK_20150904T105042	92	S2A_MSIL1C_20160214T110142_N0201_R094_T32VLP_20160214T110150	71
4	S2A_MSIL1C_20161107T105242_N0204_R051_T32VMQ_20161107T105238	18	S2A_MSIL1C_20170205T105221_N0204_R051_T32VMQ_20170205T105223	72
5	S2A_MSIL1C_20160620T105032_N0204_R051_T32VNR_20160620T105028	167	S2B_MSIL1C_20170630T105029_N0205_R051_T32VNR_20170630T105305	208
6	S2A_MSIL1C_20161107T105242_N0204_R051_T32VMP_20161107T105238	53	S2A_MSIL1C_20170211T111201_N0204_R137_T32VMP_20170211T111155	43
7	S2A_MSIL1C_20161107T105242_N0204_R051_T32VMQ_20161107T105238	74	S2A_MSIL1C_20170205T105221_N0204_R051_T32VMQ_20170205T105223	16
8	S2A_MSIL1C_20161021T110102_N0204_R094_T33WVP_20161021T110101	97	S2A_MSIL1C_20170208T110211_N0204_R094_T33WVP_20170208T110209	13
9	S2A_MSIL2A_20170503T104021_N0205_R008_T32VPP_20170503T104024	15	S2A_MSIL2A_20170503T104021_N0205_R008_T32VPP_20170503T104024	5
10	S2A_MSIL2A_20170705T105031_N0205_R051_T32VNP_20170705T105026	19	S2A_MSIL2A_20170827T105651_N0205_R094_T32VNP_20170827T105652	34
11	S2B_MSIL1C_20170915T104009_N0205_R008_T32VMK_20170915T104215	17	S2A_MSIL2A_20171102T105211_N0206_R051_T32VMK_20171102T131812	31
12	S2A_MSIL2A_20171112T105301_N0206_R051_T32VLM_20171112T124940	11	S2A_MSIL2A_20180121T105341_N0206_R051_T32VLM_20180121T130138	59
13	S2A_MSIL2A_20171009T110951_N0205_R137_T32VLM_20171009T110946	59	S2A_MSIL2A_20180223T110041_N0206_R094_T32VLM_20180223T131657	78
14	S2A_MSIL2A_20171112T105301_N0206_R051_T32VLM_20171112T124940	41	S2A_MSIL2A_20180121T105341_N0206_R051_T32VLM_20180121T130138	29
15	S2B_MSIL2A_20180416T105029_N0207_R051_T32VNR_20180416T112038	14	S2B_MSIL2A_20180509T105619_N0207_R094_T32VNR_20180509T112216	1
16	S2A_MSIL2A_20180904T110621_N0208_R137_T32VLM_20180904T143104	22	S2A_MSIL1C_20181011T105951_N0206_R094_T32VLM_20181011T112731	15
17	S2A_MSIL1C_20181110T110251_N0207_R094_T32VNR_20181110T111728	55	S2A_MSIL1C_20190205T105231_N0207_R051_T32VNR_20190205T110320	32
18	S2B_MSIL1C_20190531T105039_N0207_R051_T32VNN_20190531T125247	6	S2A_MSIL1C_20190615T105031_N0207_R051_T32VNN_20190615T112558	9
19	S2A_MSIL2A_20190728T105621_N0213_R094_T32VLP_20190728T135007	2	S2B_MSIL2A_20190802T105629_N0213_R094_T32VLP_20190802T135403	3
20	S2A_MSIL2A_20191016T110041_N0213_R094_T33WXS_20191016T122142	49	S2B_MSIL2A_20200212T104049_N0214_R008_T33WXS_20200212T123248	70
21	S2B_MSIL2A_20191130T110319_N0213_R094_T32VLN_20191130T123218	29	S2B_MSIL1C_20200122T111249_N0208_R137_T32VLN_20200122T112042	24
A	S2A_MSIL2A_20190915T080611_N0213_R078_T35MQT_20190915T105801	80	S2A_MSIL2A_20191214T081331_N0213_R078_T35MQT_20191214T111406	10
B	S2B_MSIL2A_20190425T034539_N0211_R104_T48RUV_20190425T075734	114	S2A_MSIL2A_20190927T034541_N0213_R104_T48RUV_20190927T080200	41
C	S2A_MSIL2A_20200127T131241_N0213_R138_T23KLP_20200127T151126	36	S2A_MSIL2A_20200307T131241_N0214_R138_T23KLP_20200307T152827	4
D	S2A_MSIL1C_20160922T120812_N0204_R109_T33XWG_20160922T120	23	S2B_MSIL1C_20170917T125749_N0205_R038_T33XWG_20170917T125747	337



Appendix D –  $\delta$ NDVI Analysis

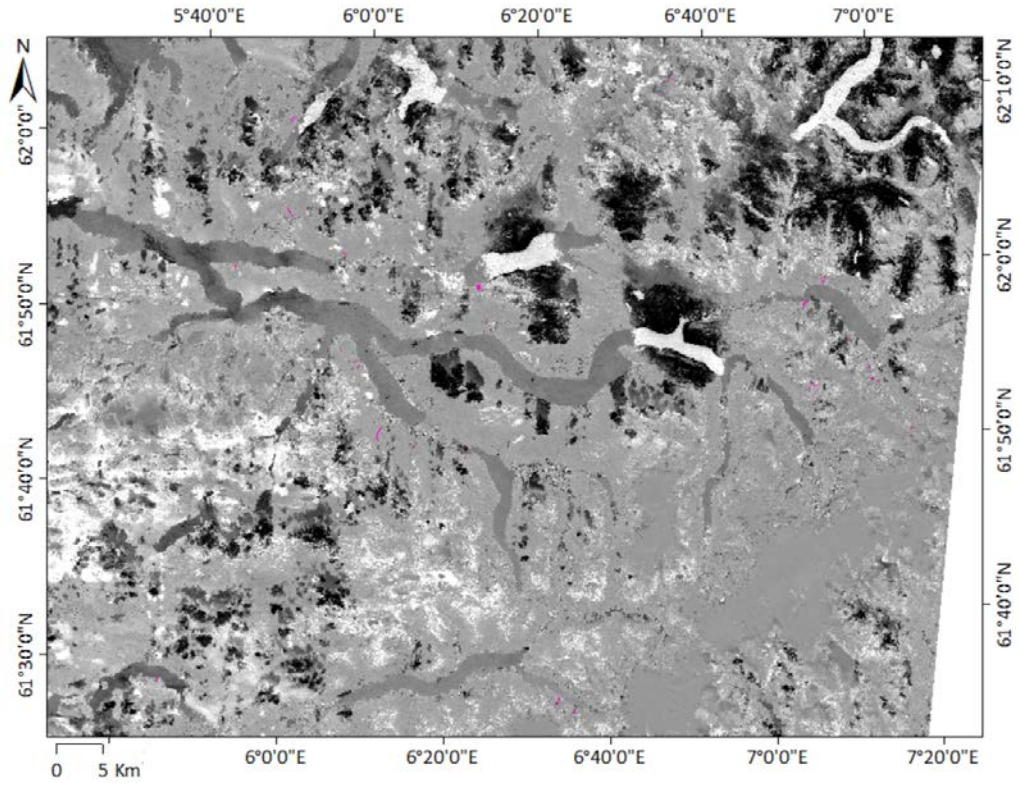


Figure D1.  $\delta$ NDVI with mapped polygons in case 2

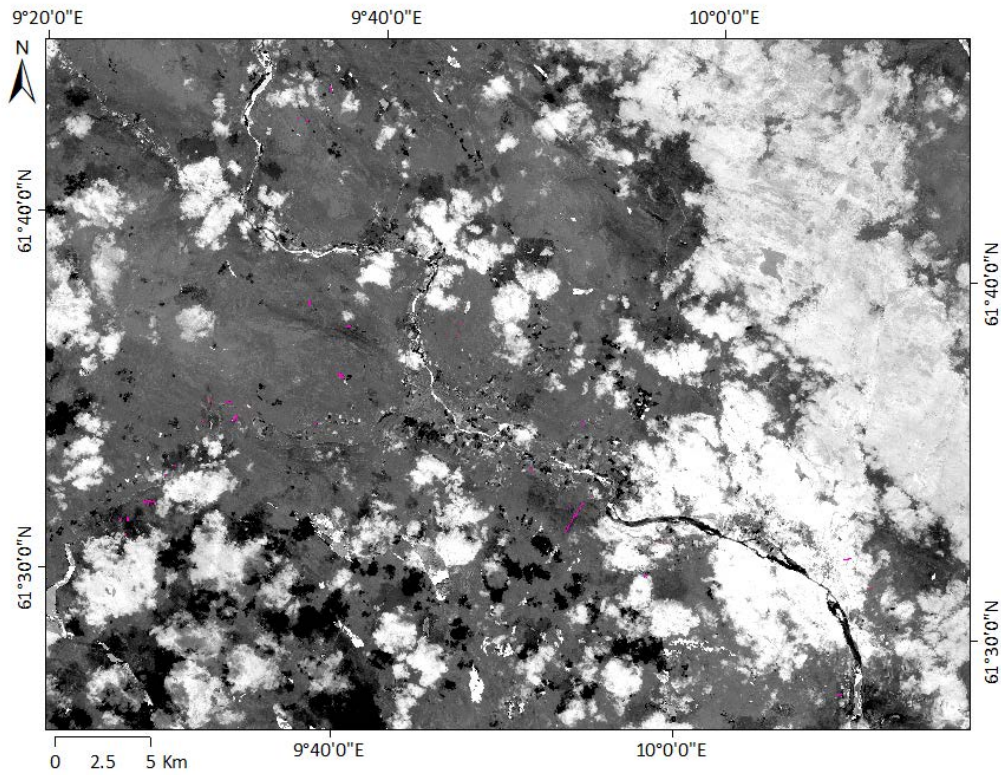


Figure D2  $\delta$ NDVI with mapped polygons in case 10

Appendix D –  $\delta$ NDVI Analysis

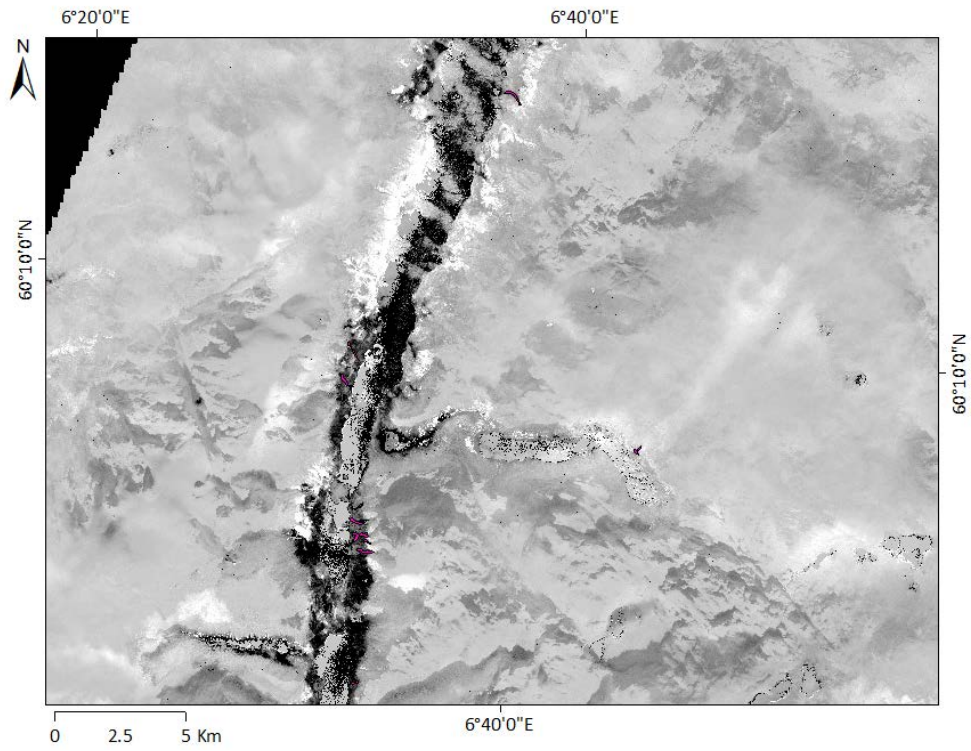


Figure D3.  $\delta$ NDVI with mapped polygons in case 12

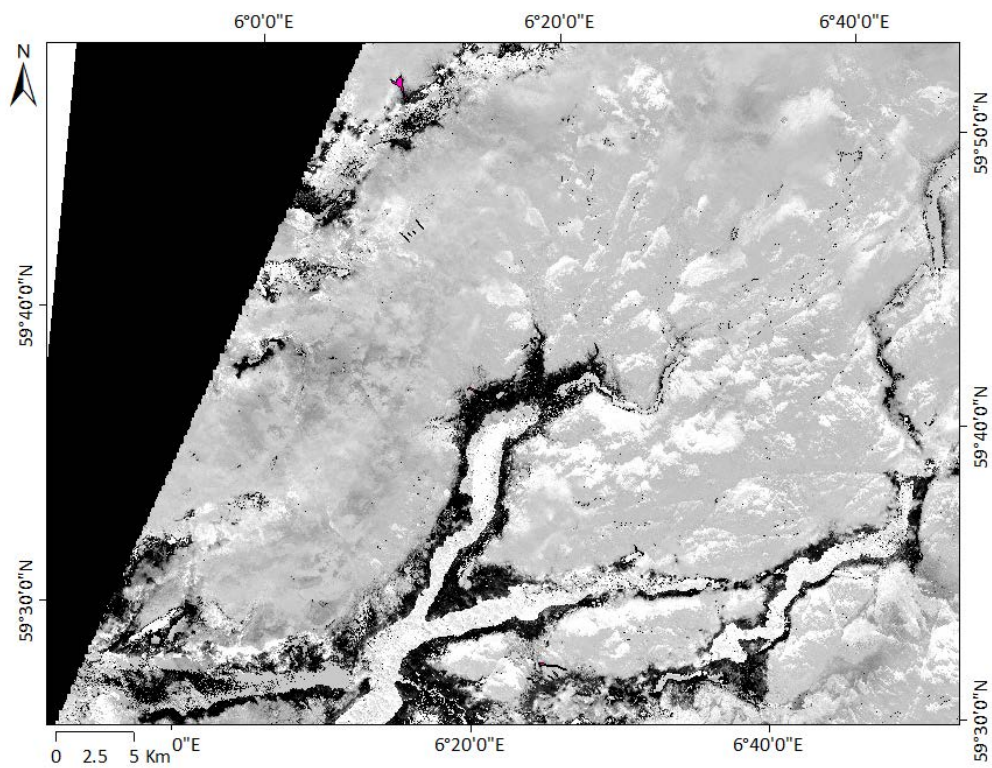


Figure D4.  $\delta$ NDVI with mapped polygons in case 14

Appendix D –  $\delta$ NDVI Analysis

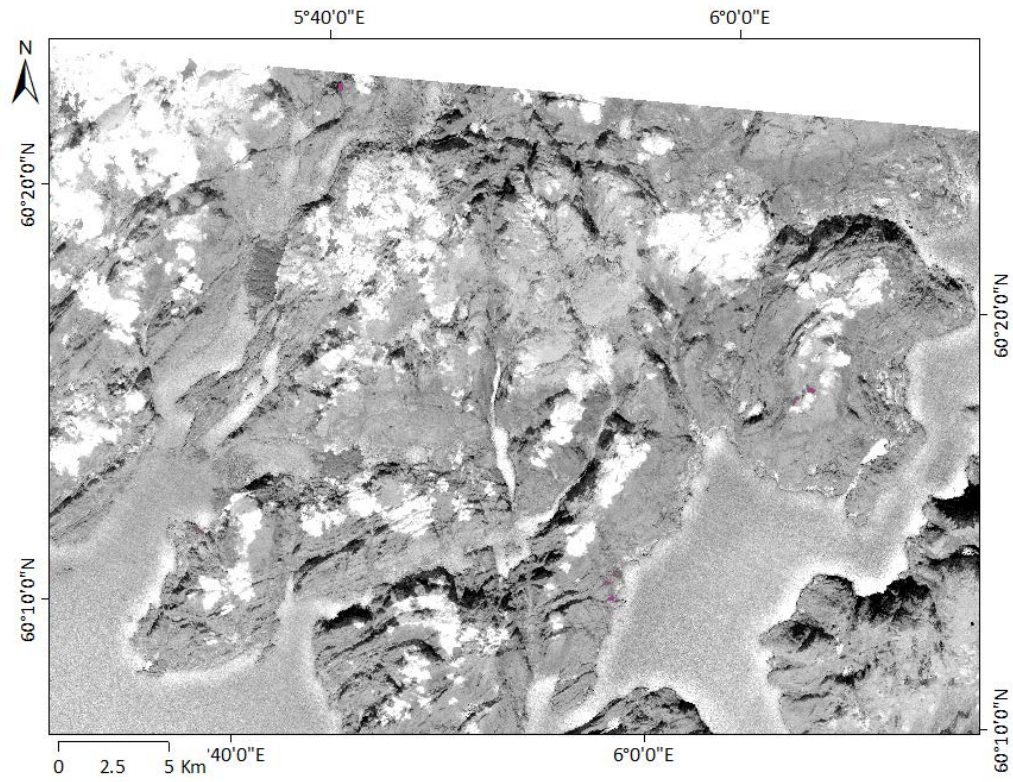


Figure D5.  $\delta$ NDVI with mapped polygons in case 16

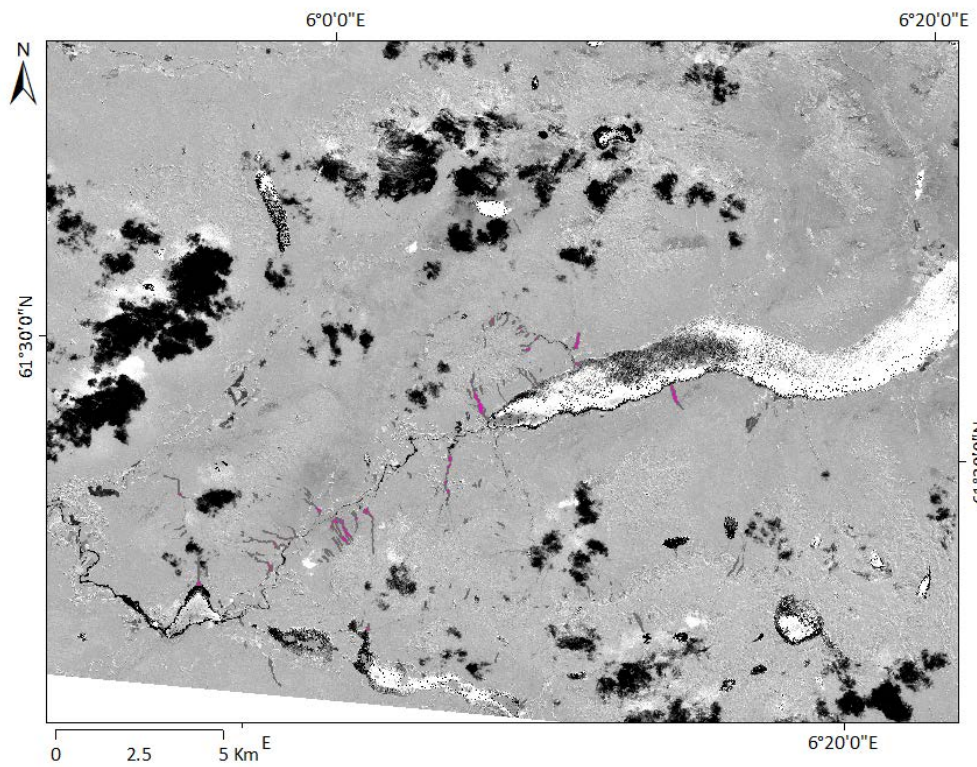


Figure D6.  $\delta$ NDVI with mapped polygons in case 19

Appendix D –  $\delta$ NDVI Analysis

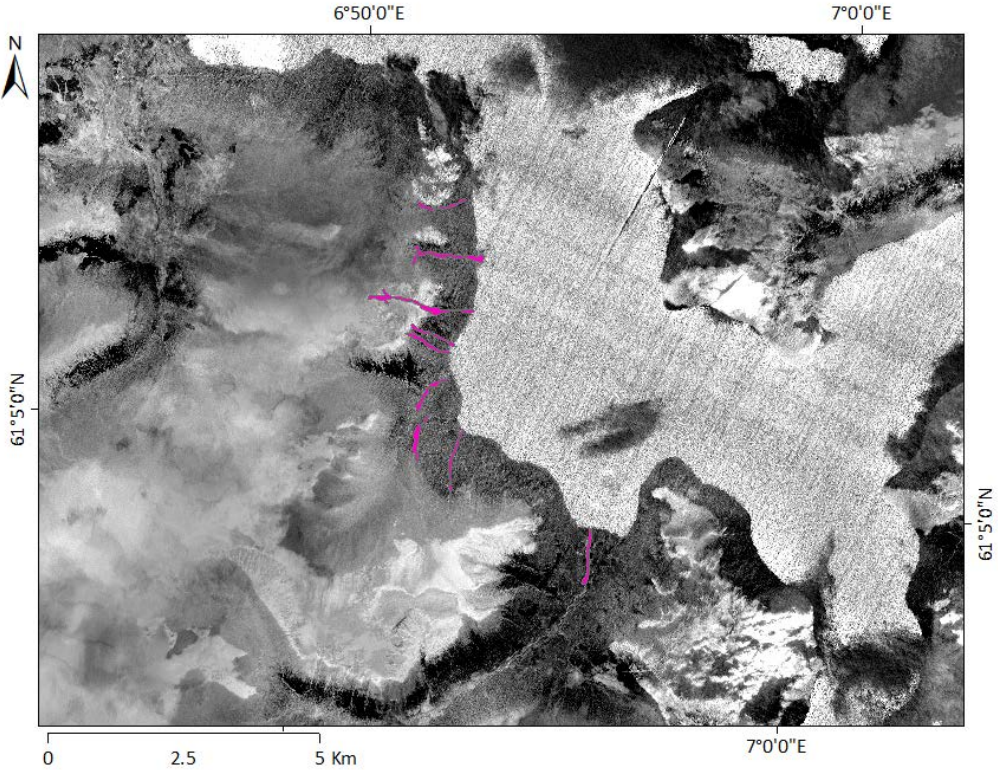


Figure D7.  $\delta$ NDVI with mapped polygons in case 21

Appendix E: Weather Data

Appendix E – Weather Data

Table E1. Weather station data

ID	Date	Nearest Hourly Weather Station	Antecedent 1 Day	Antecedent 3 Day	Maximum Hourly Rainfall	Maximum 3 Hr Rainfall	Maximum 24 Hr Rainfall	Max 1 Day Precipitation	Max 3 Day Precipitation	Snowmelt (xgeo.no)	Rain Gauge Ref	Latitude (m)	Longitude (m)	Elevation (m)
1	20150917	Gvarv-Nes	9.3	62	7.5	15.9	53.3	52.2	103.1	0	32060	171307	6596960	93
2	20151126/27	Ørsta-Eitrefjell	23.9	26.1	6.5	17.7	88.6	72	129.1	8	59695	47112	6922527	690
3	20151205/06	Elk-Hove	61.4	90.2	8.9	24.1	139.2	135.7	247.3	10	43010	5607	6516535	65
4	20161125	Innerdalen	15	26.9	7.1	14.2	41.9	41.9	86.5	10	64700	181944	6970110	405
5	20161204/05	Trondheim-Voll	14	26	4.5	9.9	29.2	20.2	47.1	10	68860	273087	7039283	127
6	20161230	Myrkdalen-Vetlebotn	10.7	22.2	8.1	23	90	73.5	117.4	9	51990	37734	6778197	700
7	20170120	Innerdalen	31.2	38.2	5	13.4	56	31.2	68.9	11	64700	181944	6970110	405
8	20170126	Glomfjord-Skihytta	36.4	44	5.4	13.7	79.7	69.8	106.2	10	80705	453648	7412463	520
9	20170518	Rena-Ørnhaugen	2.5	7.3	6.6	18.5	45.7	45.7	52.1	3	7420	312778	6810063	872
10	20170724	Skåbu	2.7	2.7	10.5	29.5	52.4	49.7	53.3	0	13655	202602	6834728	928
11	20171002	Åseral	54.8	163.2	11.7	31.9	75.9	66.5	197.1	0	41480	59794	6522462	268
12	20171123	Sauda	21	21.3	10.6	18.8	83.9	73.9	129.1	6	46610	13312	6643831	5
13	20171207	Kvamskogen-Jonshøgdi	49.6	118.9	9.1	25.1	82	78.2	169.2	7	50310	2972	6728890	455
14	20171223	Sauda	27.4	40.3	11.3	29.3	125.7	113.4	145.5	15	46610	13312	6643831	5
15	20180418	Vest-Torpa II	0	0	1	2	2	2	2	19	21680	230990	6765866	542
16	20180926	Gullfjellet	8.8	27.2	15.7	45.7	138.8	124.2	181.6	0	50865	20221	6731505	345
17	20190104	Trondheim-Voll	8	25.7	2.3	5.3	23	23	42.6	11	68860	273087	7039283	127
18	20190606	Hamar II	1.6	4.9	15.1	25.5	35.6	29.2	39.9	0	12290	287541	6746888	141
19	20190730	Haukedal	0.5	0.8	22.8	43.6	113.6	107.8	114.2	0	56960	40609	6839990	311
20	20191204	Malangen-Pålfinnmoen	15.6	57.8	4	7.6	37.6	29.2	66.2	10	90100	644184	7704933	124
21	20191229	Vangsnes	7.7	7.8	5.3	12	76.2	57.3	100.7	10	53101	51345	6810852	49

Appendix E – Weather Data

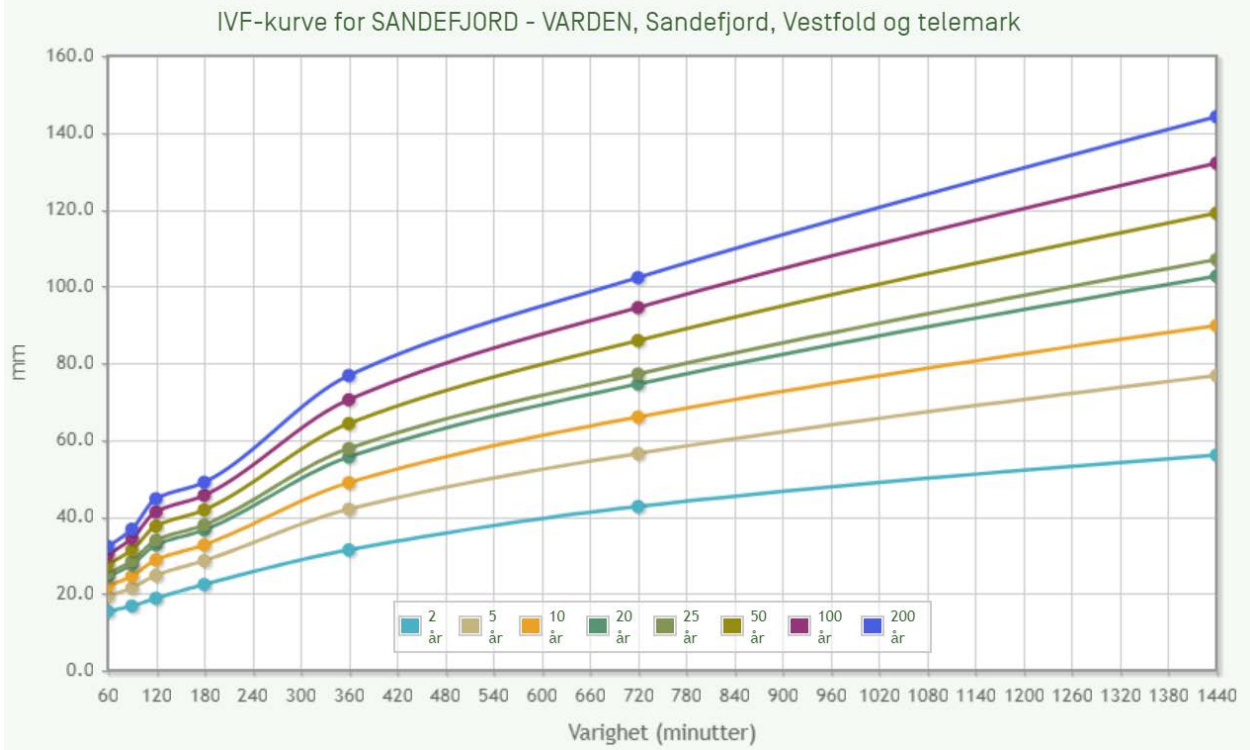


Figure E1. IDF Curve for case 1

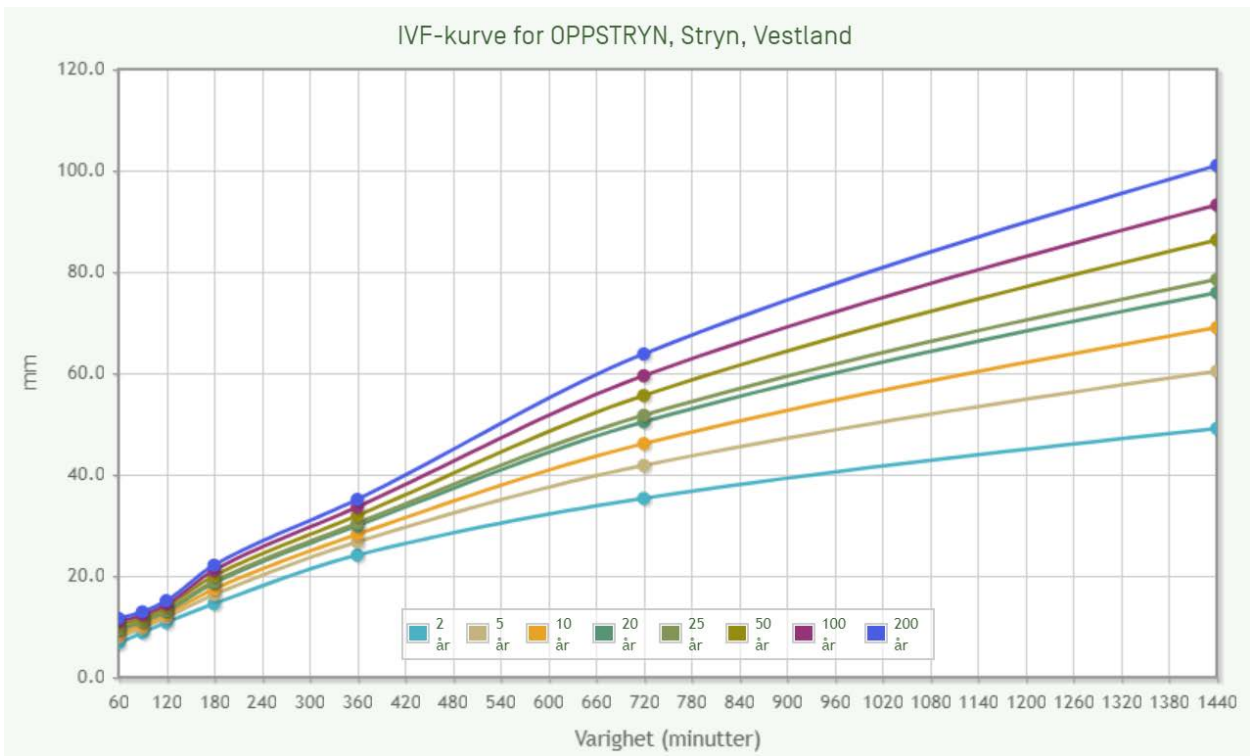


Figure E2. IDF Curve for case 2, 19

Appendix E – Weather Data

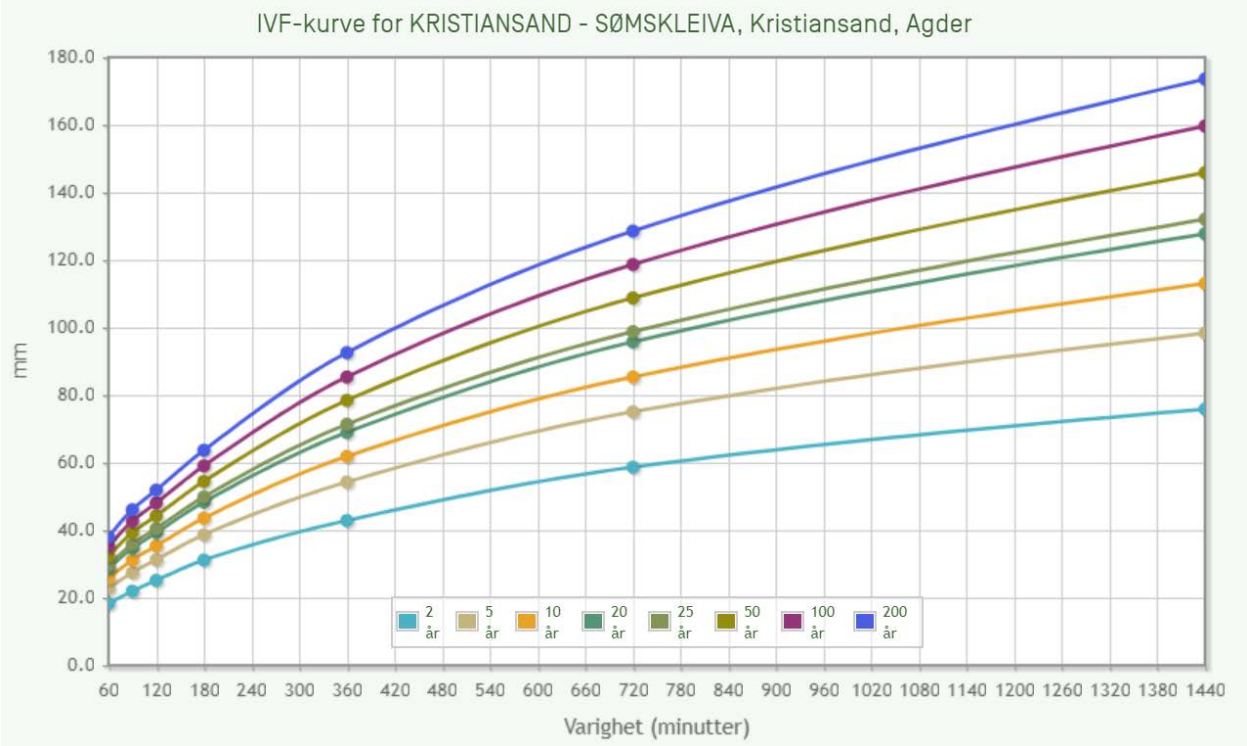


Figure E3. IDF Curve for case 3

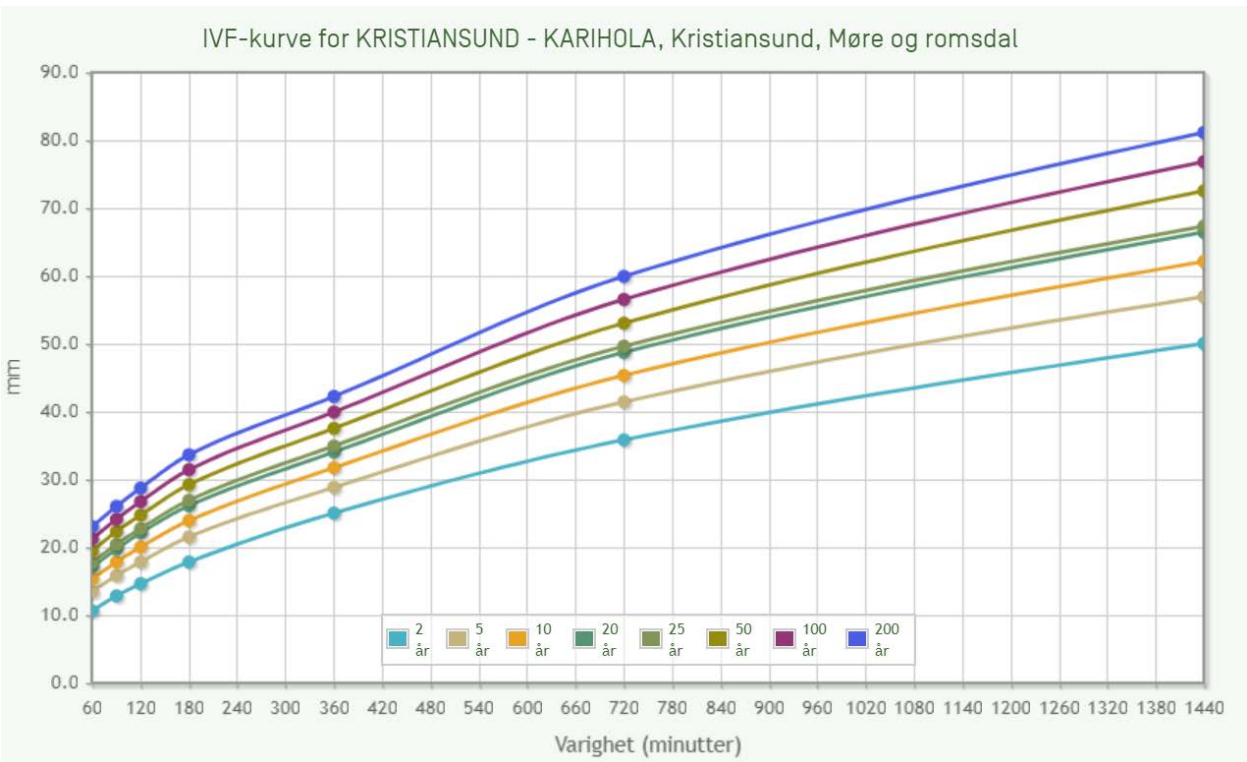


Figure E4. IDF Curve for case 4, 7



Appendix E – Weather Data

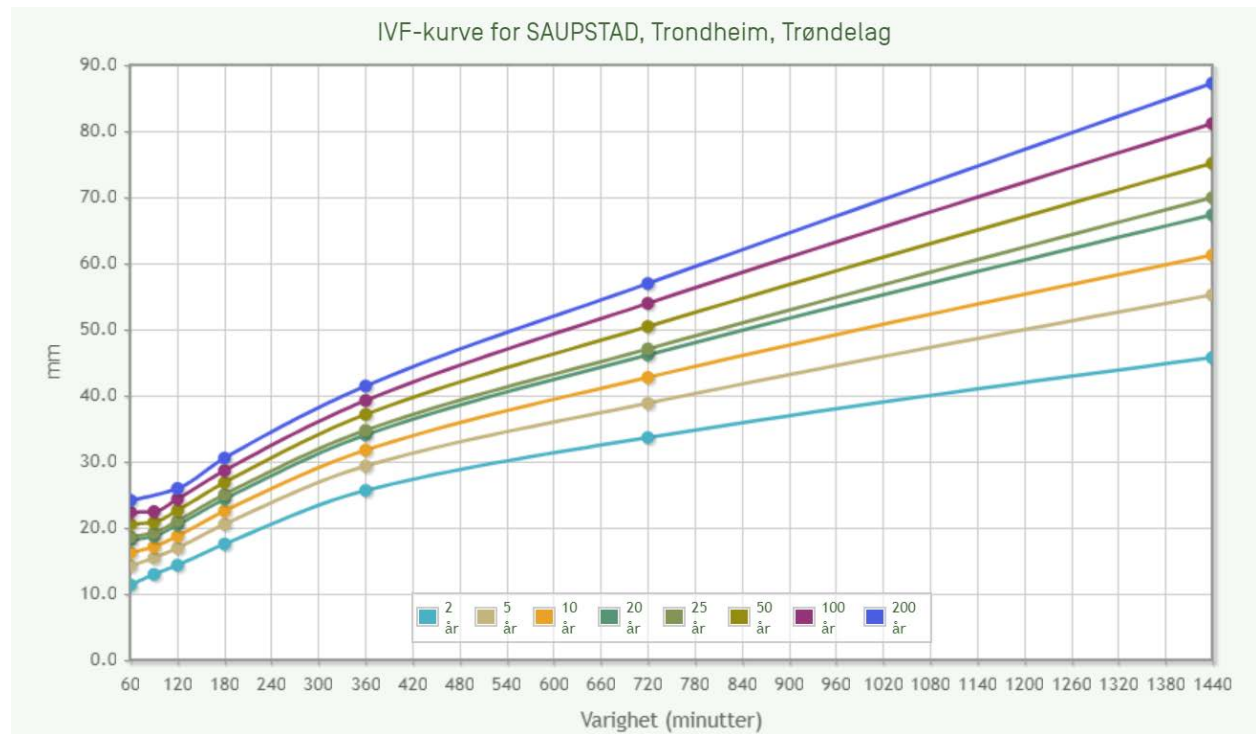


Figure E5. IDF Curve for case 5, 17

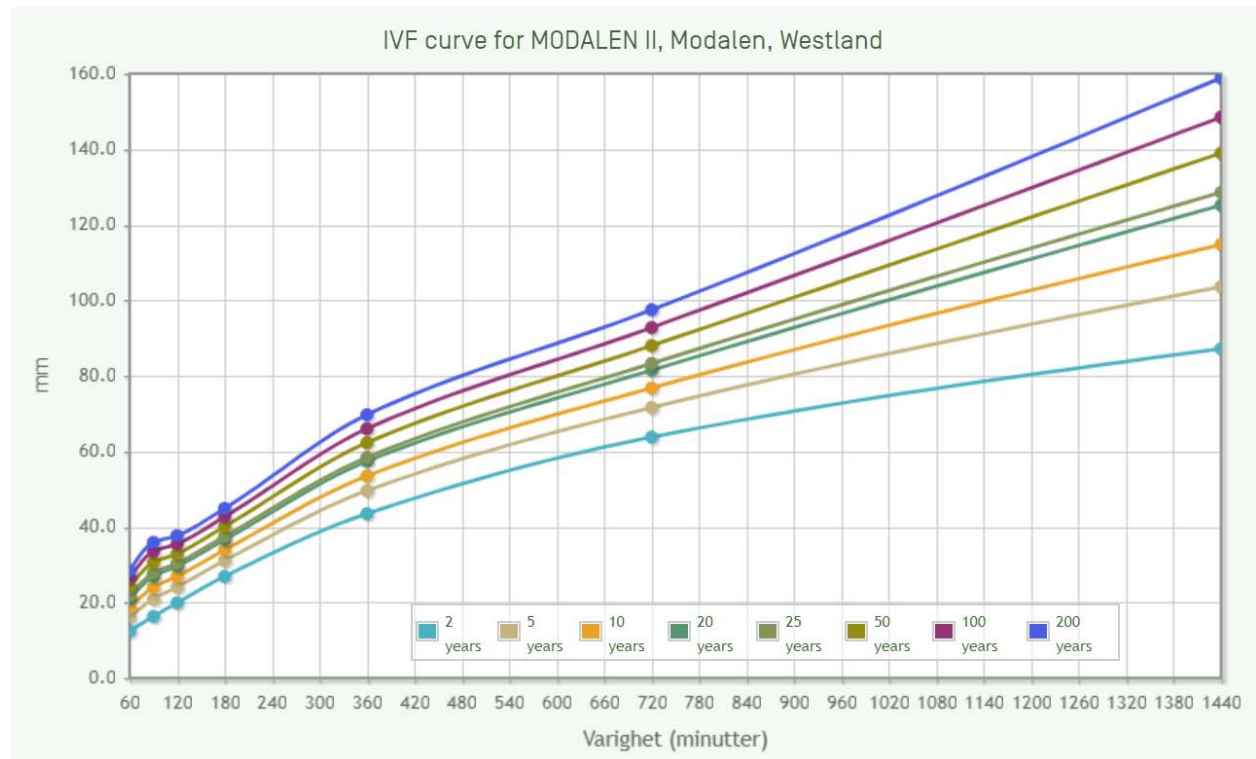


Figure E6. IDF Curve for case 6, 21

Appendix E – Weather Data

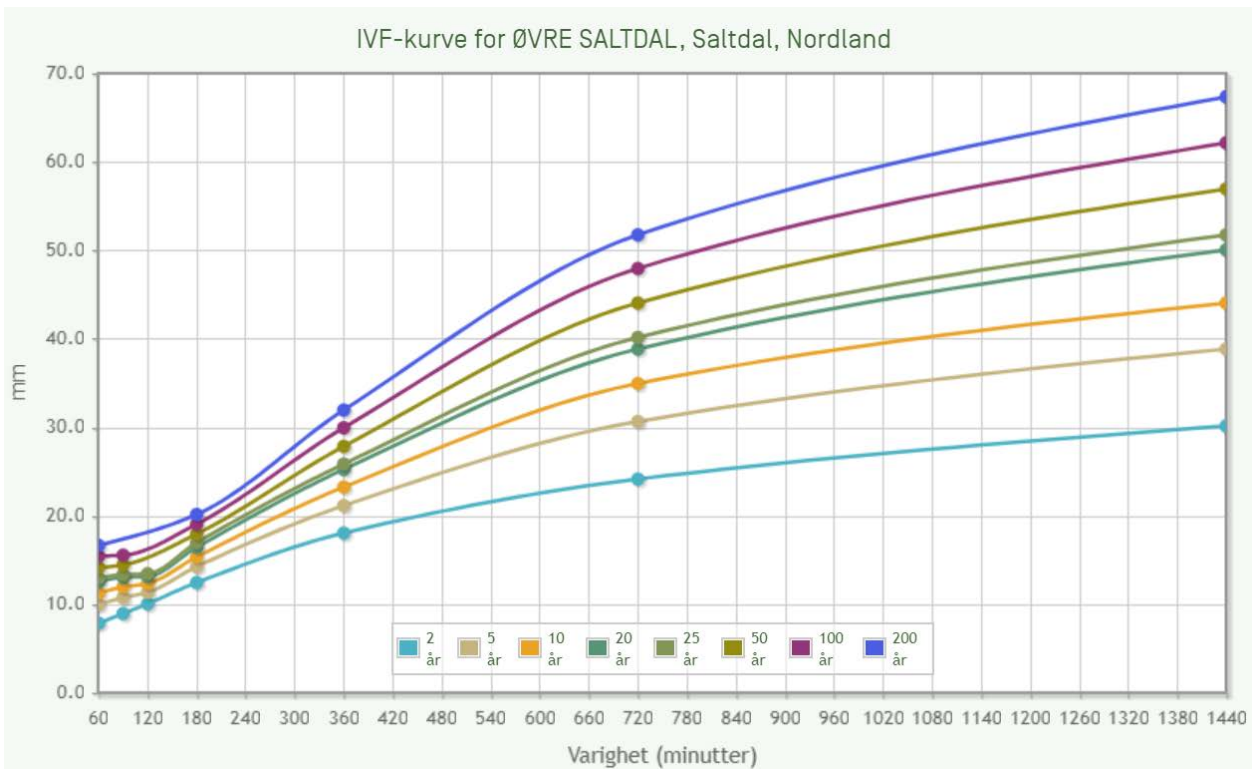


Figure E7. IDF Curve for case 8

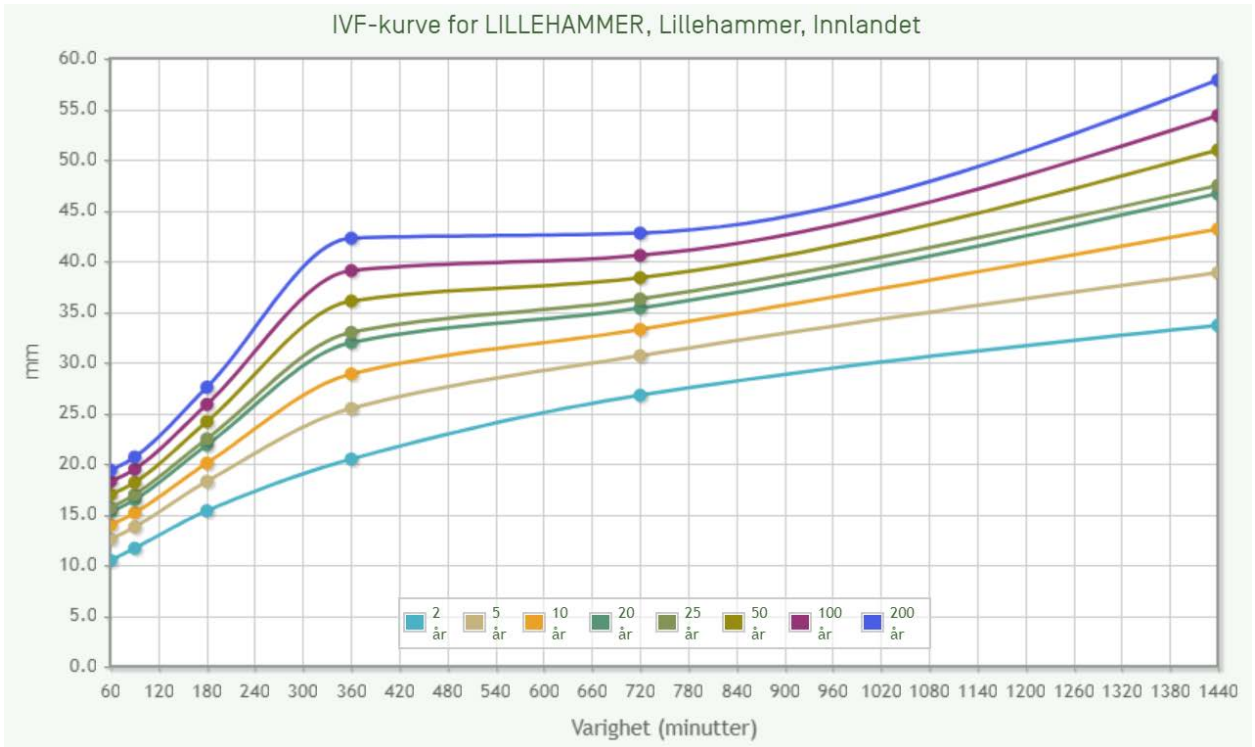


Figure E8. IDF Curve for case 9, 10

Appendix E – Weather Data

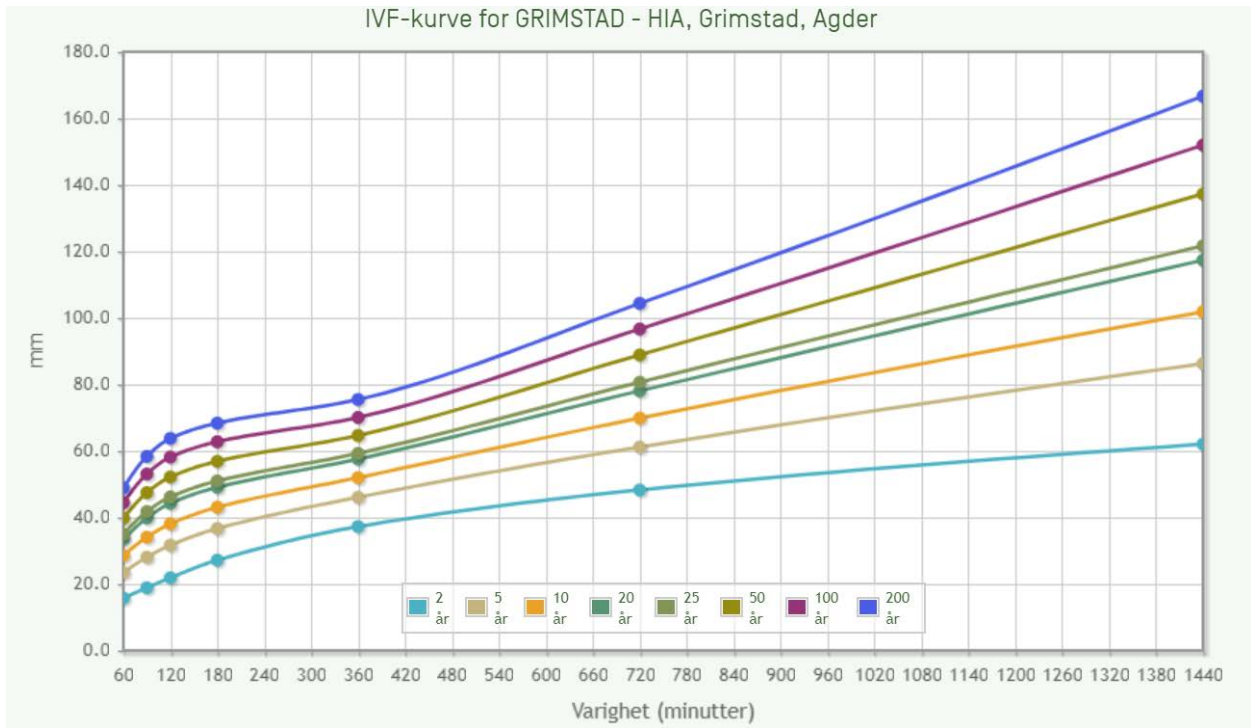


Figure E9. IDF Curve for case 11

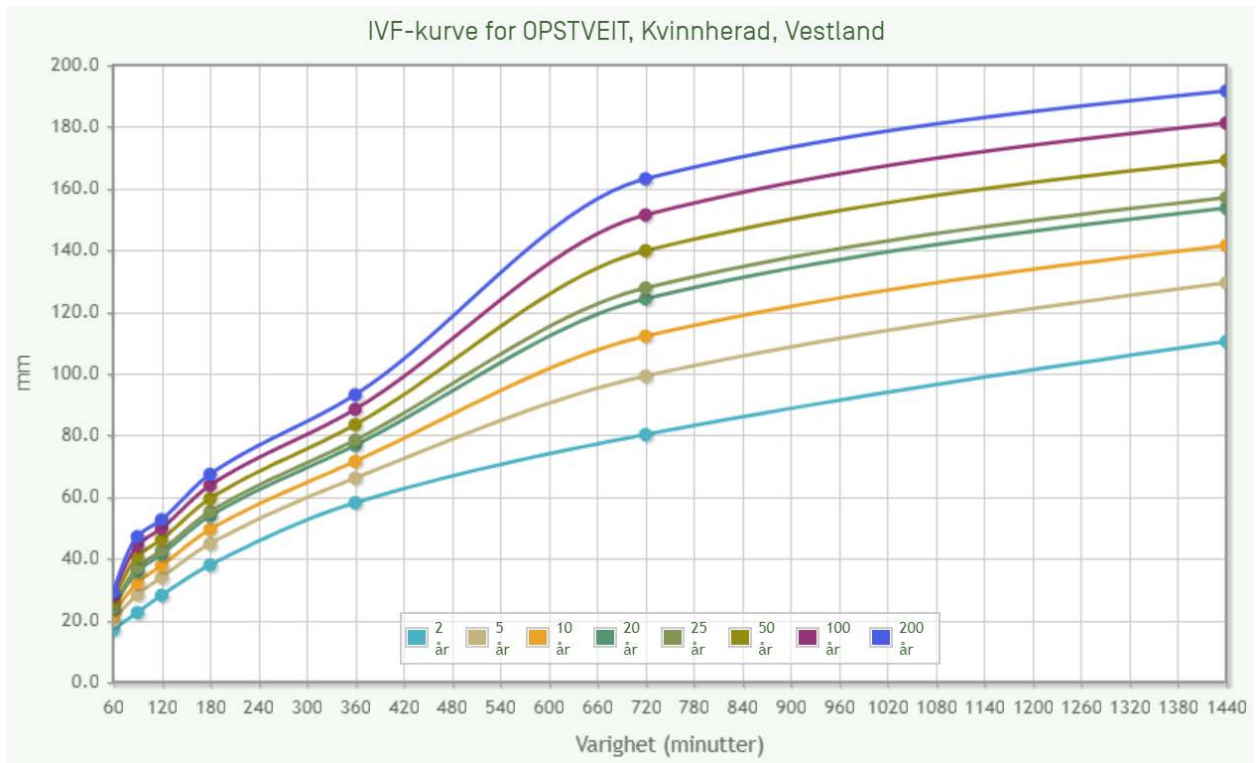


Figure E10. IDF Curve for case 12, 14

Appendix E – Weather Data

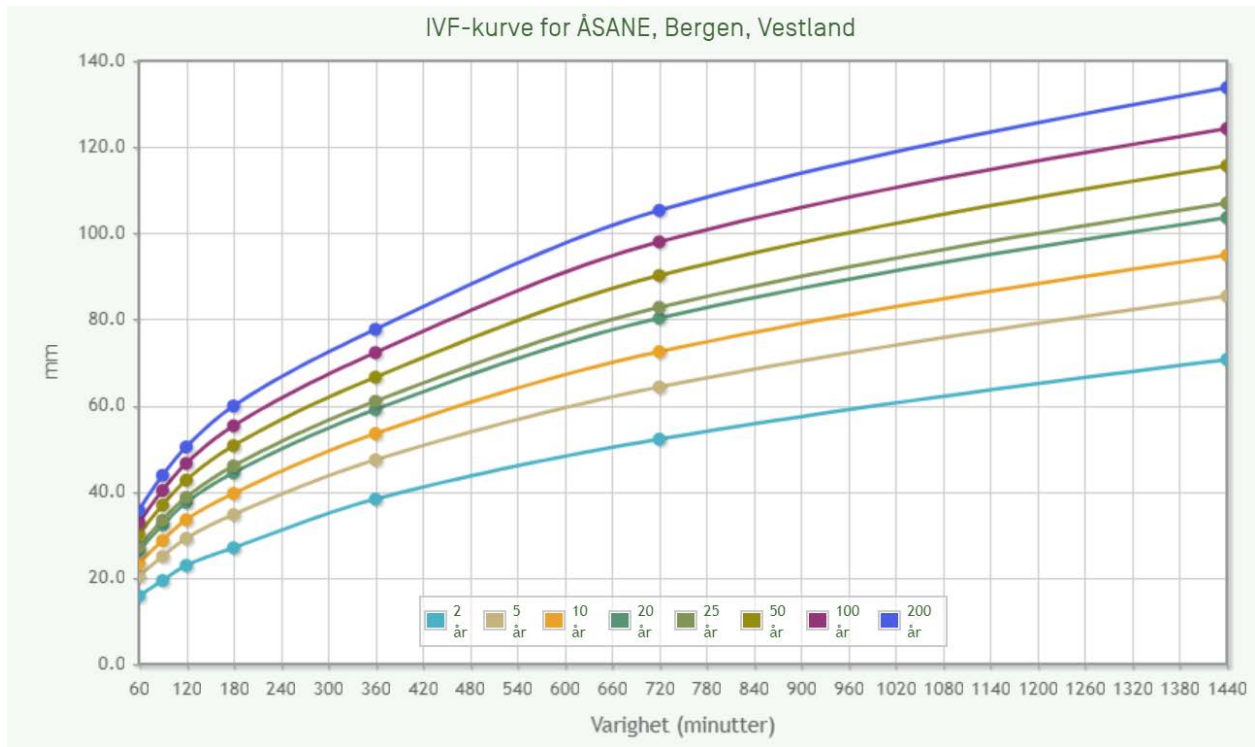


Figure E11. IDF Curve for case 13, 16

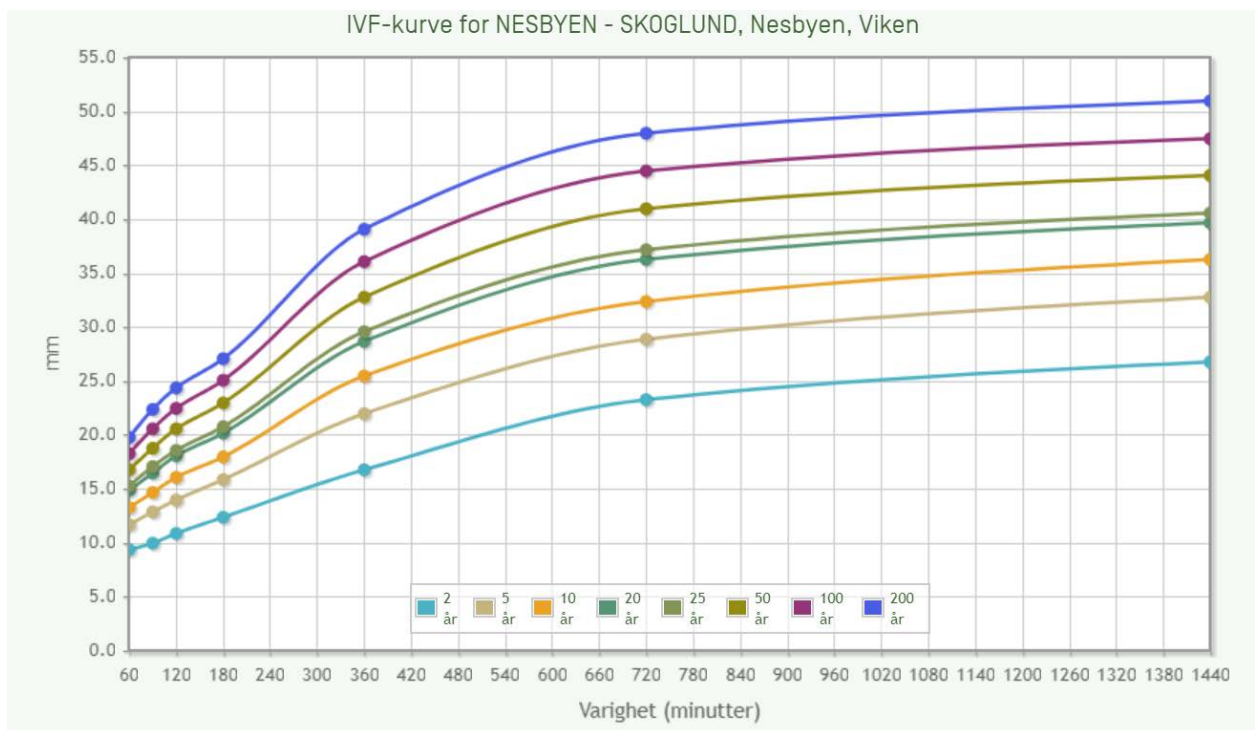


Figure E12. IDF Curve for case 15

Appendix E – Weather Data

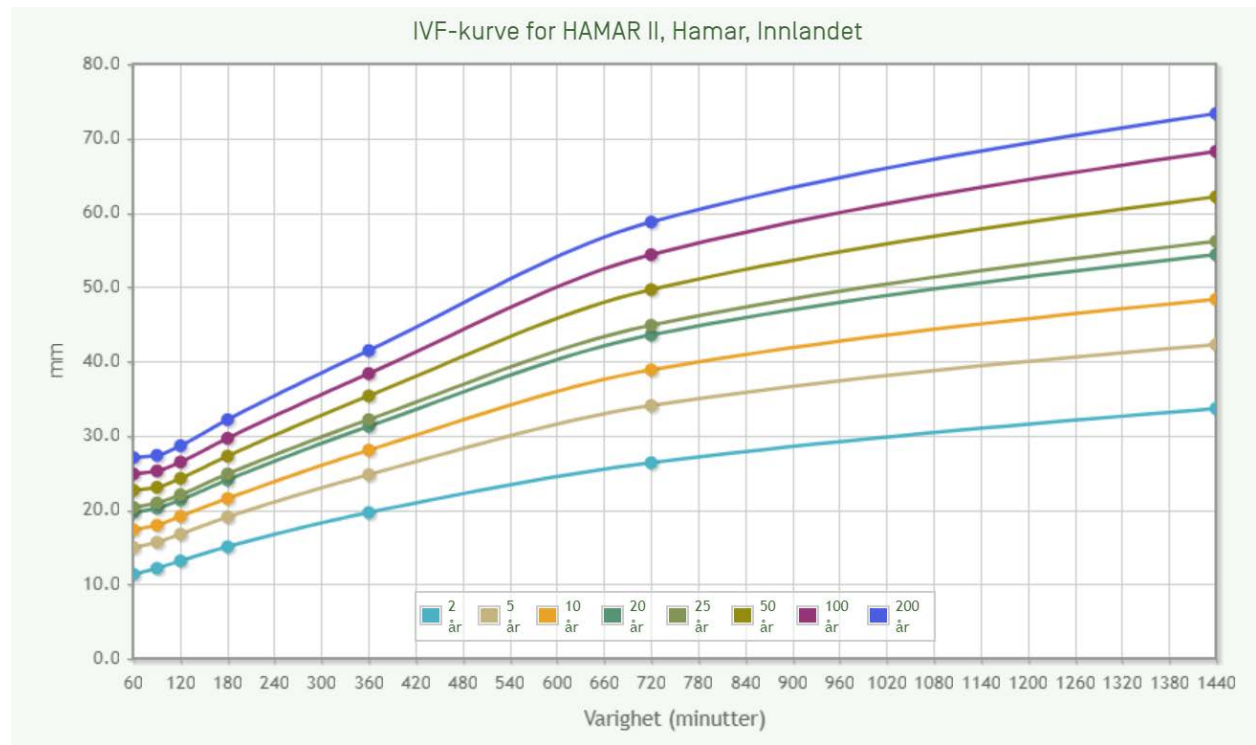


Figure E13. IDF Curve for case 18

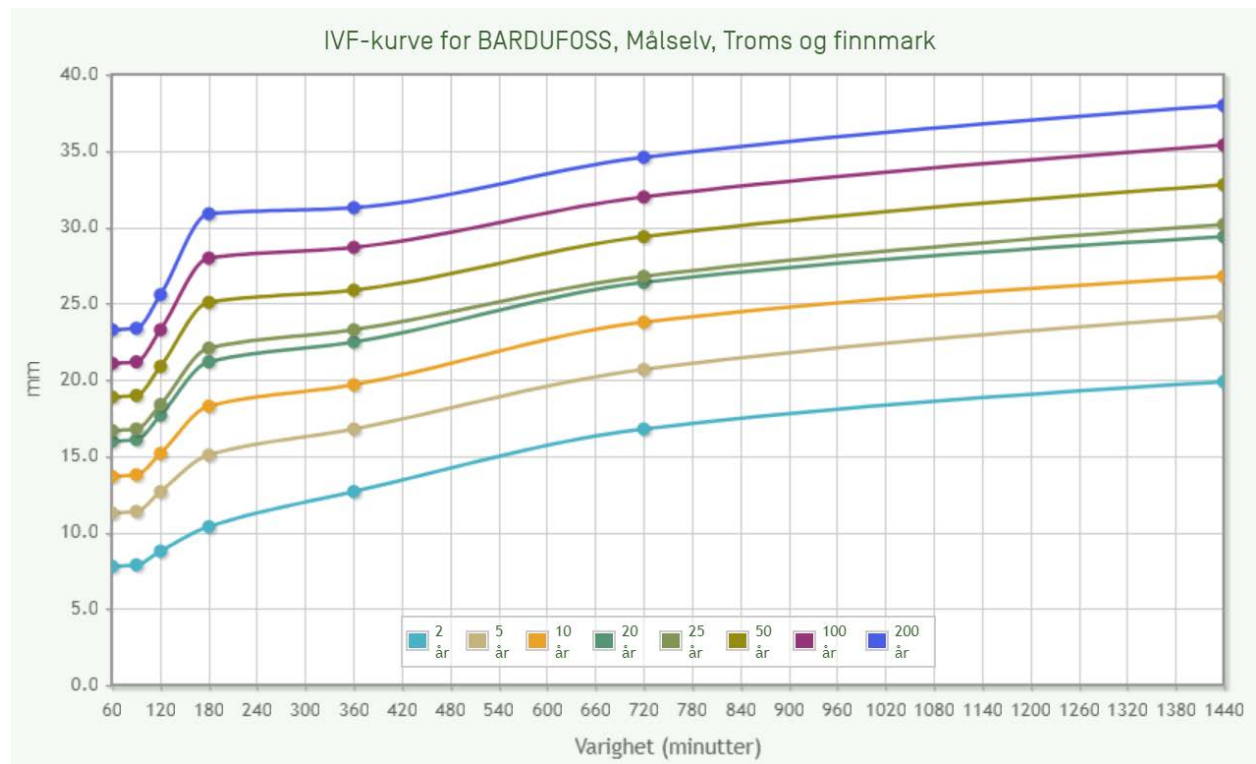
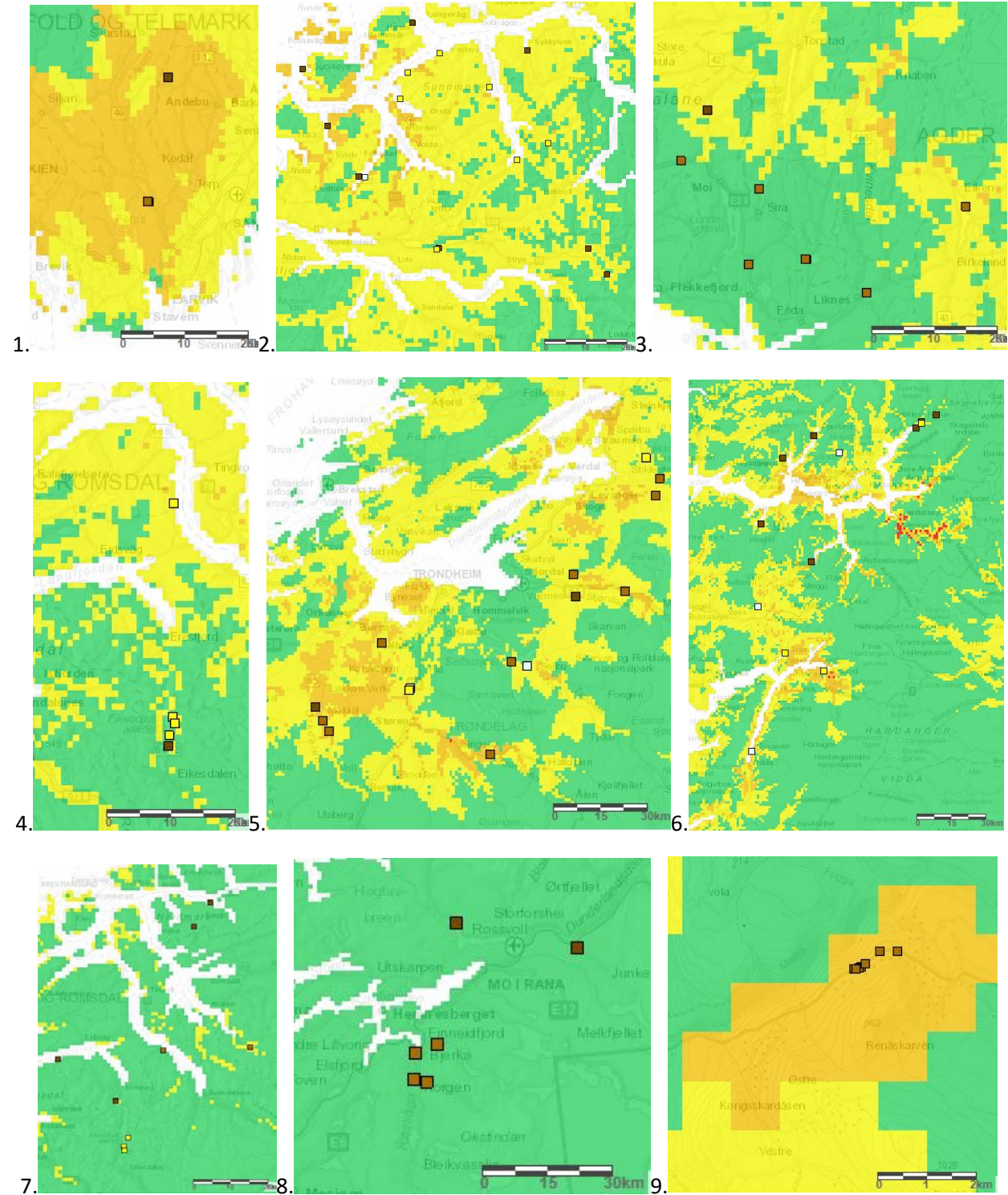


Figure E14. IDF Curve for case 20

Appendix F: HYDMET Model Results

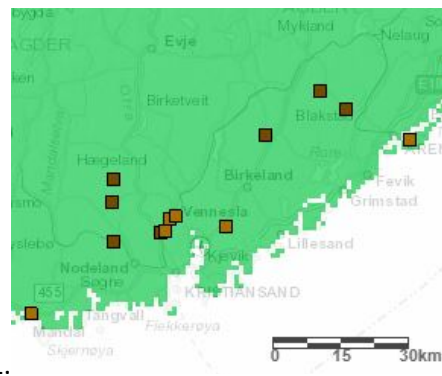
Appendix F – HYDMET Model Results



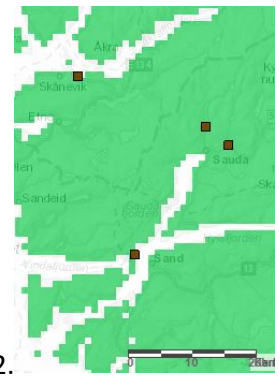
Appendix F – HYDMET Model Results



10.



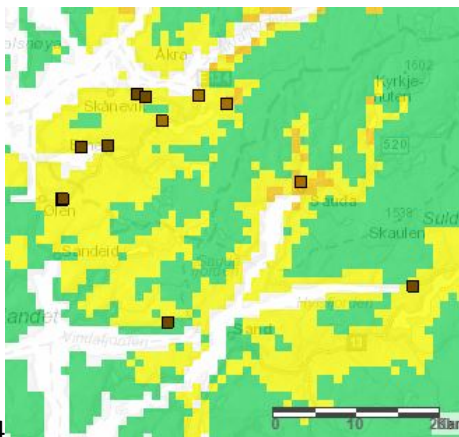
11.



12.



13.



14.



15.



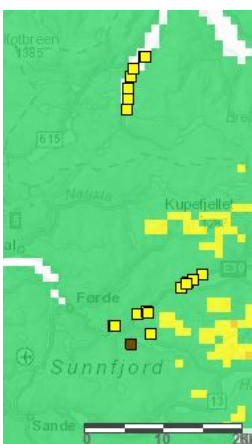
16.



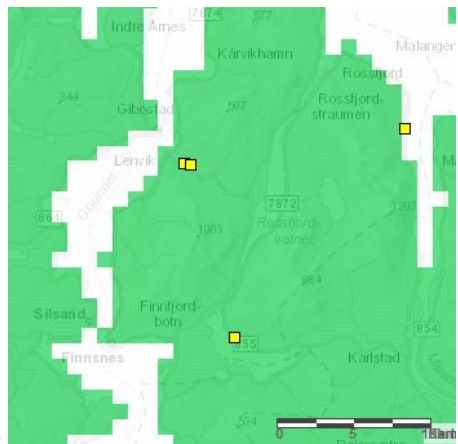
17.



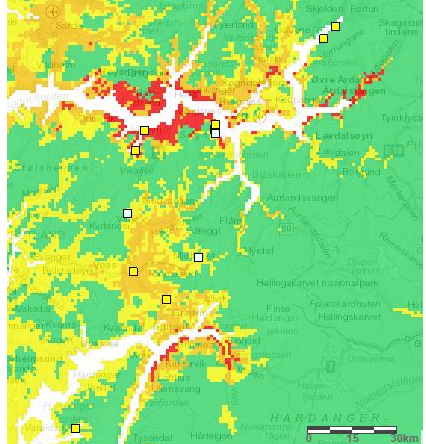
18.



19.



20.



21.



